ENRICHMENT OF SWNT SPECIES WITH CHEMICAL APPROACHES AND MECHANISM INVESTIGATION

ENRICHMENT OF SWNT SPECIES WITH CHEMICAL APPROACHES AND MECHANISM INVESTIGATION

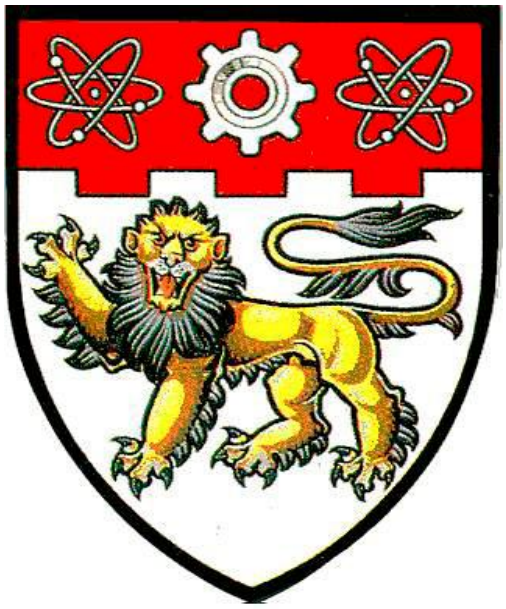

PAN XIAOYONG

SCHOOL OF CHEMICAL & BIOMEDICAL ENGINEERING
NANYANG TECHNOLOGICAL UNIVERSITY

PAN XIAOYONG

2011

2011

Enrichment of SWNT Species with Chemical Approaches and Mechanism Investigation

Pan Xiaoyong

School of Chemical & Biomedical Engineering

A thesis submitted to the Nanyang Technological University in fulfilment of the requirement for the degree of Doctor of Philosophy

2011

Acknowledgements

The author would like to thank Dr Mary B. Chan-Park for her invaluable advice and encouragement throughout the duration of this project. She has continuously shared her time, intellect, creativity, and enthusiasm with me. I thank her for her many, many hours advising and shaping my work.

The author would like to express my heartfelt thanks to all graduate students and technologists in our group. In particular, I would like to appreciate Dr Wang Weizhi, Dr Sun Zhipeng, Dr Zhou Chuncai, Dr Feng Junluo, Dr Poon Yin Fun, Mr Wang Yilei and Ms Yuan Wei for their help and willingness to share their knowledge.

Thanks also go to the Competitive Research Program grant from the Singapore National Research Foundation (NRF-CRP2-2007-02). The author acknowledges the support of Nanyang Technological University through a Research Scholarship. Assistance provided by technical staff in the school of SCBE, NTU is also gratefully acknowledged.

My family and all of my friends are greatly thanked for being my powerful backing forever.

Table of Contents

List of Figures

List of Tables

Table of Abbreviations

SWNT	Single Walled Carbon Nanotubes
HiPco	High-pressure carbon monoxide
pa-18-C-6	N-methyl(18-Crown-6)pyrene-1-acetamide
pb-18-C-6	N-methyl(18-Crown-6)pyrene-1-butyramide
pc-18-C-6	N-methyl(18-Crown-6)pyrene-1-formamide
RRS	Resonant Raman Scattering
RBM	Radial breathing mode
G mode	Tangential mode
FTIR	Fourier-Transform Infra Red Spectroscopy
UV-Vis	Ultraviolet-Visable absorbance spectroscopy
UV-Vis-NIR	Ultraviolet-Visable-Near Infra Red absorbance spectroscopy
CoMoCAT	Cobalt–Molybdenum catalyst SWNTs
PMMAFA	Poly(methyl-methacrylate-*co*-fluorescein-*o*-acrylate)
PAMMA	Poly(9-anthracenylmethyl-methacrylate)
PNMA	Poly(2-Naphthylmethacrylate)
DMF	Dimethylforamide
PLE	Photoluminescence excitation
FETs	Field-effect transistors
SDBS	Sodium dodecylbenzenesulfonic acid
D_2O	Deuterium oxide
HSP	Hansen Solubility Parameters
PBMA	Poly(benzyl methacrylate)
PMMA-*c*-PAMA	Poly(methylmethacrylate)-co-(9-anthracenylmethyl acrylate)
TMS	Tetramethylsilane
NMR	Nuclear Magnetic Resonance
RET	Resonance Energy Transfer
PPyrBT	Poly[(2,7-pyrenyl)-*co*-2,2'-[5,5'-bis(3-dodecylthiophenyl)]]
PFluPyr	Poly[2,7-(9,9-didodecylfluorenyl)-*alt*-(2,7-pyrenyl)]
THF	Tetrahydrofuran
AFM	Atomic Force Microscope
I	Irradiance
D	Donor
A	Acceptor

Summary

Current available SWNT growth methods will inevitably produce mixture of various structures and electronic properties while SWNTs with uniform electronic property or species chirality are highly desired for many applications. Although many techniques for SWNT species enrichment have been successfully developed and effectively applied, all of them suffer from various disadvantages. Most approaches to chemical separation of *sem*-/*met*-SWNTs are based on small neutral molecules or conjugated aromatic polymers which characteristically have low separation/dispersion efficiency or difficulty of post-separation removal of the polymer, so that the resulting field-effect transistors (FETs) have poor performance. Moreover, the insufficient unravel of separation mechanism makes searching of new separating agents and enrichment improvement difficult.

This thesis is devoted to both development of new chemical approach for SWNT species enrichment as well as deciphering of the mechanism underlying the selective processes. With these aims, three similar amide-functionalized pyrene derivatives (N-methyl(18-Crown-6)pyrene-1-acetamide, N-methyl(18-Crown-6)pyrene-1-butyramide and N-methyl (18-Crown-6)pyrene-1-formamide), denoted as pa-18-C-6, pb-18-C-6 and pc-18-C-6 respectively, with different alkyl chain lengths between the amide groups and pyrene moieties have been successfully synthesized and for the first time, their separation effects on single walled carbon nanotubes (SWNTs) according to their electronic structures (metallic/semiconducting) and diameter have been demonstrated. Experimental results have suggested that the side functional groups of pyrene moieties are quite critical for

their species enrichment. However, the separation efficiency of pyrene derivatives was severely limited by their poor dispersion ability.

To improve the dispersants' dispersion ability so as to improve their separation efficiency, three polymethacrylates with different pendant aromatic functional groups were employed to separate CoMoCAT SWNTs according to metallicity and diameters. Ultraviolet/visible/near infrared (UV-Vis-NIR) spectroscopy indicates that Poly(methyl-methacrylate-*co*-fluorescein-*o*-acrylate) (PMMAFA) and Poly(9-anthracenylmethyl-methacrylate) (PAMMA) preferentially disperse semiconducting SWNTs while Poly(2-Naphthylmethacrylate) (PNMA) preferentially disperses metallic SWNTs, all in dimethylforamide (DMF). The polymers' different selective behaviors in different solvents suggest that the diameter selectivity is resulted from the change of polymer conformation. On the other hand, metallicity selectivity is presumably resulted from the photon induced dipole-dipole interaction between polymeric chromophore and SWNTs. The involvement of photon in the separation processes is first time identified and the metallicity selectivity is tentatively ascribed to Resonance Energy Transfer induced intermolecular pairing force.

The investigation of selective behaviors of more flexible polymers with similar chemical structures has strengthened our conclusion. Also, the contribution of different building blocks has been further identified. Moreover, with speculation based on some preliminary results, the different role of radiative/non-radiative RET processes played in the separation processes has been suggested.

To clarify the role of photon/Resonance Energy Transfer induced intermolecular pairing force in the separation process, two conjugated polymers with distinct optical properties

were employed in SWNT species enrichment. The involvement of RET induced intermolecular pairing force was brought out by their different illumination responsive behaviours. The magnitude of this kind of weak interaction scales with an external stimuli parameter, *i.e.*, illumination irradiance *(I)* and thus tuneable. This suggests a facile technique to modify molecules/polymers' selectivity towards some specific SWNT species by altering the corresponding intermolecular interaction. The species selectivity driven by this novel technique is dependent on SWNT interband transition (E_{ii}) energies as well as dispersant's fluorescent properties. Many fluorescent molecules/polymers with appropriate fluorescent properties are thus suggested to be potential separating agents towards certain species. RET induced intermolecular pairing force, which universally existed between two entities between which RET can occur, was first time verified and applied. The significant magnitude of this interaction suggests direct manipulation of molecules/particles possible and paves its way in the application of molecular engineering.

Chapter 1 Introduction

1.1 Background

Owing to their exceptional electronic, mechanical, optical, chemical and thermal properties,[1-9] single-walled carbon nanotubes (SWNTs) have been envisioned as one of the best candidates for many potential applications.[10-14] For nanoelectronic applications, metallic SWNTs (met-SWNTs) are exceptional nanoscale leads with ballistic electron transport over several μm and current densities up to 10^9A/m^2.[15] Semiconducting SWNTs (sem-SWNT) can be wired up to function as fast nanoscale transistors or sensitive nanoscale sensors. For most electronic applications, pure metallic or semiconducting SWNTs are highly desirable.[16-17] The poor growth selectivity of *sem*-SWNTs[18] and low efficiency of destroying *met*-SWNTs make efficient post-synthesis separation schemes necessary[19-20].

Although the techniques of ac dielectrophoresis,[21] anion exchange chromatography of DNA-wrapped carbon nanotubes,[22-25] and density gradient centrifugation method[26-27] *etc.* have been successfully employed in separation of *met*- and *sem*- SWNTs, the difficulty of scaling up limits their application.

As a promising alternative, chemical methods, on the other hand, are more easily scalable and thus more attractive separation techniques. There are two main strategies for the chemical methods, one is covalent functionalization[28-32] of SWNTs and the other is noncovalent attachment[33-37] of functional groups to the sidewall of the SWNTs. Non-covalent approaches are particularly attractive due to their ability of preserving nearly all of the SWNTs' intrinsic properties as well as the mild operation condition. Normally,

noncovalent attachment is controlled by thermodynamic criteria and it is called wrapping for some polymers. Attachment of small molecules such as octadecylamine,[34] bromine[35] and flavin mononucleotide[38] has been demonstrated to be effective in assisting SWNTs enrichment but these methods still achieve limited selectivity. The adhesion of all these small molecules is substantially facilitated by weak linkage similar to hydrogen bond between SWNTs and adsorbents or intermolecular hydrogen bond. Selectivity towards certain species is presumably resulted from the distinguished thermodynamic pairing force of SWNTs/adsorbent for different SWNTs species. It can be anticipated that other forms of the weak interaction such as electrostatic interaction, Van der Waals interaction and π-π stacking interaction may also contribute to the SWNTs/adsorbent pairing force and modify the dispersants' selectivity behavior.[39-43] Experimental investigation has proved the feasibility of using pyrene derivatives[44-45] or conjugated aromatic polymers[46-48] to selectively suspend certain SWNTs species. The π-π stacking interaction is believed to be critical for the enrichment. However, increased dispersion is required for achieving better separation with small neutral molecules and the notorious strong π-π interaction is highly unfavorable with respect to the post-separation removal of the polymer. Despite of the above mentioned non-covalent strategies, understanding of separation mechanism is still inadequate. As a result, further attempts aiming at developing new approach with novel molecular design are formidable and the progress towards the improvement of separation efficiency is slow.

1.2 Objective and work scope

The overall objective is to produce substantial quantities of suspensions containing only metallic SWNTs or only semiconducting SWNTs of pristine quality for applications.

Also, the mechanism responsible for the selectivity will be investigated. To these ends, a variety of chirality selective surfactants will be employed and their effects on SWNTs separation will be explored. A series of pyrene derivatives were synthesized and their separation effects on SWNTs based on the electronic properties and diameters have been demonstrated. To overcome the problem enforced by the poor dispersion with the amide-functionalized pyrene derivatives, a series of Polymethacrylates with pendant aromatic functional groups were investigated for their selectivity in SWNTs separation. The separation mechanism, whose origin may be traced to different forms of weak interaction, was first time experimentally investigated. Different factors responsible for diameter and metallicity selectivity were identified. The relationship between the chirality selectivity and the chemical structures of the polymer may provide some instructive criteria for the search and design of molecules/polymers with novel structure for the purpose of SWNTs separation.

1.3 Organization of the thesis

This report is divided into 7 chapters. The first Chapter covers the background and objectives of this PhD project. Chapter 2 is a detailed literature review and discussion on SWNTs and their properties as well as their preparative methods and various applications. Chapter 3 lists the materials and characterization methods. Chapter 4 describes the SWNTs separation with amide-functionalized pyrene derivatives. Chapter 5 focuses on SWNTs species enrichment with a series of Polymethacrylates with pendant aromatic functional groups. Chapter 6 elaborates the different role of the building blocks in separation and building blocks' contribution to selectivity is determined. Chapter 7 identifies the role of RET induced intermolecular pairing force in the separation process.

Chapter 8 summarizes some important conclusions from the experimental results and outlines some recommendations for future work.

Chapter 2 Literature Review

2.1 Structure

SWNTs were first discovered by Iijima in 1991[49] in fullerene soot.[50-51] It was produced by the arc discharge method, which is similar to the method used for the preparation of fullerenes. Due to its exceptional properties, Single-Walled Carbon Nanotube (SWNT) has attracted much research attention and many interdisciplinary fields aiming at exploring its extraordinary features has been established. Conceptually, SWNTs can be regarded as perfect seamless cylinder structures resulting from the rolling up of small strips of single graphene sheets.[52] Each carbon atom in the graphene plane can be identified with a pair of integers (*n*, *m*) and a pair of graphene lattice primitive vectors (a_1, a_2), with the roll-up vector being defined as: $C_h = na_1 + ma_2$ (Fig. 2.1).[53] The translation vector T is perpendicular to the roll-up vector C_h and directed along the SWNT axis.

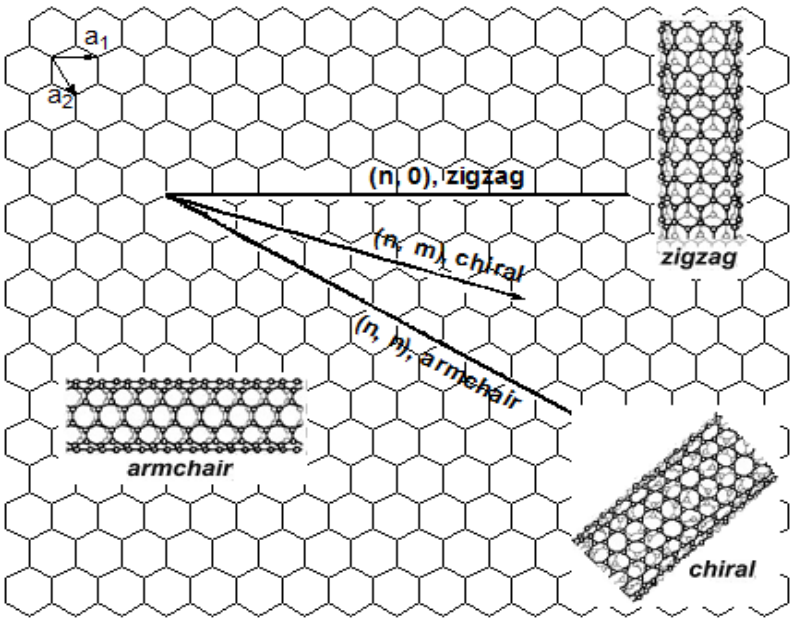

Figure 2. 1 Models of SWNTs with different helicities showing the rolling of a graphene sheet along different chiral vectors.

Typically, the diameter of a SWNT ranges between 0.5 nm and 2 nm, whereas its length reaches in the order of centimeters.[54] SWNTs' critical parameters such as diameter and chiral angle, are determined by the (n, m) indices. Conceptually, the magnitude of translattion vector T corresponds to the length of the (*n*, *m*) SWNT unit cell while the magnitude of the roll-up vector determines the SWNTs' diameter, $d = C_h/\pi$.[55-57] Concretely, once (*n*, *m*) is specified, other structural properties, such as diameter (*d*) and chiral angle (θ) which is defined as the angle between the vector C_h and the zigzag direction a_1 can be determined: $d = (3^{1/2}/\pi)a_{cc}(m^2 + mn + n^2)^{1/2}$ and $\theta = \tan^{-1}[3^{1/2}m/(2n + m)]$,[58-59] where a_{cc} is the carbon-carbon bond length of 0.142 nm and *n* and *m* are the indices that specify the chirality of SWNTs.[60] Depending on the orientation of the graphite sheet (the hexagonal lattice of carbon atoms) relative to the tube axis T, three types of SWNTs are obtained: "armchair," "chiral," and "zigzag" SWNTs.[61-62] Among them, "zigzag" and "armchair" are two inequivalent high symmetry directions, designated by (*n*, 0) and (*n*, *n*), respectively.[16,63]

The unique structure of SWNT, which is composed of slightly strained sp^2 hybridized carbon that is highly stronger than the sp^3 hybridized counterpart,[64] offers them attractive chemical stability, outstanding tensile strength and fascinating elastic Young's modulus, making them extremely useful in material chemistry and highly potential candidate for mechanical materials. [65]

2.2 Properties

2.2.1 Electronic properties

SWNTs were endowed with unique electronic properties because of small dimensions and high aspect ratio. Depending on the chiral vector in which the graphene

was rolled up to form the SWNTs, *i.e.*, the (n, m) indices, SWNTs can be either metallic or semiconducting.[55-56] SWNTs are metallic when n-m = 3k, where k is an integer, and semiconducting otherwise.[55-56] "Armchair" SWNTs are metallic since they satisfy the criteria while SWNTs with the other configurations, "chiral" and "zigzag", can be either metallic or semiconducting. Approximately 67% of SWNTs are semiconducting while 33% of SWNTs are metallic provided that the preparative method is not selective.

To some approximation, the band gap of semiconducting SWNTs scales inversely with the tube diameter. In the tight-binding theory, the band gap, E_{gap} can be represented by $\gamma(2d_{c\text{-}c}/d_{SWNT})$, where γ stands for the hopping matrix element and $d_{c\text{-}c}$ is the single carbon bond length while d_{SWNT} is the SWNT diameter.[58] Figure 2.2 shows the typical electronic band structures of metallic/semiconducting SWNTs.

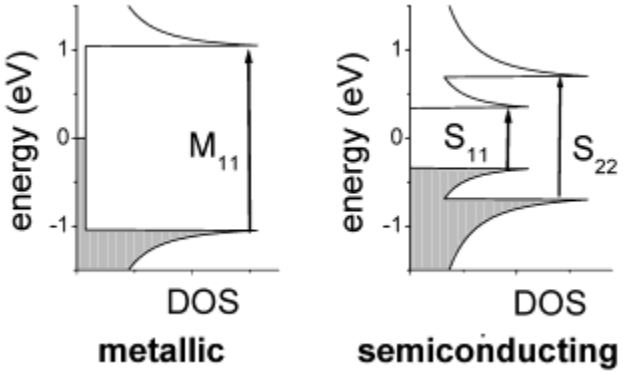

Figure 2. 2 Schematic representations of the interband electronic structures of a typical metallic and semiconducting SWNTs. (reprinted from ref. 153 with permission)

At low-bias, charge transport in metallic SWNTs can be ballistic over distance at the scale of micrometer. This is presumably due to the extremely weak acoustic phonon scattering in this unique one-dimensional structure as well as the ignorable defects which will act as scattering centres. However, optical phonons of SWNTs will be strongly excited at high bias, which will result in energy dissipation and current saturation[66].

SWNT has promising application as a field effect transistor (FET), a device that uses semiconducting SWNTs to switch. Associated with the SWNTs' exceptional electronic properties are the desirable properties such as high current density, carrier mobility and on/off ratio as well as easy scalability[15]. It is superior to and compatible with the well established silicon technology and makes fabrication of complementary logic devices possible.

2.2.1.1 Metallic SWNTs

For most one-dimensional materials, there exhibit a Peierls instability that opens an energy gap in their electronic band structures.[66] As a consequence, it undergoes a metal-insulator transition. The driving force of the Peierls instability is the release of the one dimensional chain's total energy by doubling the unit cell. However, due to the strong carbon-carbon bond in graphitic materials and the cylindrical arrangement of the atoms in SWNTs framework, a Peierls instability cannot be observed for SWNTs. Tight-binding calculations indicate that achiral SWNTs (n=m) are indeed metallic while 2/3 of the chiral SWNTs are semiconducting [(n-m) mod 3 = 1 or 2] and the rest are semimetallic with a small band gap on the scale of mev.[55-56] The semimetallic SWNTs with small band gap are included in metallic category in the following discussion because at room temperature with k_bT= 26 meV, the effects of the band gap is trivial.

Ballistic transport and current saturation

For one-dimensional conductors, their resistance is determined by the number of the available conduction channels as well as the transmission efficiency at the contacts and is independent of their length or composition.[67-69] Specifically, for a conductor with single

conduction channel and fully transparent contacts, the resistance (quantum resistance or contact resistance) is given by

$$R_Q=h/e^2\approx 26\text{K}\Omega.$$

This property is often referred to as ballistic transport since electrons travel between two ends without scattering. It is noteworthy to point out that even though it is scattering free, the resistance of a conductor cannot be zero. The contact resistance arises from the mismatch between the large number of the modes in the contacts over which the current is distributed and the few available modes in the conductor. Theoretical limit for the resistance of a single metallic SWNTs is represented by $R = h/(4e^2) = 6.5\text{K}\Omega$.[70] Experimentally, low bias resistance of an individual metallic SWNTs was found to be between 10KΩ[71] and 100KΩ.[72] Chemical vapour deposition grown SWNTs in contact with Pd were found to show the best contacts with almost completely transparent transmission.[73-74]

Scattering is substantially suppressed in SWNTs because there is no localized surface state and large momentum transfer is needed for backscattering. (Small angle scattering is unlikely to add up to 180° in a SWNT.) At low bias, acoustic phonon scattering[75-76] and defects induced elastic scattering[77] are the two major scattering sources in metallic SWNTs. At room temperature, acoustic phonon scattering dominates while defects induced elastic scattering plays the leading role at low temperatures with the mean free path on the order of several micrometers.

2.2.1.2 Semiconducting SWNTs

Field effect transistor (FET) is one kind of device uses semiconducting materials to switch. Transistor is a kind of current-control device, and its generating current includes

electron flow and hole flow. The most important feature of a FET device is on /off ration, which defined as ratio of current at the on-state and off-state. It indicates the switch capability of FET devices.[78] Higher on/off ratio is desired for FET industrial application. Another important feature of a FET device is the modulation of the source-drain current by a gate voltage.[78-79] An ideal MOSFET turns on at a gate voltage $V_g = V_{th}$, the so-called threshold voltage. At this voltage, the inversion layer below the gate oxide that connects source and drain with a current path is formed. However, in reality, the turn-on at $V_g = V_{th}$ is not instantaneous because even below the threshold voltage, thermally excited carriers can carry a diffusion current. This subthreshold current is especially important for logic devices, since it limits the switching speed of the transistor. One finds that the current in the subthreshold region depends exponentially on the gate voltage and decays below V_{th}, with a rate that is mainly dependent on temperature. Because of the exponential gate voltage dependence of the current, the inverse subthreshold slope, defined as $[d(\log I)/dVG]^{-1}$, is a convenient measure for the switching.[78] S can be easily determined graphically when the current as a function of the gate voltage is plotted on a log scale. At room temperature the subthreshold slope is typically between 70 and 100 mV/decade.[78] The theoretical limit at room temperature is 60 mV/decade.[78]

The band gap of semiconducting SWNTs scales inversely with their diameters and can be expressed as $E_g \approx 0.84\text{eV}/d[\text{nm}]$, where d stands for the SWNTs diameter. This makes them as promising active material for FET device fabrication. Charge carrier transportation through semiconducting SWNTs is governed by the relative position of the Fermi level with respect to the edge of conduction/valence band.

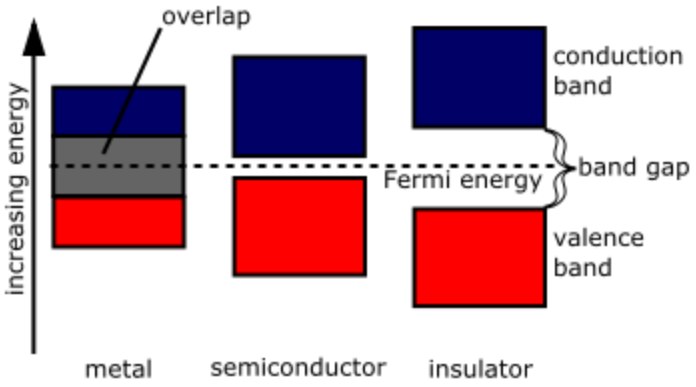

Figure 2. 3 Schematic representations of the electronic band structures of typical metal, semiconductor and insulator.

As a result, chemical or electrostatic doping which can shift the Fermi level of SWNTs can be employed to tune their conductivity. The property of electrochemical potential dependent conductivity of semiconducting SWNTs can be used to fabricate a device that acts as a switch. It functions as a conductor if the SWNTs Fermi level is shifted into the valance/conduction band by the gate potential while acts as an insulator when the Fermi level lies in the band gap. In semiconductor industry, the device with this kind of switch behaviour is well know and named as field effect transistor (FET).[78] Replication of silicon metal-oxide semiconductor based FET by replacing the silicon with a semiconducting SWNT is conceptually straightforward.[79] The first SWNT-FETs were fabricated at Delft and at IBM in 1998.[79] Laser ablation grown SWNTs were used by both groups.[80] Singly dispersed SWNTs were deposited onto a Si/SiO_2 surface. A conduction channel was formed with semiconducting SWNTs bridging the two prefabricated electrodes. By tuning the applied back gate potential, modulation of the channel conduction and the corresponding FET behaviour was achieved. Normally, the SWNT-FETs fabricated show typical *p*-type characteristics, with on/off ratios of about several orders. However, the resistance in the ON state is high, exceeding 1 MΩ. In addition, due to the thick dielectric layer, high gate voltages were required for switching.

Moreover, the subthreshold slope is much higher as compared with the MOSFETs thermal limit. To some extent, thermal treatment can improve the contact conductive property and resistance below 100KΩ has been reported for SWNT-FET with titanium contacts, in which the resistance decrease was ascribed to the formation of TiC/SWNT contacts upon annealing.[81] Improvement of the contact conductivity has also been achieved by direct growth of SWNTs such as Chemical Vapour Deposition (CVD) on the substrate, presumably due to the clean surface of the as-grown SWNTs as contrast to the solution deposited SWNTs, the surface of which will inevitably be covered by some residue. Pd, as a metal with quite good wetting properties, comes to produce the best contacts with SWNTs of diameter above 2nm. Almost unity transmission can be achieved for holes travel in the ON state.[73] However, formation of Schottky barrier at the contacts can be reasonably anticipated for SWNTs with diameters smaller than 2nm. The SWNT-FETs performance can also be improved by optimizing the gate stack.[81] Regarding this approach, SWNTs are much more applicable than silicon because there is no dangling bond on the surface of SWNTs and the associated surface scattering is thus ignorable. Dielectrics with high dielectric constant κ such as HfO_2, Al_2O_3, $SrTiO_3$ and ZrO_2,[82-84] have been successfully applied in SWNT-FETs. However, the most available SiO_2 is employed in most research work on SWNTs. As a contrast, SiO_2 is the only choice for MOSFETs because the good interface between silicon dioxide and silicon is quite crucial for achieving the optimal device performance. Silicon MOSFETs with high κ dielectrics inevitably suffer from mobility decrease. In the FET device fabrication, SWNTs well dispersed in solution can in principle be deposited at any stage provided that the solvent can withstand the process condition. On the other hand, growth of SWNTs by CVD

method onto the patterned and pre-deposited electrodes on an appropriate substrate may offer many advantages. The metal needs to stand the high temperature of the growth process. Two approaches have been advanced as solution for the temperature issue: the first approach is to decrease the growth temperature, by using methanol as the carbon source or by using methane as the feedstock gas with plasma-enhanced CVD method, down to 600℃,[85] a temperature that most metals can stand. The second approach is to limit the electrode material to the choice of metals that are stable and make good contacts with SWNTs at the normal growth temperatures. Tungsten-platinum and molybdenum are appropriate for this purpose.[86] With SWNTs' nano-scale diameter, the scaling for SWNT-FETs has been proved much more efficient than conventional MOSFETs even though they look quite similar in schematic structure. With the contact conductivity governed by the number of channels that contribute to semiconducting SWNTs conduction in FET devices, quantum effects are also involved in the function determining the device current. As a consequence, the device current is much lower than that of the MOSFETs. On the contrary, their current densities, which are on the order of $10^8 A/cm^2$, are substantially higher than that in silicon MOSFETs. On the other hand, closely spaced parallel SWNTs arrays would be needed for the delivery of the high current in a SWNT-silicon hybrid structure. With conduction path shorter than hundreds of nanometers, semiconducting SWNTs are also ballistic at low bias,[81] which is similar to metallic SWNTs in this respect. Decrease of the length scale below this critical value cannot improve its conductivity. If the factor of flight time is taken into consideration, the device will switch faster. If the conduction channel is longer than 10 μm, the SWNT-FETs show characteristic behaviour similar to that of bulk MOSFETs. Both of them show current

saturation behaviour because the channel resistance is much higher that of the contact barriers. In this case, the transportation of charge carriers is dominated by drift through the charge gradient inside the channel. Because of their cylindrical structure, the gate capacitance of SWNTs in long channel scales inversely with the logarithm of the thickness of the oxide $C_{ox} \sim 1/(\ln t_{ox})$. The SWNT depletion capacitance $C_D = 0$ and the subthreshold S is theoretically 60mV/decade at R.T. since they are completely depleted. However, due to the involvement of Schottky barriers, S decreases as the oxide thickness decreases. The other benefit with increasing oxide thickness besides subthreshold improvement is the low voltage operation of SWNT-FETs. When t_{ox} scales up, the Schottky barriers decrease due to the SWNTs' one-dimensional structure. As a result, tunneling through the barrier as well as ambipolar characteristics can be observed. The tunable band gaps of SWNTs with various diameters produced by different synthetic methods is the other advantage associated with SWNT-FETs with respect to MOSFETs.

One interesting property for both metallic and semiconducting SWNTs is that the dominant interband transitions vary with diameter and chiral vector. Consequently, to achieve uniform electrical properties, SWNTs need to be monodisperse in both their diameter and electronic type because SWNTs with nearly identical diameters can have different chiral vectors and thus different electronic properties. This makes chirality enrichment inevitable for many applications.[87-88]

A two dimensional network, often referred to as a thin film, of SWNTs can be viewed as a novel transparent electronic material with good and tunable optical, electrical and mechanical properties.[89] The networks exhibit high conductivity, high mobility and good optical transparency in addition to robustness, flexibility and environmental

resistance. These characteristics coupled with ambient temperature spraying or printing technology, indicate that this material will have a substantial impact on various emerging technologies and markets, ranging from solid state lighting to macroelectronics, smart fabrics and organic solar cells.[89]

The ability of SWNT to form networks with known length and density distributions is of crucial significance to the development of various electronic materials that incorporate this smart electronic component. Specifically, low density networks of SWNTs are of substantial technological interest since they can be tuned from semiconducting to metallic behaviour as the density of SWNTs increases. As a consequence, a number of methods of forming such networks have been developed. High temperature methods usually involve growth of SWNTs in desired place using chemical vapour deposition (CVD) method.7,8 Much more effort has been devoted to low temperature, suspension-based deposition techniques because they makes usage of various kinds of substrates and incorporation of distinct SWNT purification/modification/enrichment techniques possible. As a result, many ambient temperature deposition techniques for SWNT thin film formation have been developed. Techniques have been demonstrated to be effective and wildly employed include dip-coating,[90] spray-coating,[89,91] suspension evaporation,[92-93] spin-coating,[43] and layer-by-layer assembly.[94] While there are distinct utilities for each of these techniques, they all suffer from the problem of SWNT bundle formation. Bundle formation will exclusively result in metallic behaviour of SWNT networks.[95]

In order to facilitate solution deposition of SWNTs for integration into electronic devices, they need to be purified and well dispersed into solutions. Vigorous sonication is

normally needed for the preparation of SWNT dispersion although this process inevitably leads to cutting in SWNT length and introduction of defects on the sidewall of SWNTs, resulting in compromise of electronic properties. Understanding the sonication effects of solution processing steps on network electronic properties thus has important implications in the design and electronic applications of SWNT networks. Generally, as sonication time increases, SWNTs are shortened. This will inevitably result in the decrease of electrical current due to the increasing of the number of junctions as well as introduction of more structural defects.[95]

Another important parameter which will strongly influence the device performance is the concentration of SWNT networks.[89,96] The increase of density of SWNT network will ultimately result in the exhibit of metallic behavior of SWNT network. Alignment of SWNT network also has quite significant implication on the network properties since good alignment will surely result in the decrease in the number of intertube junctions bridging the electrodes.[89,96]

Besides all the above-mentioned parameters, SWNT intrinsic properties (metallic vs semiconducting) are also quite crucial for the network properties.[43] For example, pure semiconducting SWNTs or even single chiral species are highly desired for the fabrication of network transistors. This makes the enrichment of SWNTs according to electronic properties or chiral species necessary for some electronic application.

2.2.2 Optical and Optoelectronic Properties

SWNTs with perfect crystal structures have direct band gaps in the momentum (K) space and their band and subband structures are well defined, making them ideal candidate for optical and optoelectronic applications.[97-98] For direct band gap materials,

no momentum transfer is needed to induce interband transitions and direct light absorption and emission is possible since the minimal-energy state in the conduction band and the maximal-energy state in the valence band coincide in terms of wavevector.

Absorption/emission of photons with suitable wavelength will excite/relax substances with appropriate electronic band structures.[59,99-100] Depending on the detailed electronic band structures, the wavelength and intensity of these optical transitions vary from substance to substance. In a typical SWNT structure, each carbon bonds to three neighbouring atoms by σ bond and the remaining pi electron contributes to the formation of delocalized π electron system. Electronic states of SWNTs delocalize along the periodic axis and are bound in the transverse direction.

Optical properties have been investigated for individual/bundled SWNTs with Ultraviolet-Visible-Near infrared (UV-Vis-NIR) spectroscopy,[99,101] Resonant Raman Scattering[102-103] as well as Photoluminescence maps.[104-105] Moreover, electroluminescence and optoelectronic properties such as photoconductivity have also been explored.

For single dispersed SWNTs, their optical band gaps slightly depend on their microenvironment.[106] However, SWNT photoluminescence is extremely susceptible to microenvironment and quite sensitive to aggregation and chemical functionalization. The characteristics of optical excitations in SWNTs as well as the microenvironment effects are reflected in the absorption spectra/PLE maps, *i.e.* their wavelengths and shapes.[103,107] PLE maps investigation is nevertheless an efficient method for identification of chiral species (n, m). In a typical Photoluminescence map, when the excitation energy matches the secondary optical transition levels E_{22}, the emission from SWNTs' primary electronic

transitions E_{11} will be resonantly enhanced. (with the schematic mechanism included in the section 2.4 Characterization Methology) Also, when the excitation energy matches higher electronic transitions such as E_{33}, E_{44}, *etc*. emission from the same E_{11} bandgap will also be resulted. This constitutes the theoretical foundation of the assignment of (n, m) indices.[103,108] Each of the peaks in a typical PLE map can be identified as an individual semiconducting species by careful analysis of its intensity fluctuation with varying excitation and emission wavelengths. The PLE map analysis offers a great deal of information about the precise interband transition energies for a wide range of SWNTs species. Moreover, the PLE intensity of different species in a single PLE map works as an effective proxy of their relative content in the mixed samples.[103,108] In addition, an empirical "Kataura plot" of semiconducting SWNTs can be constructed from the electronic band structures derived from the related optical properties.[109] The near-infrared emission from semiconducting SWNTs makes them promising candidates for optical detection and imaging in complex environments.

SWNTs' optoelectronic properties make them highly promising for widespread applications in electrically driven light emitting devices and light detectors.[110-111] Current generation from SWNTs upon photon excitation has been reported.[112] In previous studies, SWNTs bundles were used. Recently, individual SWNTs in SWNT-FETs have also been investigated for photocurrent or photovoltage generation.[112] Theoretical calculation suggested that the quantum efficiency of photon to current conversion is about 10% in SWNT-FETs.[112] This makes SWNT-FETs promising in photodetector application. In ambipolar SWNT-FETs devices[113] with symmetric electrode structure, equal currents of carriers (holes and electrons) are generated from their injection from the opposite ends of

SWNTs provided $V_g = V_d/2$.[114] Due to the 1 D structure of SWNTs, electron and holes are localized transversely and travel freely along the axis direction. Under certain circumstance which is governed by momentum and spin selection rules, *etc.* electron and hole will recombine with generation of one photon. IR emission has indeed been observed with ambipolar SWNT-FETs. When $V_g = V_d/2$, the maximum of the emission intensity was observed, which is in good agreement with the theoretical anticipation.

In optical spectroscopy, the emission peaks coincide with the band gaps of the SWNTs used in the devices. However, the dependence of the peak shapes in the electroluminescence emission spectra on SWNT length was observed. Long SWNTs (>5μm) resulted in sharp and symmetric peaks while short SWNTs (~200-300nm) gave broad and asymmetric bands.[115] This phenomenon was explainable with the extent of relaxation (completed or partial) of the excited carriers during the periods of their residence in long or short SWNT channels. The energy distribution of the carriers can be derived from the wavelength and peak shape of their electroluminescence band. Recently, much information about the electrical transport process in a SWNT-FET was obtained by investigation of the spatially resolved light emission from very long SWNTs (~50μm), *i.e.* their dependence on the applied drain and gate voltage. As contrast to the LEDs where doping modulate the light emission location, in ambipolar SWNT-FETs, the position of the light emission is determined by the gate voltage. The spot of emission works as a precise proxy of the location where the recombination of electron and hole occurs.[113,115]

2.2.3 Chemical and Electrochemical Properties

2.2.3.1 Covalent chemistry

SWNTs covalent functionalization

Covalent chemistry focuses on the functionalization of the outside wall of SWNTs. It can be classified into two main categories. The first category is functionalization of the defect sites on the sidewall or at the tube ends which are generated by ozonation or oxidation.[116-118] The generated functional groups can be converted to their corresponding derivatives.[119-134] The second category includes various addition reactions which result in the direct covalent functionalization of SWNTs sidewall.[135-142] Fluorination and aryl dizaonium are among the typical effective addition reagents. The most common effective covalent functionalization of SWNTs was carried out in oxidizing mixtures of sulphuric acid and nitric acid/hydrogen peroxide under sonication.[20] Besides purification, this method also cuts SWNTs. Various kinds of functional groups such as carboxylic acids, quinines, esters, and anhydrides, are generated on the sidewall as well as at the ends of SWNTs by following this approach. Normally, the carboxylic acid groups are activated by thionyl chloride treatment for further functionalization. Peptide, which is an extremely important derivative, is also accessible from carboxylic acid. An obvious advantage of this approach is that the bulk properties of the SWNTs are almost preserved upon functionalization due to the limited defect sites introduced to the SWNTs sidewall although the ends are destroyed more severely. In 1998, sidewall functionalization by direct fluorination was reported by Mickelson et al and various spectroscopic techniques were employed to confirm the substantial covalent functionalization.[135] The presence of covalently bound fluorine was corroborated by Infrared spectroscopy and the characteristic Raman spectral properties of the pristine SWNTs were substantially suppressed upon reaction. More importantly, the attached fluorine can be removed by treatment with hydrazine, which makes the recovery of the spectroscopic properties of

SWNTs possible. The attached fluorine groups are also susceptible to the replacement with other strong nucleophiles such as Grignard reagents and metal alkoxides.

Other reagents which functionalize SWNTs directly include dichlorocarbene, carbene derivatives, nitrenes[143-144] and azomethine ylides.[145-146] Similar to oxidation functionalization, the spectroscopic properties of SWNTs are changed upon reaction with these reagents.

Covalent chemistry, as an effective approach for SWNTs' structural modification, provides many promising pathways for SWNTs' potential application in various fields. The most severe problem with covalent functionalization is that SWNTs bundles are not disrupted in most cases. However, covalent functionalization of singly dispersed SWNTs is desired for many applications. Structural modification of SWNTs with specific chirality will probably be needed for their future application.

In order to enhance the degree of covalent functionalization of SWNTs and fully utilize the unique properties of SWNTs, much effort has been devoted to developing approaches for reproducible dispersions of individual SWNTs.[147] The thermodynamic drive toward aggregation must be overcome to stabilize the singly dispersed SWNT solution. A dispersion method, as a component step of the manufacture chain, has thus to be developed according to the processing conditions of the SWNT based material.[147]

There are two main approaches for SWNT dispersion: the mechanical approaches and approaches that are developed to alter the surface energy of SWNTs, either non-covalently or covalently.[148] Mechanical approaches such as ultrasonication can separate SWNTs from each other, but can also cut the nanotubes, decreasing their aspect ratio.[148] Chemical methods (either covalent or non-covalent) use surface modification of SWNT

to improve their affinity to the dispersing medium.[148] However, aggressive chemical functionalization such as nitric acid treatment at high temperatures, may introduce structural defects and compromise the properties of the SWNTs.[148] Non-covalently physical approaches have been proven capable of debundling SWNTs as well as stabilizing individual tubes while maintaining SWNT integrity and intrinsic properties and are thus quite attractive dispersion techniques.[148]

In the last dacade, the non-covalent functionalization by surfactants or polymers has been widely employed in the preparation of SWNT dispersion in both aqueous and organic solvents to obtain high fraction of individually dispersed species.[148]

For the dispersion of SWNT in aqueous solvent, a notable achievement is the use of the ionic surfactant sodium dodecylbenzene sulfonate (SDBS).[147] Further developments indicate selective interactions with hence dissolution of semiconducting and metallic SWNTs and SWNTs of different diameters.[147]

Noncovalent functionalization of SWNTs with polymers was shown to enhance the dispersion of SWNT in both water and organic solvents, as well as to facilitate separation of SWNTs from metal and carbonaceous impurities.[148] Two mechanisms were advanced: "wrapping" which is believed to rely on specific interactions between a given polymer and the SWNT species. Kinetic mechanism suggests that long ranged entropic repulsion among polymer functionalized SWNTs acts as a barrier that stabilizes the SWNT dispersion.[148]

The curvature for SWNT reactivity

Generally, the reactivity of both Fullerene and SWNTs depends strongly on their structure and scales with their curvature of the carbon framework. SWNTs are less curved than Fullerene while they are more curved with respect to graphene.[64,149-151] As a result, SWNTs are anticipated to be more inert than Fullerene and more reactive than graphene sheet.[152-154] Moreover, the reaction of a single carbon atom will facilitate the reaction of the atoms in its vicinity. This is due to the fact that the relaxation of strain at one point will increase the total strain among the remaining carbon atoms. Consequently, the strain relaxation will accelerate the addition reactions in SWNTs.

Selective covalent chemistry of SWNTs

For most of the application of SWNTs in electronic devices, the most severe barrier is the difficulties associated with the preparation of SWNTs with pure electronic properties. All of the reported synthesis approaches will inevitably produce mixture of metallic and semiconducting SWNTs. Although some preferential growth of certain species has been partially achieved in some techniques, their selectivity is low and improvement is highly desired before their widespread application. Some reported SWNTs chemistry offers a unique and effective covalent functionalization of SWNTs and makes manipulation of SWNTs according to their electronic properties possible. In most of these approaches, metallic SWNTs are selectively functionalized and this allows the separation of metallic SWNTs and semiconducting SWNTs scalable. As a result, electronic devices manufacture based on SWNTs with specific electronic properties is feasible.

With SDS as the surfactant, SWNTs are well dispersed in aqueous solution. Upon reaction with diazonium salt,[28] the individually suspended metallic tubes show substantial

higher activity as compared to their semiconducting counterparts. With the reaction conditions carefully controlled, functionalization of SWNTs with benzene diazonium salt even shows discrimination between metallic and semimetallic SWNTs. The reaction of water soluble diazonium salts with SWNTs proceeds via charge transfer intermediate with electrons extracted from SWNTs by dizaonium moieties and covalent aryl bond formed subsequently. The diazonium reagent participates in the charge transfer process, acting as one component of the complex. Electron transfer from SWNTs can stabilize the transition states and covalent bond formation for electrons near the Fermi level (EF) is thus highly preferred. As a consequence, metallic SWNTs show higher reactivity due to the more readily available electrons at the Fermi level. Due to the acceleration effects of the defects on adjacent atoms, the selectivity is amplified once the reaction is initiated. This trend continues until the complete reaction of the whole SWNTs.[28] The selective functionalization of SWNTs was confirmed with UV-Vis-NIR absorbance spectra as well as Resonance Raman Scattering spectra. After functionalization with dizaonium salt at appropriate dizaonium salt/SWNTs ratio, the characteristic interband transition bands of metallic SWNTs disappear while those of the semiconducting SWNTs are preserved. Resonance Raman Scattering spectra corroborated the conclusion that the functionalization proceed with a prominent selectivity towards metallic SWNTs. The intensity of disorder (D) band, a phonon mode at ~1330cm^{-1} arises from the sp^3 hybridized carbon, increases dramatically after reaction. This confirms the conversion of sp^2-hybridized carbon to sp^3-hybridized carbon on the SWNTs sidewall during aryl-SWNTs bond formation. The intensity of the D band indicates the degree of covalent bond formation. It is thus easily understandable that the D band intensity scales with

increasing reaction extent. On the contrary, the tangential mode decreases because of the loss of electronic resonance upon functionalization. Moreover, covalent functionalization of SWNTs destroys the symmetry of the Radial Breathing Mode (RBM) and will eventually suppress the characteristic RBM features of the corresponding chiral species. This kind of behaviour can't be observed with non-covalent surface adsorption, which decreases the resonance enhancement without complete removal of the RBM features. PLE maps of the semiconducting SWNTs, which are quite sensitive to covalent functionalization, also verified the metallic SWNTs selectivity of the reaction.

The recovery of the SWNTs' spectroscopic features can be achieved by thermal treatment of the reacted material at 300℃ in an inert atmosphere.[28] The cleavage of the aryl moieties from the SWNTs sidewall is believed to be involved in and responsible for their property restoration. Comparison of the Raman spectra obtained before reaction and after thermal treatment indicated almost full recovery of the RBM mode, suggesting the reversibility of the chemical functionalzation. Moreover, complete restoration of the characteristic absorbance features after thermal treatment manifest the recovery of the intrinsic electronic structure. The facts listed above suggest that selective covalent chemistry can be employed as a reversible pathway for manipulation of SWNTs with specific electronic properties which makes recovery of intrinsic electronic and optical properties possible.

Other reported reagents which will selective functionalize SWNTs include dichlorcarbene reactions, and osmylation, *etc.*[143-144]

2.2.3.2 Non-covalent chemistry

Molecular Adsorption and desorption

Molecular adsorption was first discovered during the measurement of electrical transport properties and was brought out by the difference between the resistance of semiconducting SWNTs in vacuum and that in air.[155]

Systematical investigation of the electrical properties of SWNTs in various chemical environments revealed that various small gas molecules adsorb onto SWNTs and undergo charge transfer.[155] Exposure of semiconducting SWNTs to NO_2 at ppm level results in 10^3 times increase of conductance in a few seconds. On the contrary, decrease of the conductance up to 2 orders can be observed if the SWNTs are exposed to NH_3. Similar sensitivity of SWNT conductance to O_2 adsorption has been observed by Collins and co-workers.[156] These results suggested the potential application of SWNTs as chemical sensors. O_2 and NO_2 are strongly adsorbed on SWNTs and desorption of them is quite slow at room temperature. However, the physisorption of NH_3 on SWNTs is weak and desorption of NH_3 can thus be easily achieved by pumping in vacuum. Density functional theory (DFT) has been employed in the calculation of the binding energy between SWNTs and various molecules. Theoretical calculation suggested a binding energy of ~0.4eV to 0.9eV between NO_2 and SWNTs as well as ~e/10 electron transfer from SWNTs to NO_2.[157-158] For O_2, DFT calculation yields a binding energy of ~0.25 eV and ~e/10 charge withdraw from SWNTs.[159] However, DFT calculation suggests very trivial binding energy between NH_3 and SWNTs. It is thus advanced that they bind together via Van der Waals interaction. In spite of the ignorable charge transfer, dramatic change of SWNTs electrical properties can be observed upon NH_3 adsorption.

Photoinduced desorption of molecules from SWNTs was reported recently.[160] Thermal treatment at ~200℃ can also assist in the molecular desorption.[156,161] In the

presence of Ultraviolet (250nm) light at low flux, rapid desorption of molecules can be observed at room temperature.

This kind of photoinduced desorption is universal for various molecules. Wavelength dependent results indicate that electronic excitation of SWNTs is responsible for this intrinsically nonthermal process. Electron-hole pairs are generated via Landau damping following π-plasmon excitation by UV illumination.[162] As a result, desorption is suggested to be due to the attachment of photon generated electrons/holes to the adsorbed molecules.

The results highlighted the roles of photochemistry and surface chemistry in the application of SWNTs as molecular wires. With SWNTs as probes, surface science can be explored.

Polymer adsorption and wrapping

With the assistance of wrapping with various polymers such as polyvinyl pyrrolidone (PVP) and polystyrene sulfonate (PSS), SWNTs solubilisation in water up to g/l concentration has been reported by Smalley et al.[163] They also observed that there is no dependence of the SWNTs/polymer association on the free (excess) polymer in solution, which suggests the strong interaction between polymer and SWNTs. For the purpose of the investigation of SWNTs' application in optoelectronic devices, conjugated luminescent polymers such as poly-{(m-phenylenevinylene)-co-[(2,5-dioctyloxy-p-phenylene)-vinylene]}(PmPV) and its derivatives,[164] poly{(2,6-pyridinylenevinylene)-co-[(2,5-dioctyloxy-p-phenylene)vinylene]} (PPyPV)[165] and poly{(5-alkoxy-m-phenylenevinylene)-co-[(2,5-dioctyloxy-p-phenylene)-vinylene]}(PAmPV),[166] have been successfully employed in the dispersion of SWNTs. The stabilization of the suspension is

ascribed to the wrapping of the polymers around SWNTs and π-π stacking interaction as well as Van der Waals interaction between polymers and SWNTs is believed to be involved. It is obvious that SWNTs' structure and properties can be preserved with noncovalent functionalizations. Stilbenoid dendrimer, a branched variant of the PmPV polymer has been successfully synthesized and the demonstration of it as an effective dispersant of SWNTs has been reported.[167]

SWNTs dispersed with biological molecules such as nucleic acids and protein peptides show great potential for bioengineering and nanotechnology application.[168] DNA may wrap around or be encapsulated inside SWNTs due to the Van der Waals interaction between DNA and SWNTs.[169] Macromolecular structures have been successfully build with SWNTs dispersed with an amphiphilic α-helical peptide via the interaction between adjacent peptides wrapping around SWNTs.[170] Individually suspended SWNTs, possibly end to end connected, can also be successfully isolated using amphiphilic α-helical peptide with specific structure.[171] Starch has also been demonstrated to be an effective dispersant in the presence of iodine and starch/iodine complex is believed to be involved.[172] Other macromolecules which have been established as effective dispersant for SWNTs include Gum Arabic, another polysaccharides, Potato and waxy corn amylopectins *etc.*[173-174]

Doping

For SWNTs' application in Field Effect Transistor (FET) devices, device performance (p type or n type) is in principle determined by type of charge carrier (electron or hole). This makes the control of the type of charge carrier extremely crucial in devices application. Both SWNTs based p-type and n-type FETs are desired.[65]

However, most preparative method will produce p-type SWNTs-FETs. Doping method with alkali metal as the dopants has been reported to be effective for preparation of n-type FETs.[175-176] Nevertheless, the dopants are readily oxidable and the device performance will drop significantly. Doping with an amine rich polymer, polyethyleneimine (PEI), has been demonstrated to be effective for fabrication of n- type FETs that are stable in air.[177] Analysis suggests that approximately 1 electron was transferred from the wrapped polymer PEI to every 1000 carbon atoms on the SWNTs. As an alternative to alkali metals which ionized completely, functional groups on organic material with partial electron donating and withdrawing capability can be efficiently used to dope the SWNTs embedded in the devices and switch the charge carriers between electron and hole.

Selective non-covalent chemistry of single-walled carbon nanotubes

A noteworthy aspect of noncovalent chemistry of SWNTs is that there are approaches that show preferential reactivity toward metallic SWNTs over semiconducting SWNTs or *vice versa*. Such selective surfactants include bromine, amines and DNA.[22,34-35] This is important because it offers researchers the ability to manipulate SWNTs by band gap and makes preparation of pure metallic or semiconducting SWNTs possible.

2.2.4 Mechanical Properties

σ bond is the strongest among all kinds of chemical bonds. SWNTs with structures all σ bonding are thus regarded as the ultimate fibre with strength in tube axis. Both experimental investigation and theoretical calculations suggest that SWNTs are stiffer than or at least as stiff as diamond with the highest Young's modulus and tensile strength.

Most theoretical investigations are performed for defect free structures and yield coincident results.[178-179] Generally, various SWNTs with perfect structures are stronger than graphite,[6,180-181] which is presumably due to the substantial increase of the axial component of σ bonding upon rolling of a graphene sheet into a tube. Young's modulus is dependent on SWNTs' diameter but independent on chirality. SWNTs with diameter between 1nm and 2nm show highest Young's modulus, *i.e.* ~ 1TPa. In a SWNTs bundle or SWNTs rope, the Van der Waals force induces a strong shearing among the SWNTs with Young's modulus decreased. It has been demonstrated that the Young's modulus scales with decreasing bundle diameter. As the diameter of a bundle increases from 3nm to 20nm, Young's modulus decreases from 1TPa to 100GPa. The elastic property of SWNTs is also marvellous. Because of dislocations and defects propagation, most hard materials crack with a strain of 1% or even less. As contrast, theoretical and experimental investigation both indicate that SWNTs can tolerate up to 15% tensile strain before fracture.[182] As a result, the tensile strength of individual SWNTs can be up to 150GPa provided the Young's modulus is 1TPa.

2.2.5 Thermal Properties

Diamond and graphite have exceptional heat capacity and thermal conductivity. In parallel, SWNTs can be anticipated to have similar thermal properties at room or elevated temperature. However, at low temperatures, some unusual behaviour can be observed for SWNTs due to phonon quantization. Both experimental investigation and theoretical calculation indicate that the coupling between tubes in SWNTs bundles is weak at 100K or above.[183] In this temperature region, single SWNT or SWNT bundle shows heat relation similar to that of graphite. Nevertheless, at lower temperature, a new

phenomenon named quantum confinement effects arises for SWNTs. As an example, the heat capacity is 0.3(mJ/gK) for a (10,10) SWNT and 0 for graphite and SWNT bundle.[183-184] The on-tube phonon structure is manifested by the thermal conductivity of SWNTs, independent on their stacking state, *i.e.* single or bundled. Thermal conductivity of bulk SWNTs are quite different from that of graphite. A linear temperature dependent characteristic can be observed for SWNTs at low temperature, which corroborate the occurrence of one-dimensional phonons. As electrical conductivity, thermal conductivity of SWNTs is one dimensional. Consequently, investigation yields a wide range of thermal conductivity from 200W/mK to 6000W/mK with a prominent dependence on the sample quality. Experimental measurements and theoretical investigation indicated that the thermal conductivity of a SWNT rope at room temperature scales between 1800W/mK and 6000W/mK.[184-185]

2.2.6 Magnetic and Electromagnetic Properties

Normally, magnetic properties of SWNTs are investigated with electron spin resonance (ESR), which applies widespread in the study of electronic properties of conjugated materials and graphite. Although the experimental results[186] qualitatively agree with theoretical conclusion, there is prominent deviation among different experimental measurements, presumably due to the SWNTs quality and alignment.

Theoretically, SWNTs magnetic properties such as susceptibility and anisotropic g-factor are predicted to be close to those of graphite although SWNTs may show some unique properties.

SWNT electrical response to magnetic field has also been anticipated to be unusual. Metal insulator transition and band gap change have been corroborated by both experimental and theoretical investigation. Theoretically, the band gap of SWNTs under uniform magnetic field parallel to the tube axis is given by the following expression in which $\beta = 3\phi(h/e)$ where h/e is the magnetic flux quantum.[187]

For metallic tubes of $n - m = 3q$

$E_g = E_{go}\beta, \quad 0<\beta<3/2$

$E_g = E_{go}|3-\beta| \quad 3/2<\beta<3$

For semiconducting tubes

$E_g = E_{go}|1-\beta| \quad 0<\beta<3/2$

$E_g = E_{go}|2-\beta| \quad 0<\beta<3/2$

With E_{go} defined as:[53,98,188]

$$E(k_x,k_y) = \pm\gamma\{1+4\cos(\frac{\sqrt{3}}{2}k_x a)\cos(k_y a/2) + 4\cos^2(k_y a/2)\}^{1/2}$$

Where γ is the nearest neighbor-hopping parameter in the range of 2.5eV-3.2eV and a is lattice constant with value of 0.246 nm. With the above expressions, metal insulator transition can be predicted and the band gap variation under axis-parallel magnetic field can be calculated. Similar behaviour can also be observed with a transverse magnetic field.

A major characteristic of the theory is that the change of the band gap is oscillatory[189] and SWNTs can be shifted between metallic and semiconducting by application of an external magnetic field, which is called Aharonov-Bohm effect.

2.3 Synthesis

Since its discovery, several preparative methods have been advanced for the large scale production of high quality SWNTs. Laser ablation, electric arc discharge and chemical vapour deposition are among the most successful and widely employed approaches.[65,190-193]

2.3.1 Laser Ablation

Laser ablation for SWNT production was established by Smalley and his colleagues in 1996.[194]

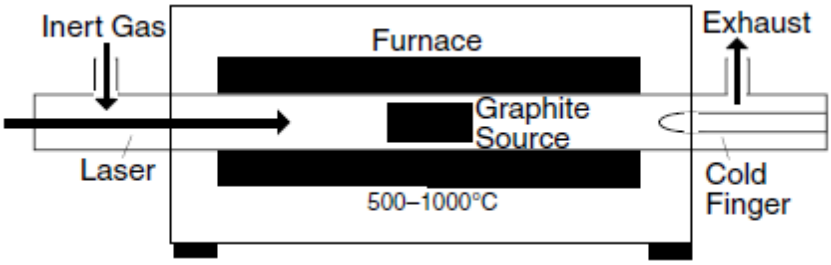

Figure 2. 4 Schematic of a laser ablation furnace. (reprinted from ref. 193 with permission)

In this method, ablation of a carbon target was conducted with a high power laser in a hot inert (helium or argon) atmosphere. Once the temperature is elevated to 1200℃, a pulsed laser beam is used to trigger the evaporation of carbon from the graphite target. Carbon atoms are swept by the flowing gas from the hot area to a low temperature collector on which SWNTs are formed by condensation. Impregnation of the carbon target with catalysts, which are normally transition metals, is the prerequisite for the generation of SWNTs with laser ablation technique. Experimental investigation indicated that the growth of SWNTs can be finished in a few milliseconds. Besides SWNTs bundles, fullerenes, amorphous carbon as well as other carbon by-products are also

produced by this technique. The properties of the produced SWNTs are highly dependent on various different parameters including furnace temperature, light intensity, type of carrier gas and hydrocarbon as well as the gases flow rate. For instance, no SWNTs growth can be observed below 800℃. The most severe disadvantage of this technique is its high cost due to the involvement of high quality graphite source and high power lasers.

2.3.2 Electric Arc Discharge

Electric are discharge is one of the first reported techniques for SWNTs growth.[49,52,195]

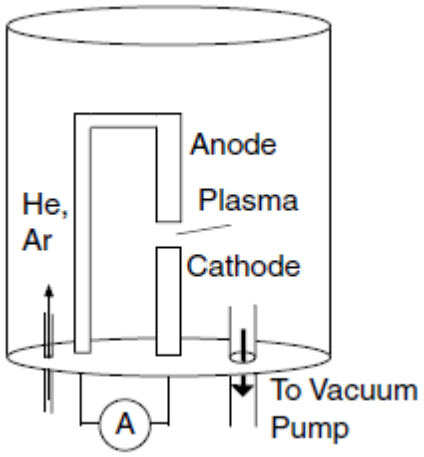

Figure 2. 5 Schematic of an arc discharge chamber. (reprinted from ref. 193 with permission)

In this technique, two graphite electrodes with diameters in the range of 6-12mm and separating distance in the scale of 1-4mm are placed inside a chamber under the protection of inert gas. With 50-100A current passing through the electrodes, carbon atoms are ejected from the anode to the cathode, where they aggregate to form SWNTs. The length of the anode thus decreases as the SWNTs growth proceeds. From the graphite anode is the carbon vaporized as crystallites and small clusters are generated subsequently, with rearrangement of the clusters into a cylindrical structure forming

SWNTs follows. The produced SWNTs then drift towards and deposit on the cathode. The unavoidable production of unwanted graphite crystallites which do not form SWNTs limits the yield of this technique. SWNTs growth in arc discharge method are usually catalyzed by various metallic nanoparticles such as Fe, Co, Ni, Cu, Ag, Al, Pd, Pt, Fe/Co, Fe/Ni, Fe/Co/Ni, Co/Cu, Co/Ni, Co/Pt, and Ni/Cu, etc.[196-198] SWNTs with diameters in the range of 1-5nm and length in the scale of 1mm are normally produced by this method.[196-198] The production rate of this method is as high as several hundred mg of pristine SWNTs in every 10 minutes. However, high reaction temperature of 1500℃ is necessary for high yield production.

2.3.3 Chemical Vapour Deposition

As a relatively slow method, chemical vapour deposition (CVD) can produce long SWNTs in large scale.[199-202]

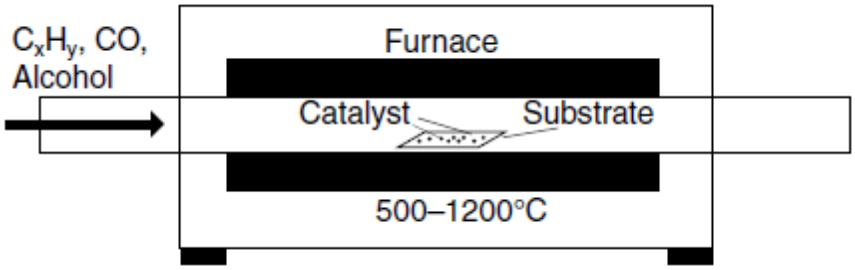

Figure 2. 6 Schematic of a CVD furnace. (reprinted from ref. 193 with permission)

The hydrocarbon source is elevated to 700℃-1000℃ in a quartz tube in the presence of catalyst. SWNTs growth follows the thermal deposition of the carbon containing gas on catalyst. The catalyst on the substrate provides the nucleation sites for SWNTs growth. At elevated temperature, the decomposition of hydrocarbon into hydrogen and carbon is followed by the dissolution and diffusion of carbon atoms into

the metal surface. Subsequently, rearrangement into a network consisting of carbon atomic hexagons occurs and it finally precipitate out as SWNTs. When the metal surface is covered by amorphous carbon, *i.e.* the catalyst is "poisoned", the carbon atoms are blocked from the contact with the catalyst and SWNTs growth is terminated. Hydrocarbon used in the CVD method can be in either gas state, liquid state or solid state. Acetylene, methane and ethylene are the widely used gaseous hydrocarbons and alcohol, benzene and hexane are typical choices of liquid while naphthalene, camphor, etc. are among the solid hydrocarbon sources. Typically, inert gas such as He or Ar is used to flush the quartz tube in a thermal CVD setup for about 10 minutes. After that, hydrogen is introduced to reduce the catalyst at about 400℃ for ~30 minutes.[199] The effect of hydrogen on the catalyst size has been explored. Next, SWNTs growth is initiated by the introduction of the hydrocarbon source. The whole catalytic system is made up of two parts: the metal catalyst and the metal support. Fe, Ni, Co or Mo is usually used as the catalyst and MgO, Al_2O_3, Si or $CaCO_3$ are among the choices of the metal support. Catalytic systems consisting of two different metals are beneficial for their high yield production and the ratio of the metal components is quite critical for SWNTs yield and morphology.[200] Thermal evaporation is one of the most widely employed techniques for preparation of catalyst as small particles. Theoretical calculation and experimental investigation indicated that the SWNTs diameter is closely related to the particle diameter. The size of the SWNTs diameter scales with that of the metal particle. Two growth mechanisms, *i.e.* tip growth and base growth, are possibly involved in the growth. If the interaction between the support and metal particles is strong, carbon atoms will precipitate from the metal particles. This results in the growth of SWNTs on top of the

particles. On the other hand, weak interaction between support and metal particles will facilitate the precipitation of the carbon atoms from the bottom of the metal. In this circumstance, SWNTs growth occurs between the support and metal particles. This is called the tip growth.

Horizontal and vertical furnaces are the two widely employed CVD configurations.[65,203-204] The former one is possibly the most popular configuration for SWNTs growth. By tuning the deposition time of hydrocarbon, the length of SWNTs can effectively be controlled. For the purpose of mass production of SWNTs, the vertical furnace is normally employed. In this configuration, hydrocarbon gas is injected from the top and the SWNTs are collected at the bottom of the chamber. The most obvious advantage of CVD technique is its scalability for high quality SWNTs growth at low cost. The tunability of SWNT quality and production rate with adjustment of various reaction setups such as temperature, hydrocarbon source, catalyst and gases flow rate is another superiority of CVD method.

Although SWNTs growth can be conducted in various conditions, the basic prerequisites include an active catalyst, a carbon source and elevated temperature.

2.3.4 Selective growth of SWNTs

As compared with other preparative methods which produce SWNTs in a narrow diameter range, CVD method usually results in SWNTs with diameters scaling from 0.4nm to 5nm and its diameter control is relatively difficult.[202-203] Many techniques have been established for diameter control with most research focusing on the control of sub steps such as catalyst design, particle formation as well as tuning of growth conditions.

The preferential growth of certain chiral species is even more difficult, presumably due to the one-to-many relationship between the diameter and chiralities of SWNTs. As a result, much effort has been devoted to the post synthetic separation.

Particle production for narrow-diameter SWNTs

Driven by the argument that the diameter of produced SWNTs will presumably be controlled by the diameter of metal particles, exploration of SWNTs growth directly on unsupported individual particles has been conducted.[203,205-206] For example, ferritin has been used to produce particles with narrow diameter distribution. Via tuning the ferritin concentration, SWNTs with different diameter distribution can be produced.

CoMoCAT: chirality selectivity

A very efficient selective method based on supported catalyst, which is referred to as CoMoCAT method,[207-210] has been developed for the chirality control of SWNTs growth. Mesoporous silica was used as the support and CO was introduced as the carbon source. By controlling the ratio of Co and Mo, chirality selectivity can be achieved. PLE maps suggest that few semiconducting chiralities are produced.

PECVD production of narrow-diameter and chirality SWNTs

It has been well established that plasma-based SWNTs growth such as laser ablation and arc discharge methods will produce SWNTs with relatively narrow diameter distribution. Production of SWNTs with very narrow diameter distribution (0.8 to 1.5nm) has been successfully demonstrated by using a catalyst based on ferritin in a modified plasma enhanced CVD system.[18,211-213] Electrical transport data suggests that ~90% are semiconducting SWNTs.[18] The deviation from theoretical value (67%) for random

chirality distribution is very obvious although the mechanism for the preference toward semiconducting SWNTs is not clear. It has been suggested by density functional theory that less energy is needed for the formation of semiconducting SWNTs with large band gaps than that is needed for metallic SWNTs. The semiconducting SWNTs preference may be resulted from the selective etch of metallic SWNTs by plasma generated H • . Alternatively, the selectivity may possibly be ascribed to the lower external energy supply for the formation of smaller diameter SWNTs since the higher strain energy associated with smaller SWNTs can partially compensate the energy requirement for their growth. PECVD method can also be conducted directly on substrates at temperatures as low as 550℃.

2.4 Characterization Methology

Associated with the fast advancement of SWNTs research and their expanding applications is the rapid development of the techniques for SWNTs characterization. Due to the existence of various growth methods, characterization protocols are needed to assist the scientific community to standardise the assessment of SWNT properties. Various techniques have been adapted in the investigation of SWNT features.

2.4.1 Thermogravimetric analysis

TGA is an analytical technique[214-215] used to determine the thermal stability of materials and the fraction of volatile components by monitoring the weight loss that occurs as a sample is heated. The measurement is normally conducted in air or in an inert gas such as He, N_2 or Ar. The weight loss is recorded as a function of increasing temperature. In most cases, TGA is performed with a linear temperature ramp. With this

kind of analysis, ash content and oxidation temperature can be obtained. For the pristine SWNTs, TGA analysis is normally complicated since the weight loss due to carbon oxidation is usually accompanied by the oxidation of catalyst which will result in the increase of the overall weight. Under certain circumference, this will result in an upward slope of the TGA curve before the bulk weight loss. It is common to notice that different TGA analysis results will be obtained with SWNTs from the same batch sample, especially the TGA traces. This confirmed that SWNT samples are not pure chemicals and therefore are not homogeneous and uniform as usually observed for pure chemicals. This can explain why there is always some discrepancy between the results of different characterization beyond the reproducibility and accuracy of the instruments. The solution to this problem is three (or more) times analysis and calculation of the mean average.

2.4.2 Optical Spectroscopic characterisations

Optical techniques have been widely used to characterize SWNTs. The advantages of optics rely on both experimental and fundamental aspects. Experimentally, the techniques are readily available, relatively simple to perform, quick, and can be performed at room temperature and under ambient pressure. Fundamentally, the optical techniques are non-destructive and non-invasive because they use the photon, a massless and chargeless particle, as a probe. Furthermore, optical experiments can be carried out at the single tube level due to the unusually high optical response of SWNTs, which is a consequence of the one-dimensional confinement of their electronic structure.

Basic Principles

Despite the diversity of optical techniques, the underlying physics of the apparent distinct optical phenomenon observed for SWNTs is common and can be explained in the

context of the so-called Kataura plot,[216] which was proposed by *Kataura*, et al. in 1999.[106]

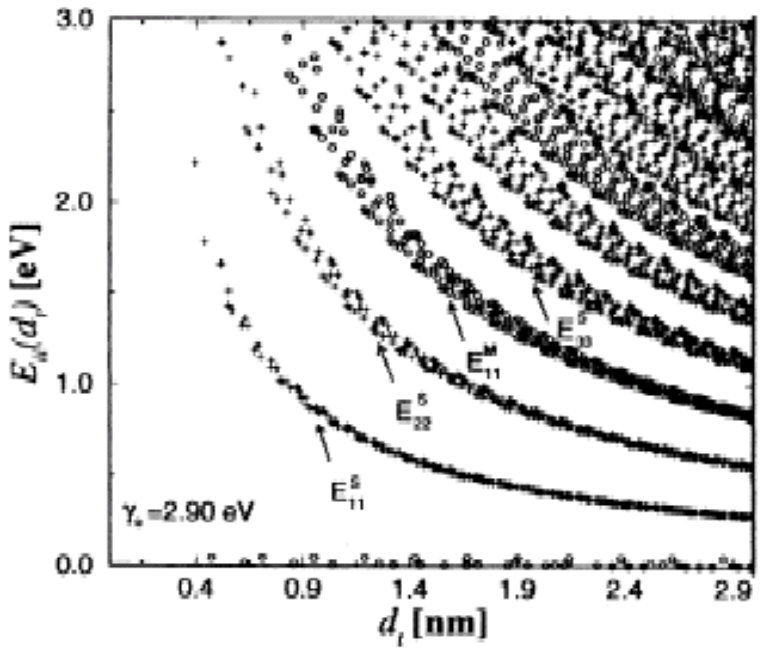

Figure 2. 7 Kataura plot generated for SWNTs in a diameter range of 0.4 to 3nm. (reprinted from ref. 215 with permission)

A *Kataura* plot is shown in the above figure. Each point in the plot stands for one optical transition energy E_{ii} for certain (n,m) SWNT species as a function of tube diameters. Specific SWNT species absorb light and exhibit corresponding optical response in case the photon energy matches the interband transition energy. Significant efforts have been devoted to both theoretical and experimental studies for the sake of establishing the *Kataura* plot. Good agreement between theoretical and experimental studies has been obtained. However, the E_{ii} value of SWNT species is quite sensitive to its micro environment and thus susceptible to external experimental parameters.

2.4.2.1 Resonantly enhanced Raman spectroscopy.

Raman spectroscopy[217-218] is widely used for the characterization of SWNTs due to its high sensitivity along with the little work needed for the sample preparation. The information of the Raman signal is quite rich and can be used in the investigation of isolated, aligned as well as bundled SWNTs. Generally, the resulted spectra depend strongly on the energy of the excitation laser. Raman signal of SWNT species with their interband transition energies match the laser energy will be substantially enhanced. Under this circumference, nomenclature of Resonance Raman Spectroscopy (RRS) is normally used. Light polarization will also influence the signal intensity since it is a crucial factor of the selection rule governing the optical absorption processes.

A typical Raman spectrum of SWNTs consists of two dominant spectroscopic features, *i.e.* the low frequency radial breathing mode (RBM, between 100–300 cm^{-1}) and the high frequency tangential mode (G band between 1500–1600 cm^{-1}). Disorder-induced D mode is another feature presented with reasonably strong intensity. Since the RBM frequency, ω_{RBM}, depends linearly on the reciprocal tube diameter d_t, each (n, m) spceies in a sample with a wide diameter distribution will have a different RBM shift. This can be used to characterize the species abundance of both pristine and enriched SWNTs. Analysis of the G band is usually conducted regarding the two prominent peaks, which originate from the symmetry breaking of the tangential vibration when the graphene sheet is rolled. The two intense G peaks are labelled G^+ and G^- for modes corresponding to atomic displacement along the tube axis and atomic displacement along the circumferential direction respectively. The line shape of the G bands for semiconducting and metallic SWNTs is quite significant in terms of G^- band. In contrast to the Lorentzian line shape G^- band for semiconducting species, the G^- band for metallic species is

substantially broadened due to the phonon-electron coupling. G mode and RBM mode are informative for SWNT structural and electronic characterization. Because of the resonant nature of the SWNT Raman signal, SWNT species are selectively probed by different wavelength lasers. As a consequence, multiple excitation wavelengths are needed in order to get more comprehensive information. Another feature of Raman spectra which is rich in structural information is the D band (disorder band), which is normally located at 1200–1400 cm^{-1}. This mode is resulted from the disordered structure, *i.e.* the sp^3-hybridized carbon atoms on the sidewall of SWNT as well as other carbon sources in carbonaceous impurities. Specifically, the intensity ratio of G band and D band is used for the estimation of the extent of functionalization of SWNTs. The Raman features of RBM and G modes are also sensitive to the degree of functionalization with their intensities decrease with increasing functionalization.

2.4.2.2 UV-Vis–NIR absorption spectroscopy.

Optical absorbance spectroscopy is the simplest optical technique, from both theoretical and experimental point of view. Optical absorbance[106,219] can be used to detect the existence of SWNT species or estimate the concentration of the presented species from the optical features corresponding to the first and second interband transition from semiconducting SWNTs (E_S^{11} and E_S^{22}) and the first interband transition of metallic species (E_m^{11}). Optical features of higher level interband transitions are blurred due to low density of states governing the optical process and the overlap with absorption from σ-bonded electrons.[219] Since the optical absorption intensity is roughly proportional to the species concentration, optical absorbance can be used to determine the degree of SWNT separation based on electronic properties. Theoretically, light will be absorbed when its

photon energy is in resonance with E_{ii} values for certain SWNT species. The resonance width depends strongly on the sample processing conditions and the broad peaks are normally resulted from the unresolved absorption features from different species and it is often difficult to resolve the in the optical absorbance spectra the features from tubes with different (*n*,*m*) that have similar E_{ii}. The analysis of species abundance is compromised with small change in species E_{ii} value. This is the great challenge associated with environmental changes. The species dependent optical absorbance spectra can be resolved if the sample has a small diameter distribution, and this is normally the case for smaller diameter SWNTs. For absolute population analysis, optical absorbance efficiency of relevant species is needed. Covalent functionalization of SWNTs will induces modification to their electronic structure.[220] As a result, their corresponding absorption features will be influenced. The disruption of π conjugation is increased with increasing functionalization degree. At low degree of functionalization, the characteristic absorbance features can still be identified in the UV-Vis-NIR spectrum with suppressed intensity. Complete loss of the absorbance features can be observed at high functionalization degree.

2.4.2.3 Infrared spectroscopy.

Because of the strong absorption of SWNTs in the IR region, relative less information about the vibrational properties of SWNTs can be obtained from Infrared spectroscopy as contrast to Raman spectroscopy.[221] For SWNTs, A_{2u} and E_{1u} are the two main active modes at about 874 and 1598 cm^{-1} respectively.[221] The number of infrared active modes depends on the species chiral indices. There are three, three and six Infrared active vibrational modes for zigzag, armchair and chiral tubes respectively. IR

spectroscopy is normally employed to characterize the impurities and identify the functional groups introduced by organic functionalization.[222] Specifically, IR is quite useful to characterize oxidised SWNTs. The finger print of the resulted C=O stretching band appears at around 1700cm^{-1} and the characteristic bands of C-H vibration locate between 2800 and 3000cm^{-1}. These spectroscopic features[222] are absent in non-functionalized SWNTs and are thus can be easily identified upon functionalization.

2.4.2.4 Emission spectroscopy.

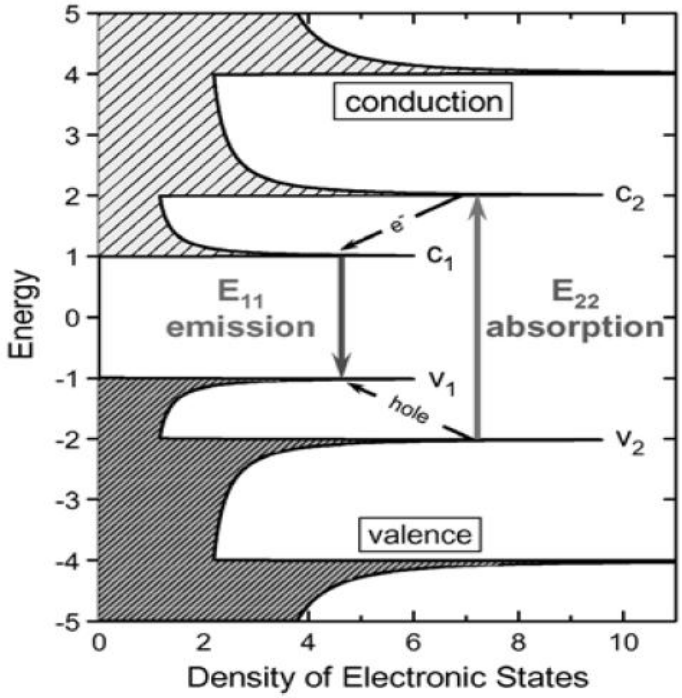

Figure 2. 8 Schematic density of electronic states for a semiconducting single-walled carbon nanotube. Van Hove singularities are labeled with "v" for valence band and "c" for conduction band, along with subscripts giving the sub-band index. Vertical arrows show intense optical transitions for light polarized along the tube axis. (reprinted from ref. 222 with permission)

Among the various optical characterization methods, photoluminescence exhibits the most intense signal.[103,108,223] One prominent shortcoming with this characterizing technique is the sample preparation. Since the photoluminescence of SWNT species are strongly quenched upon formation of bundles, solution with individually suspended

SWNT species are highly desired for this characterization. Another shortcoming is that metallic species cannot be detected by this technique since metallic SWNTs do not fluoresce. As contrast to Raman spectra which exhibit a unique feature (E_{ii}, ω_{RBM}) for each (n,m) species, photoluminescence excitation spectra (PL emission as a function of the excitation energy) suggest another unique finger print, that is obtained by measurement of the (E_S^{22}, E_S^{11}) signal intensity for each specific tubes.[103,108] The (E_S^{22}, E_S^{11}) pairs can be well established once a complete photoluminescence excitation map is conducted. The peak intensity of semiconducting SWNTs is roughly proportional to their individually suspended species concentrations and thus can be used as a proxy for the estimation of enrichment degree of various semiconducting species. For the determination of species abundance, PL quantum efficiency of each species is necessary. PL emission is substantially suppressed after chemical functionalization and thus can be used to track the reaction preferentiality towards certain species.

2.4.3 Scanning probe microscopy

All scanning probe microscopy techniques such as Atomic force microscopy[224-225] and Scanning tunnelling microscopy[58,226] involve the scanning action of a sharp tip across the surface of an object. The tip is attached on a flexible cantilever; this allows it to follow the surface profile. When the tip scans across the surface, the interaction between the tip and the surface influences the cantilever movement. The modification of the cantilever movement is detected by selective sensors. Various interactions can be investigated depending on the mechanics and working mechanism of the probe. The two most widely employed scanning techniques for SWNT characterization are atomic force microscopy (AFM) and scanning tunneling microscopy (STM). AFM tracks the

interaction force between the surface and the tip while STM measures the tunnelling current between the tip and the surface at a fixed distance.

2.4.4 Electron microscopy

Scanning electron microscopy[227] and Transmission electron microscopy (TEM)[228] are the two main characterization techniques used to visualize the SWNTs, measure their lengths and diameters as well as access their purities. Due to its low resolution, SEM provides little information on the attachment of functional groups on the sidewall of SWNTs. On the other hand, direct imaging of the single tube chirality can be achieved with HRTEM.

2.5 Separation techniques & Resonance Energy Transfer

2.5.1 Separation techniques

In order to realize its potential in nanoelectronic devices, great effort has been devoted to the development of new techniques for the sake of preparing metallic or semiconducting SWNTs with high purity. Preferential growth and selective enrichment are the two main strategies for this purpose.

Plasma enhanced chemical vapor deposition (CVD)[18] is one of the typical preferential growth method for the production of semiconducting SWNTs. The semiconducting content of the produced SWNTs at 600℃ with assist of plasma can achieve as high as 90%. This qualitative estimation was conducted based on electrical characterization. It demonstrated an effective preferential growth of semiconducting SWNTs over metallic ones. The characterization methods employed for the content estimation have also been applied to other SWNTs materials and the results revealed that

HiPco SWNTs consists of ~61% metallic while laser ablation produce metallic with slight preferentiality (~70%). These control experiments suggest plasma enhanced CVD method to be an effective method for the preparation of semiconducting SWNTs. High performance field-effect transistors (FET) are obtained with the sem-SWNTs enriched product. However, the met-SWNTs content of the produced mixture is still high and limits its application.

Separation of semiconducting and metallic SWNTs was first demonstrated with individually SWNTs suspension using alternating current dielectrophoresis.[21,229-230] This physical technique was borrowed from the life sciences and makes use of the different polarisabilities of semiconducting and metallic SWNTs in the presence of an external electrical field. Theoretically, the dielectric constant of metallic SWNTs is of the order of $1000\varepsilon_0$ (ε_0 is vacuum permittivity), much higher than that of aqueous surfactant solution ($\sim 80\varepsilon_0$). However, the dielectric constant of semiconducting SWNTs, which is on the scale of $5\varepsilon_0$, is much lower than that of aqueous media. Due to the large difference of dielectric constants between metallic and semiconducting SWNTs, effective sorting according to electronic type can be achieved with the application of a strong and inhomogeneous electrical field. In the presence of an alternating current electrical field, the force on SWNTs, generated by the interaction between the induced dipole moment and the electrical field, drives the metallic SWNTs towards the high field region while semiconducting SWNTs are driven oppositely towards the lower field region. When SWNTs are suspended in aqueous media, the electrophoretic response owing to the interaction of the charges on the SWNTs and the applied field is inevitably involved and will compete with the dielectrophoretic response. Nevertheless, besides the SWNTs'

intrinsic electronic properties, diameter and length are quite critical to this static charge effects, making it unsuitable for separation of metallic and semiconducting SWNTs.

Another effective technique for separation by SWNTs electronic type and diameter is anion exchange chromatography of DNA-wrapped SWNTs.[22] In this technique, SWNTs were strongly encapsulated with single stranded DNA and a stable SWNTs-DNA hybrid that can effectively assist in the dispersion of SWNTs in aqueous solution was formed. Due to the screening of the charge by met-SWNTs, (met-SWNTs)-DNA has less surface charge than its counterpart (sem-SWNTs)-DNA. To make use of the above mentioned difference for SWNT separation, ion exchange chromatography experiment is conducted. Experimental observation suggests that small diameter SWNTs ($d<1.2nm$) were encapsulated with priority as contrast to large diameter ones. With ion exchange chromatography technique, separation according to diameters and electronic types has been achieved from optical absorbance spectroscopy. Raman spectroscopy and PLE maps also confirm successful species enrichment based on electronic properties and diameters. Theoretical work has suggested that the hybrid's effective charge density, which is primarily determined by DNA helical pitch, is the major factor governing the ion exchange chromatography sorting process.

One fascinating approach which allows effectively enrichment of SWNTs according to their density was the density gradient ultracentrifugation (DGU) method.[26] In this approach, the well dispersed SWNTs were loaded carefully into an intentionally prepared medium with density gradient in the centrifuge tube. During ultracentrifugation, density gradient of the medium assists in the SWNTs sediment according to their corresponding densities so that they can reach the point of the medium with matched density. The

consequence is that the SWNTs will sort in the centrifuge tube according to their distinguished density, forming various layers. Provided that the dispersing surfactant is uniform in density for all loaded SWNTs solution, the SWNTs density will be determined exclusively by their diameters. A theoretical model describing the SWNTs motion during DGU has been developed.

For the above mentioned methods, *i.e.* ac dielectrophoresis, anion exchange chromatography of DNA-wrapped SWNTs and density gradient centrifugation method, the difficulty of scaling up limits their application.

As a promising alternative, chemical methods, on the other hand, are more easily scalable and thus more attractive separation techniques. There are two main strategies for the chemical methods, one is covalent functionalization of SWNTs and the other is noncovalent attachment of functional groups to the sidewall of the SWNTs. Generally, an increase of the curvature of the carbon framework leads to a more pronounced pyramidalization of the sp^2 hybridized carbon atoms and therefore an increased tendency to undergo addition reactions. The structure effect is evident in fullerene and can be extended to SWNTs.[231] In C70, for example, the bonds at the poles are much more reactive than those around the flatter equatorial region.[231] Efficient addition at the equator takes place only with very reactive species, such as arynes, carbenes, or halogens. Normally, SWNTs bear no caps at their poles, and consist instead of graphitic sidewalls, usually with defects.[231] Thus, there are no strongly curved regions that could serve as reactive targets for direct additions. As the typical diameter of a SWNT (1 ± 2nm) is larger than that of a fullerene, its relative reactivity is even less than that of the flat regions in fullerenes.[231] Further problems in reactions with SWNTs are their low

solubility or dispersability, and their occurrence in bundles. Therefore, functionalization of the sidewalls by covalent-bond formation will only be successful if a highly reactive reagent is used. Besides the above mentioned factors, reactivity of SWNTs is influenced by other factors associated with their unique 1-D tubular structures such as the electronic properties as well as the species chiralities. The reported selective covalent functionalization so far includes diazonium reagent, nitric and sulphuric acids, osmylation, ozonation, azomethine ylides, *etc*.

Under carefully controlled condition, selective attack of metallic SWNTs has been demonstrated with diazonium reagents.[28] The model employed to explain the selective behavior describes the diazonium reagent extracting electrons, giving out N_2 gas and forming stable covalent bond with the SWNTs sidewall. The availability of electrons near the Fermi level is assumed to be responsible for the preferential formation of charge transfer state between met-SWNTs and diazonium reagent, which finally results in the higher bond formation reactivity for met-SWNTs. However, chiral angle, chemical doping, *etc.* are also anticipated to the influence the reactivity. Although the chemistry shows good selectivity towards primarily met-SWNT, extraction of the functionalized met-SWNTs from the plain sem-SWNTs is still a challenge. In this circumstance, met-SWNTs have not been separated from Sem-SWNTs but have been functionalized chemically so that they are undetectable by optical spectroscopy. Nevertheless, the destruction of semiconducting SWNTs is unavoidable and the handling of the extremely explosive diazonium reagents exposes us to high hazard.

Upon treatment with nitric and sulphuric acids,[19] selective removal/destroy of metallic SWNTs with small diameters has also been achieved. Optical and Resonance

Raman spectra were employed in the characterization of the treated SWNTs and confirmed the selectivity. The selectivity is resulted from the selective adsorption of positively charged NO_2^+ on metallic SWNTs due to the higher availability of electron densities at the Fermi level in the metallic SWNTs. The diameter selectivity is ascribed to the higher strain associated with the higher curvature of smaller diameter SWNTs. However, because the reactivity of metallic SWNTs towards the acid mixtures decreases with increasing diameter, large diameter metallic SWNTs still exist after treatment. This makes the removal of the metallic SWNTs not complete. Moreover, smaller diameter semiconducting SWNTs show some reactivity towards the treatments, which may result in its lost in the end.

Another effective covalent functionalization which can effectively discriminate between metallic and semiconducting SWNTs is osmylation of SWNTs under UV irradiation.[232] In this reaction, the interaction of OsO_4 with SWNTs in Toluene with the assistance of UV irradiation shows greater reactivity toward metallic species with a large electron density near the Fermi level. As a result, the osmylation of metallic SWNTs disrupted the conjugated π electron structure with the osmium tetroxide species converted to OsO_2 nanoparticles, which are then attached onto the sidewall of the SWNTs. Resonance Raman Scattering spectra of the functionalized SWNTs samples at three different excitation wavelengths, which selectively probe different chiral species, confirmed higher preferentiality towards metallic SWNTs with osmylation reaction. The conclusive evidence arise from the dramatic loss of resonances at 514.5nm as contrast to the trivial modification observed with the spectra features from primarily semiconducting SWNTs probed with 1064nm laser.

Solution-phase ozonolysis[233] has been demonstrated to be effective for the separation of SWNTs according to their diameters and the diameter selectivity was confirmed by the Resonance Raman spectra of the treated SWNTs. The selectivity corroborated the above mentioned theoretical prediction of the effects of pyramidalization and π-orbital misalignment on SWNT reactivity.

Selective chemistry has been observed using azomethine ylides[29] as the functionalization reagents. Resonance Raman spectra and UV-Vis-NIR absorption spectra suggests that semiconducting SWNTs are preferentially functionalized, which is possibly induced when the starting N-oxides substrates (ylide precursors) are attached to the polycyclic aromatic substituent. With the polycyclic aromatic π-stack preferentially with the more aromatic semiconducting SWNTs, the selectivity of the covalent functionalization towards semiconducting SWNTs was finally resulted.

Besides preferential chemistry, selective removal/destroy of unwanted species has also been achieved with laser irradiation.[20] Upon laser irradiation in air, metallic SWNTs in SWNT film network can be preferentially destroyed as contrast to their semiconducting counterparts provided that the laser wavelength and irradiation power intensity are appropriate and the SWNTs in the network are not severely bundled. Different rates of photolysis-assisted oxidation of metallic SWNTs and semiconducting SWNTs is the driven force of the selective destroy. This method shows good promising for the preparation of semiconducting SWNTs enriched network for Field Effect Transistor (FET) application. However, it suffers from the low efficiency of selective destroy of laser irradiation.

The most obvious disadvantage associated with all above mentioned functionalization methods is the destruction and ultimate consumption of the desired species along with the destruction of the unwanted species due to the harsh condition involved. As contrast, non-covalent approaches are particularly attractive due to their ability of preserving nearly all of the SWNTs' intrinsic properties as well as the mild operation condition.[234-237] Normally, noncovalent attachment is controlled by thermodynamic criteria and it is called wrapping for some polymers.

Selectivity by electronic type has been extensively studied for non-covalent chemistries based on amines.[33,238] In particular, selective functionalization of metallic SWNTs has been achieved with propylamine and isopropylamine in THF. On the contrary, if the SWNTs are first oxidized in acidic solution, octadecylamine selectively interacts with semiconducting species.

Charge-transfer complex formation with metallic SWNTs has been demonstrated for bromine.[35] UV-Vis-NIR absorption spectra were used as the primary characterization technique to investigate the selectivity. The driving force of the selectivity is the chemical discrimination in the charge transfer complex formation between bromine and the metallic SWNTs *vs.* semiconducting SWNTs. The resulted density difference was used to effect a centrifugation based separation.

π-π stacking interaction has also been demonstrated to be effective for selective suspension of certain SWNT species. With the assistance of this kind of discriminatory interaction, porphine[36] and pyrene[44] has been verified to be selective towards semiconducting SWNTs. In order to facilitate the dispersion of SWNTs with the aromatic compounds, long functional groups were intentionally introduced. UV-Vis-NIR

absorption spectra and electrical conductivity measurements were the primary characterization techniques. The method relies on distinct molecular recognition properties of aromatic functional groups toward the carbon graphitic structure. The π-π stacking interaction is believed to be critical for the enrichment. However, increased dispersion is required for achieving better separation.

The adhesion of all these above mentioned small molecules is substantially facilitated by electrostatic interaction or weak linkage similar to hydrogen bond between SWNTs and adsorbents or intermolecular hydrogen bond. Selectivity towards certain species is presumably resulted from the distinguished thermodynamic pairing force of SWNTs/adsorbent for different SWNTs species. It can be anticipated that other forms of the weak interaction such as electrostatic interaction, Van der Waals interaction and π-π stacking interaction may also contribute to the SWNTs/adsorbent pairing force and modify the dispersants' selectivity behavior.

In fact, another kind of weak interaction, *i.e.*, hydrogen bond has also been successfully employed in the selective suspension of certain SWNT species. With flavin mononucleotide as the dispersion agents,[38] selective wrapping of the molecules in a helical pattern around SWNTs has been observed. With the aid of intermolecular hydrogen bond, a helical ribbon between adjacent flavin mononucleotide was formed. In the presence of concentric π-π stacking interaction between flavin mononucleotide and the SWNT sidewall as well as the intermolecular hydrogen bond, prominent species selectivity was verified by photoluminescence maps as well as UV-Vis-NIR absorption spectra of SWNTs. The selectivity is possibly resulted from the dependence of strength of helical flavin mononucleotide assembly on the SWNT chirality. The selectivity was

verified by computer simulation. With the introduction of another surfactant SDBS, the flavin mononucleotide assembly is disrupted and replaced. The strong affinity of flavin mononucleotide towards (8,6) species resulted in a 85% chirality enrichment from a SWNT sample with broad diameter distribution.

Interestingly, upon laser irradiation, Triton X-100[37] has been reported to be highly selective towards small diameter SWNTs. The preferential chemical interaction can be induced by laser with power density down to $10^{-2}\mu W/\mu m^2$ as long as the photon energies match the energies corresponding to the interband transition of SWNT species. Resonance Raman spectra was used to probe the diameter distribution of the treated SWNTs because of the direct relationship between the Raman shift of the spectral features and the SWNT diameters.

Attachment of all the reported small molecules such as octadecylamine, bromine and flavin mononucleotide has been demonstrated to be effective in assisting SWNTs enrichment but these methods still achieve limited selectivity.

Another kind of chemical structures which have promising potential for the selective suspension of SWNT species is conjugated polymers. For example, depending on their chemical structures, fluorene-based polymers[48] selectively suspend SWNT species with certain chiral angles and diameters. Poly(9,9-dioctylfluorenyl-2,7-yl) and poly[(9,9-dihexylfluorenyl-2,7-diyl)-co-(9,10-anthracene)] selectively suspend SWNT species with large chiral angles while poly[(9,9-dioctylfluorenyl-2,7-diyl)-co-(1,4-benzo-{2,1',3}-thiadiazole)] preferentially wraps SWNTs with specific diameter(1.02-1.06nm). Starting with narrow diameter distributed SWNTs (Co-MCM-41), high purity of (7,5) species (up to 79%) can be obtained by polymer assisted extraction.

A more comprehensive study of selectively suspension of SWNT species by conjugated polymers was published in 2007 by Nish, etc.[46] Obvious evidence of good suspension and high selectivity was suggested by optical absorbance and Photoluminescence excitation maps. Up to ~60% relative concentration of a single species of isolated tubes was claimed. Depending on the structures of polymers,[47] distinct species in terms of chiral angles and diameters were selectively suspended. Computer simulation suggests that ordered molecular structures were formed by the rigid-backbone structures, wrapping around the SWNTs with n-fold symmetry determined by the SWNT diameters. In a following report, solvent effects on the selectivity were systematically investigated. The results indicated that highest selectivity can be observed when toluene was used as the solvent while chloroform is effective in enhancing the SWNT overall solubility.

As in the case of aromatic small compounds, the π-π stacking interaction is also believed to be critical for the enrichment. Nevertheless, the notorious strong π-π interaction is highly unfavorable with respect to the post-separation removal of the polymer.

Another interesting enrichment strategy is enrichment of SWNTs based on their helicity. With the employment of chiral 'gabletype' diporphyrin molecules,[239-240] left- and right-handed helical SWNTs were prepared by preferential extraction. This approach is worth pointing out since it is the only strategy that was developed aiming at preparation of optically active SWNTs instead of the normally developed separation techniques based on SWNT electronic properties and diameters. The driven forces are the different affinities of the diporphyrin molecules towards left- and right-handed helical SWNT

isomers to form complexes with unequal stabilities. As in the case of aromatic small compounds, the π-π stacking interaction is also believed to be critical for the enrichment. Nevertheless, the application of the enriched optically active SWNTs is still rare.

2.5.2 Resonance energy transfer

Radiative energy transfer

Radiative energy transfer is a two-step process:[241] a photon emitted by a donor D is absorbed by an acceptor that is chemically different (A) or identical (D) This process is often called trivial transfer because of the simplicity of the phenomenon, but in reality the quantitative description is quite complicated because it depends on the size of the sample and its configuration with respect to excitation and observation. Radiative transfer results in a decrease of the donor fluorescence intensity in the region of spectral overlap.[241]

non-radiative energy transfer

Non-radiative transfer of excitation energy requires some interaction between a donor molecule and an acceptor molecule, and it can occur if the emission spectrum of the donor overlaps the absorption spectrum of the acceptor, so that several vibronic transitions in the donor have practically the same energy as the corresponding transitions in the acceptor.[241] Such transitions are coupled, i.e. are in resonance. The term resonance energy transfer (RET) is often used. In some papers, the acronym FRET is used, denoting fluorescence resonance energy transfer, but this expression is incorrect because it is not the fluorescence that is transferred but the electronic energy of the donor.[241] Energy transfer can result from different interaction mechanisms.[241] The interactions may be Coulombic and/or due to intermolecular orbital overlap.[241] The Coulombic interactions consist of long-range dipole–dipole interactions (Förster'smechanism) and short-range

multi-polar interactions.[241] The interactions due to intermolecular orbital overlap, which include electron exchange (Dexter's mechanism) and charge resonance interactions, are of course only short range.[241]

Chapter 3 Materials and Methods

3.1 Materials

The reagents, 1-pyreneacetic acid (97%, brown solid), 1-pyrenebutyric acid (99.5%, brown solid), 1-pyrenecarboxylic acid (99%, brown solid), thionyl chloride (99%, colorless liquid), 2-(aminomethyl)-18-Crown-6 (99.9%, colorless liquid) and pyridine (99%, colorless liquid) were supplied by Sigma-Aldrich and used as received. The polymers poly(benzyl methacrylate) (PBMA) (white solid) and poly(methylmethacrylate)-co-(9-anthracenylmethyl acrylate) (PMMA-c-PAMA) (yellow solid), poly(2-Naphthylmethacrylate) (PNMA) (yellow solid), poly(9-anthracenylmethyl methacrylate) (PAMMA) (yellow solid) and poly(methylmethacrylate-*co*-fluorescein-*o*-acrylate) (PMMAFA) (yellow solid), as well as sodium dodecylbenzenesulfonic acid (SDBS) (99.9%, white powder) were obtained from Aldrich and were used as received. The synthesis and characterization of the polymers poly[(2,7-pyrenyl)-*co*-2,2'-[5,5'-bis(3-dodecylthiophenyl)]] (PPyrBT) and poly[2,7-(9,9-didodecylfluorenyl)-*alt*-(2,7-pyrenyl)] (PFluPyr) has been reported elsewhere.[242] Solvents dichloromethane (98%), acetonitrile (99%), chloroform (99.5%), Tetrahydrofuran(THF) (99.9%), N,N-dimethylformamide (DMF) (99%), toluene (99.5%) and deuterium oxide (D_2O) (99.5%), were purchased from Sino Chemical Company Pte Ltd and used without further purification unless otherwise specified. As-grown HiPco (super pure grade) SWNTs used are the nanotubes purchased from Carbon Nanotechnologies Inc. (CNI). CoMoCAT SWNTs were purchased from SouthWest Nanotechnologies, Inc. and were used as received.

3.2 Experimental Section

Separation with surfactants.

Suspending of specific amount of SWNTs in surfactant solution (with different SWNTs/surfactant ratio for different surfactants) was followed by sonication for different periods of time (10, 15&60 minutes) at distinct sonication power intensities (100W&175W) depending on the surfactant used. Centrifugation was then conducted (immediately or after 2 weeks standing) to removed the bundled SWNTs. Both the supernatant solution and precipitated solid were collected for further characterization.

3. 3 Characterization Methods

^{1}H NMR spectra were recorded on a Bruker ACF 300 FT-NMR spectrometer operating at 300 MHz. Deuterated chloroform was used as the solvent and tetramethylsilane (TMS) was used as the internal standard.

FT-IR absorption spectra were acquired with a Nicolet 5700 FT-IR instrument. Infrared spectroscopy gives much less information about the vibrational properties of SWNTs compared to Raman spectroscopy, mostly due to the strong absorption of SWNTs in the IR range. In this study, FT-IR absorption spectra were used to characterize the pyrene derivatives on the sidewall of SWNTs.

Raman spectra from all the samples were measured with a Renishaw Ramanscope in the backscattering configuration under the same experimental conditions (except for differing laser excitation wavelengths). Stokes spectra of all the HiPco samples were obtained with 514.5 nm (2.41 eV), 633nm (1.96 eV) and 785nm (1.58eV) lasers while Stokes spectra of CoMoCAT SWNTs were obtained with 633nm (1.96 eV) laser.

Absorption and photoluminescence spectra of polymer solutions were obtained with a Shimadzu UV-1601 PC UV-vis spectrophotometer and an AMINCO BOWMAN II luminescence spectrometer respectively. For the characterization of polymer solution with UV-Vis and photoluminescence measurements, dilute polymer solution (1×10^{-5} M) was prepared in anhydrous spectrum-grade THF.

For UV-Vis-NIR characterization, polymer solution was normally used as reference for background subtraction in supernatant scans while for the precipitates, no background subtraction was conducted during the data collection because polymer absorption features were strongly suppressed by the toluene washing. Some spectra have been magnified for comparison; this has no effect on the content ratio of different species. Some spectra exhibit a sharp edge at almost exactly 800nm due to the change of the detector during data collection. Due to the change of detector during data collection, a sharp edge at almost exactly 800nm can be observed in some of the spectra.

UV-Vis-NIR spectra of the SWNT solutions were recorded on a Cary 5000 UV-Vis-NIR spectrophotometer.

Photoluminescence excitation (PLE) measurements of the supernatant SWNTs suspended in the polymer solution as well as the precipitates, resuspended in SDBS, were performed on a Jobin-Yvon Nanolog-3 spectrofluorometer with an InGaAs detector.

The current-voltage (I-V) characteristics of the SWNTs networks were measured using an Agilent 4157B Semiconductor Parameter Analyzer System. SWNT network conductivity (σ) was estimated from the I-V behavior in the low current-low bias linear regime. The effects of air exposure on the conductivity of the SWNTs network, which was fabricated by depositing some chloroform solution of SWNTs between the two

electrodes, were investigated by the measurement of the conductivity as a function of time when heated in the air at 200ºC.

Back-gated SWNT-FETs were fabricated on heavily doped p-type silicon wafers capped with 300nm thermally grown silicon dioxide layers. Source and drain electrodes were photolithographically patterned in a 60nm layer of Au on a 10 nm layer of Ti. The channel length and width were 20μm and 100μm respectively. All electrical measurements were carried out in ambient conditions using a Keithley semiconductor parameter analyzer Model 4200-SCS.

Atomic Force Microscope (AFM) measurements were performed on a MFP3D microscope (Asylum Research, Santa Barbara, CA) with a cantilever (Arrow NC, Nanoworld) in tapping mode. Scan rate was set to be 1 Hz at various scan sizes.

Chapter 4 Species enrichment of SWNTs with pyrene alkylamide derivatives: is the alkyl chain length important?

4.1 Introduction

In this chapter, we show that amide-functionalized pyrene derivatives can preferentially suspend *met*-SWNTs with specific diameters based on non-covalent interaction. Three pyrene derivatives with different lengths of alkyl groups between the amide groups and pyrene moieties (Figure 4.1) have been successfully synthesized[243]. The three pyrene derivatives, N-methyl(18-Crown-6)pyrene-1-acetamide, N-methyl(18-Crown-6)pyrene-1-butyramide and N-methyl(18-Crown-6)pyrene-1-formamide, employed in this work are hereafter referred to as pa-18-C-6, pb-18-C-6 and pc-18-C-6 respectively, for convenience sake, corresponding to the starting material of 1-pyreneacetic acid, 1-pyrenebutyric acid and 1-pyrenecarboxylic acid. For all the three pyrene derivatives, the SWNTs in the supernatant solution as well as the precipitated solid were characterized by Raman spectroscopy using 514.5nm, 633nm and 785nm lasers. UV-Vis-NIR spectroscopy and current-voltage measurement of precipitated solids after four-pass separation using pc- 18-C-6 and pa-18-C-6 alternately were also conducted. Fourier-Transform Infra Red Spectroscopy (FTIR) was used to confirm the structural rearrangement of pa-18-C-6.

4.2 Experimental section

4.2.1 Synthesis of pyrene derivatives

Three amide-substituted pyrene derivatives were synthesized by reaction of 1-pyreneacetic acid, 1-pyrenebutyric acid or 1-pyrenecarboxylic acid and thionyl chloride

followed by further reaction with 2-(aminomethyl)-18-Crown-6. Their chemical structures were confirmed with ^{1}H NMR spectroscopy.[243] The representative synthetic strategy is outlined in Figure 4.1.

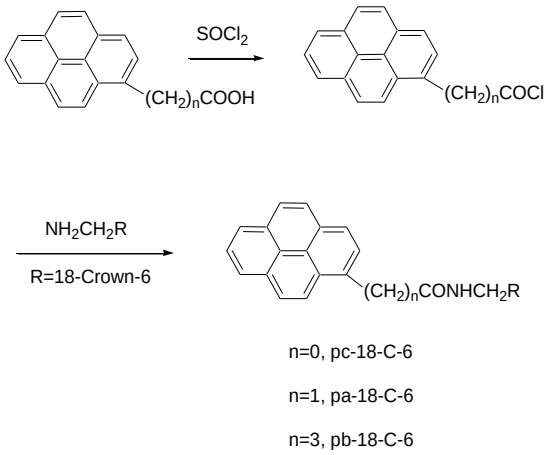

Figure 4. 1 Synthetic approach to pyrene derivatives. N-methyl(18-Crown-6)pyrene-1-acetamide, N-methyl(18-Crown-6)pyrene-1-butyramide and N-methyl(18-Crown-6)pyrene-1-formamide are referred to as pa-18-C-6, pb-18-C-6 and pc-18-C-6 respectively.

The detailed synthetic procedure with 1-pyrenecarboxylic acid as the starting material is as follows: 0.1023g 1-pyrenecarboxylic acid (0.415mmol) was added to about 20ml thionyl chloride and the reaction mixture was refluxed overnight before the excess thionyl chloride was removed by distillation. The remaining solid was dissolved in newly dried dichloromethane(DCM) and 0.1230g 2-(aminomethyl)-18-Crown-6 (0.42mmol) was added to the mixture. 0.05ml of pyridine was added and the solution mixture was refluxed for 48h under the protection of argon.

4.3 Results and Discussion

To confirm the enrichment of *sem*- and/or *met*-SWNTs in separated samples, Resonant Raman Spectroscopy[244] was used since the allowed optical transition energies depend on tube diameter and type (*i.e.* electronic property) and consequently differ for *met*- and *sem*-SWNTs. Different lasers bring different SWNTs, depending on types (*met*-

/*sem*-) and diameters, into resonant scattering since the energy of interband electronic transition depends on these two parameters.[245-246] The HiPco nanotubes have been reported to have diameters ranging from 0.8 to 1.3nm. According to the Kataura plot,[106,247-248] excitation at 514.5nm probes primarily larger diameter (D>1.08nm) *sem*-SWNTs and smaller diameter (D<1.03nm) *met*-SWNTs. Excitation at 633nm selectively probes smaller diameter (D<0.94nm) *sem*-SWNTs and larger diameter (D>1nm) *met*-SWNTs. However, RRS signal of HiPco SWNTs with 785nm excitation mainly come from *sem*-SWNTs.[106,247-248]

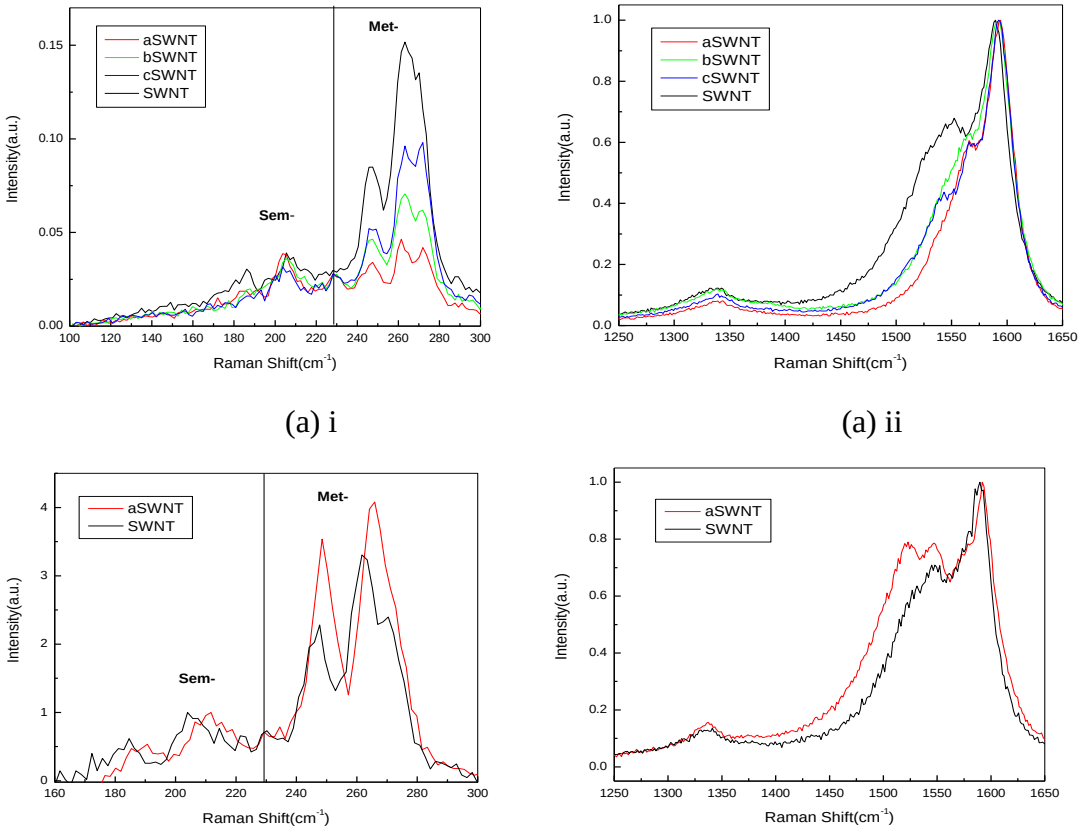

Figure 4. 2 Raman Resonant Scattering spectra using 514.5 nm laser of the (a) precipitated solids and (b) SWNTs in the supernatant solution (in chloroform), with different separation agents. (i) the RBM section (data not normalized for a(i) due to its obvious difference) (ii) the G and D bands (data normalized with G^+ band reference).

Fig 4.2 shows the enlarged radial breathing mode (RBM) and tangential mode (G mode) portions of the Resonant Raman Scattering (RRS) spectra[244-246] using 514.5nm laser. The spectra of the precipitated solids and supernatant are shown in Figures 4.2(a) and 4.2(b) respectively. The spectrum of as-received HiPco SWNTs is also included for comparison. In the RBM spectra (Figures 4.2(a)i and 4.2(b)i), the Raman peaks of *sem*- and *met*-SWNTs are clearly separated in wavenumber. The peaks with wavenumbers between 160 and 230cm^{-1} are due to *sem*-SWNTs while those between 230 and 300cm^{-1} are due to *met*-SWNTs. For the precipitated solid, the decrease of the RBM peak intensities of *met*-SWNTs for all the three pyrene derivatives indicates that these pyrene derivatives selectively suspend *met*-SWNTs in the supernatant. The separation efficiencies are in the increasing order of pc-18-C-6, pb-18-C-6 and pa-18-C-6, with pa-18-C-16 most effectively suspending *met*-SWNTs (of relatively small diameter with 514.5nm laser). The conclusion is corroborated by the G mode shapes (Fig. 4.2(a)ii),[249-250] whereby sharp G^- peak (at approximately 1567 cm^{-1}) indicates *sem*-SWNTs while the broad G^- peak with a shoulder at ca. 1530 cm^{-1} indicates *met*-SWNTs. The G band is most broad and unsymmetrical in the case of pc-18-C-6, confirming it results in the highest *met*-SWNTs content in the precipitate. Hence, from the 514.5 nm G band of the precipitate, we can confirm the separation efficiency in the increasing order of pc-18-C-6, pb-18-C-6 and pa-18-C-6.

Figure 4.2(b) shows the RRS spectrum of the supernatant solution with incident excitation wavelength of 514.5nm. Only the spectrum of the pa-18-C-6 sample was well resolved; the enlarged RBM and G modes are shown in Figures 4.2(b)i and ii. The RBM peak intensities in the 230 cm^{-1} to 300 cm^{-1} region of the pa-18-C-6 spectra indicate that

the metallic content in the supernatant solution is enriched with respect to the as-received SWNTs. The more broad and unsymmetrical G band with increasing G^- feature with pa-18-C-6 corroborates this conclusion. Under 514.5nm excitation, the observed Raman peaks of SWNTs suspended in solution with pb-18-C-6 and pc-18-C-6 were not well-resolved. The absence of nanotube peaks with pb-18-C-6 and pc-18-C-6 is due to the mismatch of the resonance energies of these suspended nanotube species to the laser excitation energy.

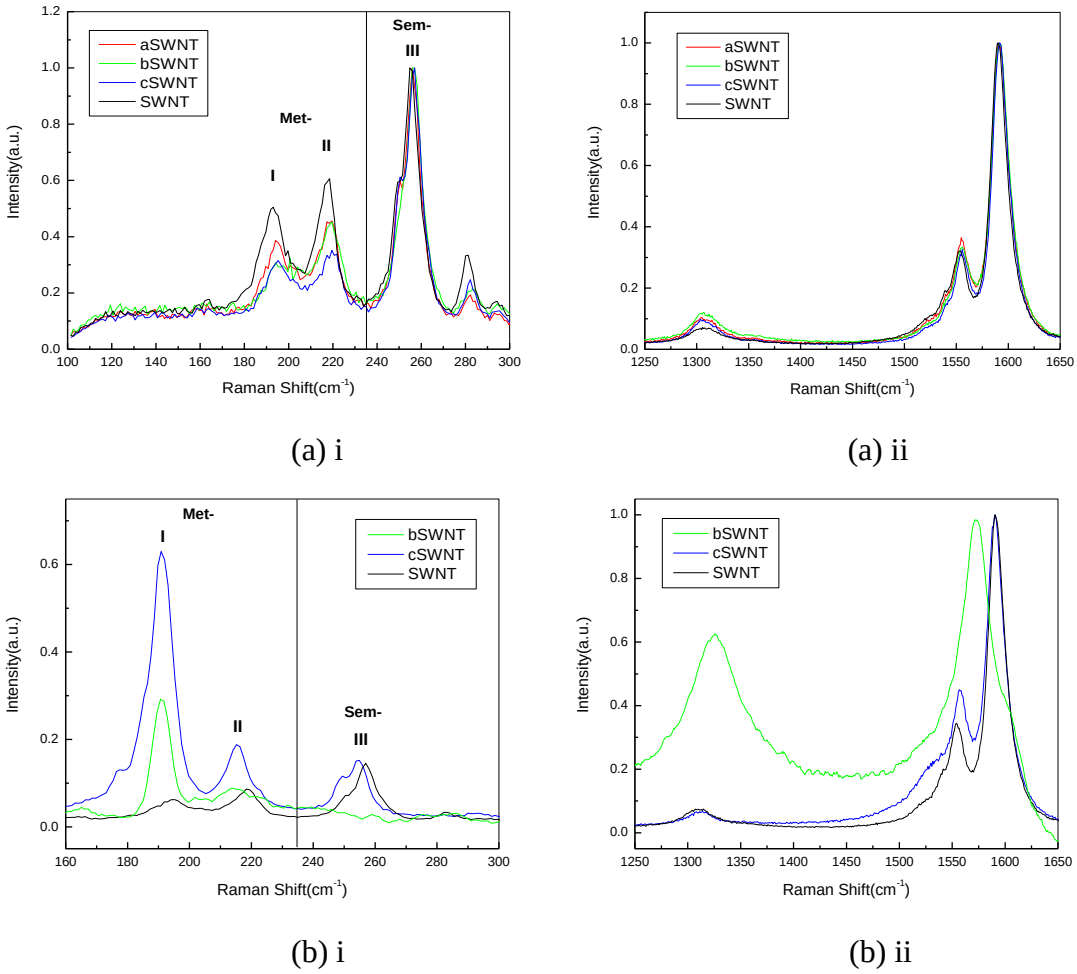

Figure 4. 3 With 633 nm laser, the Raman spectra of (a) precipitated solids and (b) SWNTs in the supernatant solution (in chloroform). (a)i RBM section of the precipitated solid (data normalized with Peak III reference), (a)ii the G and D bands of the precipitated solids (data normalized with G^+ band reference), (b)i the RBM section of the SWNTs in the supernatant solution with separation agent pb-18-C-6 and pc-18-C-6 (data not normalized), (b)ii the G and D bands of the

SWNTs in the supernatant solution with separation agent pb-18-C-6 and pc-18-C-6 (data normalized with G^+ band reference).

With 633nm excitation, according to Kataura plot[106,247-248], the RBM peaks located below 235cm^{-1} are due to *met*-SWNTs while those above 235cm^{-1} are due to semiconducting ones (Figures 4.3(a)i and (b)i). The spectra of Figure 4.3(a)i are normalized for comparison purposes with respect to the peaks located at approximately 256cm^{-1}. As in the 514.5nm excitation spectra, the decrease of the RBM peak intensities of *met*-SWNTs in the precipitate (Fig. 4.3(a)i) indicates that these pyrene derivatives selectively suspend *met*-SWNTs in the supernatant; the concentration of *met*-SWNT in the precipitate is the lowest for pc-18-C-6 and highest for pa-18-C-6. The separation efficacy implied by the relative intensities of *met*-SWNTs RBM peaks (150-235cm^{-1}) in Fig 4.3(a)i is in the increasing order of pa-18-C-6, pb-18-C-6, pc-18-C-6 which should be of relatively large diameter to be detectable by the 633 nm laser. This order is exactly opposite to that implied by the Raman spectra with 514.5 nm excitation.

Also with 633nm laser, the RBM and G mode spectra of the SWNTs in the supernatant solutions using pb-18-C-6 and pc-18-C-6 are well resolved and are shown in Figures 4.3(b)i and 4.3(b)ii. For pb-18-C-6, the RBM peaks above 235cm^{-1} are entirely absent (Fig. 4.3(b)i), indicating that almost all of the SWNTs in the supernatant solution are *met*-SWNTs. This conclusion is corroborated by the G band shape, in which the G^- band is even stronger than the G^+ band (Fig. 4.3(b)ii). However, whether or not the high intensity of the D band peak of this spectrum is related to the extremely high metallic content of this sample is not clear at this moment. Similarly, for pc-18-C-6, the relative intensities of RBM peaks indicate that the metallic content in the supernatant solution is

dramatically increased as compared with the as-received SWNTs; the broader G^- band corroborates with this.

Under 633nm excitation, the SWNTs in the supernatant solution using pa-18-C-6 are barely excitable (*i.e.* inactive) (Figure 4.3(b)i). The separation efficacy detectable by 633nm laser is in the increasing order of pb-18-C-6 and then pc-18-C-6 and pa-18-C-6 is undetectable. Under 514.5nm excitation, on the other hand, the SWNTs in the supernatant using pb-18-C-6 and pc-18-C-6 are inactive (Figure 4.2(b)i). However, Fig. 4.3(b)i and 4.2(b)i together show that the supernatants contain *met*-SWNTs for all three surfactants. The discrepancy between the trends using 633nm and 514.5nm lasers is presumably due to different diameter nanotubes which have RBM modes excitable with different laser energies and different suspension efficacy with various pyrene derivatives. (Resonance occurs when the interband electronic transition of the SWNT is typically within ± 0.1 eV of the laser excitation energy.) With pb-18-C-6 and pc-18-C-6, larger diameter *met*-SWNTs which resonates with 633nm laser are selectively suspended in the supernatant solution (Figure 4.3(b)i); with the same surfactants, the inertness of these suspended SWNTs to 514.5nm laser excitation (Figure 4.1(b)i) may then be attributed to the inability of this laser to probe *met*-SWNTs with larger diameter. (The mismatch between the energy of 514.5nm excitation radiation and the energy associated with interband electronic transition of large diameter *met*-SWNTs results in the suspended SWNTs inactiveness to 514.5 nm laser for these two surfactants.) With separation agent pa-18-C-6, small diameter *met*-SWNTs are suspended and these can be detected with 514.5 nm laser (Figure 4.2(a)i); using the same surfactant, the inertness of the suspended small diameter *met*-SWNTs to 633nm laser can be attributed to the fact that the energies

associated with the interband electronic transition are shifted out of the resonance window of the laser.

From the RRS results with excitation of 514.5nm and 633nm, we conclude that all three pyrene derivatives are metallic-selective. pa-18-C-6 has stronger selectivity towards smaller diameter *met*-SWNTs while pb-18-C-6 and pc-18-C-6 are highly selective towards larger diameter *met*-SWNTs. The Raman results of the supernatant and precipitate reinforce each other. For example, in Fig. 4.3, the preferentiality of highly effective pc-18-c-6 for the largest diameter *met*-SWNTs results in its highest enrichment in the supernatant solution (peak *I* in Fig. 4.3(b)i) and the sharpest decrease of the peak *I* intensity in the precipitated solid (Fig. 4.3(a)i).

With both pc-18-C-6 and pb-18-C-6 surfactants, the metallic RBM peak increase is larger for the peak with lower wavenumber at around 190 cm^{-1} (peak *I* in Figure 4.3(b)i). The relation between the RBM frequency and the nanotube diameter[103] is $\omega_{RBM}(cm^{-1})=C_1/d_t+C2$ (C_1=223.5 and C_2=12.5 for HiPco SWNTs) where ω is the Raman shift of the RBM of SWNTs and d_t is its diameter in nanometers. Hence, the smaller wavenumber peak (*I*) corresponds to large diameter (~1.3 nm) nanotubes whilst peak *II* corresponds to smaller diameter (~1.1 nm) nanotubes. This suggests that the degree of interaction between both of these surfactants and SWNTs is proportional to the diameter of the *met*-SWNTs. Also in Fig. 4.3b(i), for pc-18-C-6 with higher *met*-SWNT suspendability, the three RBM peaks (*I*, *II* and *III*) persist but with pb-18-C-6, peak *III* totally disappear and the intensity ratio of peak *I* to that of peak *II* increases. Hence, pc-18-c-6 which has higher suspending power for large *met*-SWNTs has lower differentiating ability between the various diameters. The higher discriminating capability

associated with the relative weaker separation agent pb-18-C-6 results in higher intensity of the peak located at 216 cm^{-1} (peak *II* in Fig. 4.3(a)i) in the precipitate as compared with pc-18-C-6, which is also consistent with the spectra obtained for the SWNTs in the supernatant solution (Fig. 4.3(b)i).

Also, the more the surfactant is consumed on larger diameter *met*-SWNTs, the less is left for attachment to other smaller-diameter SWNTs since the feed ratio of the surfactants and SWNTs is controlled to be the same for all the three surfactants. This is confirmed by the Raman results using the two excitation wavelengths. With the separation agent pb-18-C-6, as compared to pc-18-C-6, there is less consumption by the larger diameter *met*-SWNTs (Fig. 4.3(b)i) so that there is more free compounds left in the supernatant for suspending the smaller diameter *met*-SWNTs causing the higher peak intensity drop of the smaller diameter *met*-SWNTs probed with excitation of 514nm (Fig. 4.2(a)i).

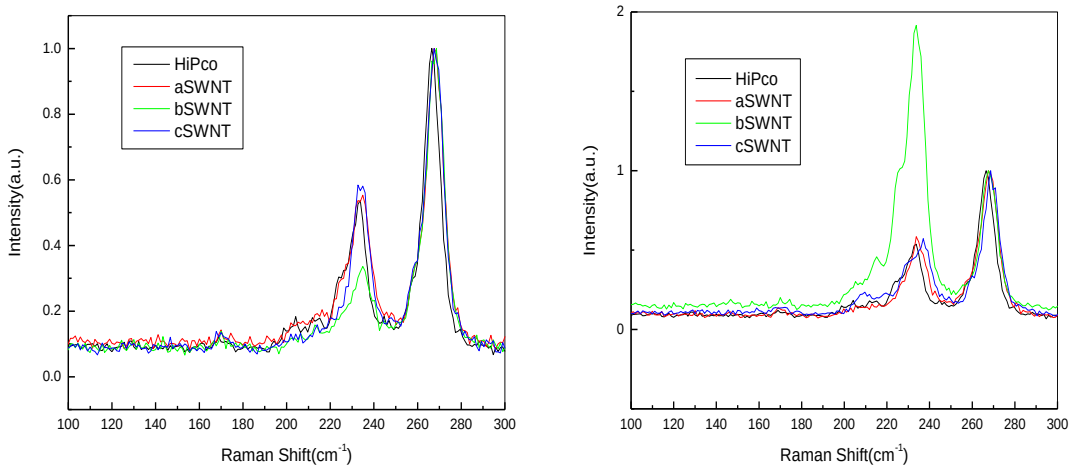

Figure 4. 4 With 785 nm laser, the Raman spectra (RBM section) of (a) precipitated solids and (b) SWNTs in the supernatant solution (data normalized with Peak at ~267cm^{-1} reference).

Fig. 4.4 shows the enlarged radial breathing mode (RBM) (tangential mode (G mode) not included because no difference can be observed) portions of the Resonant Raman Scattering (RRS) spectra using 785nm laser. The spectrum of as-received HiPco SWNTs is also included for comparison. According to Kataura plot, 785nm laser mainly probes semiconducting HiPco SWNTs with relative large diameter (D>0.9nm). It can be conveniently concluded from the spectra that pb-18-C-6 is selective to large diameter (low RBM Raman frequency) semiconducting SWNTs while pa-18-C-6 and pc-18-C-6 show no discrimination between different semiconducting species. The large diameter selectivity of pb-18-C-6 is possibly due to its longer functional group, which will facilitate the wrapping of large diameter SWNTs.

There is no contraction between the conclusions we have made based on the Raman spectra with different lasers since different lasers will selectively probe different SWNTs species, depending on the energy difference between the laser energy and interband transition energies E_{ii} of certain species. There is almost no overlap between the species chiralities which will be resonantly probed by different lasers.

To demonstrate the effectiveness of our proposed molecules for the separation of SWNTs with respect to their electronic properties (*i.e.* metallic or semiconducting), UV-Vis-NIR spectra and Current-Voltage (I-V) curves of the SWNTs in the supernatant solution and the precipitated solids were obtained. In the sample preparation, pa-18-C-6 and pc-18-C-6 were used alternately for the *met*-/*sem*- nanotube separation as pa-18-C-6 is more effective in suspending smaller diameter metallic SWNTs while pc-18-C-6 is more selective to larger diameter metallic SWNTs. In each round, the supernatant solution was removed and the precipitated residue was collected for further separation.

Both these two surfactants were used twice in the sequence of pa-18-C-6, pc-18-C-6, pa-18-C-6 and pc-18-C-6. The final residue was collected for UV-Vis-NIR spectral characterization and electrical measurement. The supernatant solutions were combined and the SWNTs from the supernatant solution were also employed in the UV-Vis-NIR characterization.

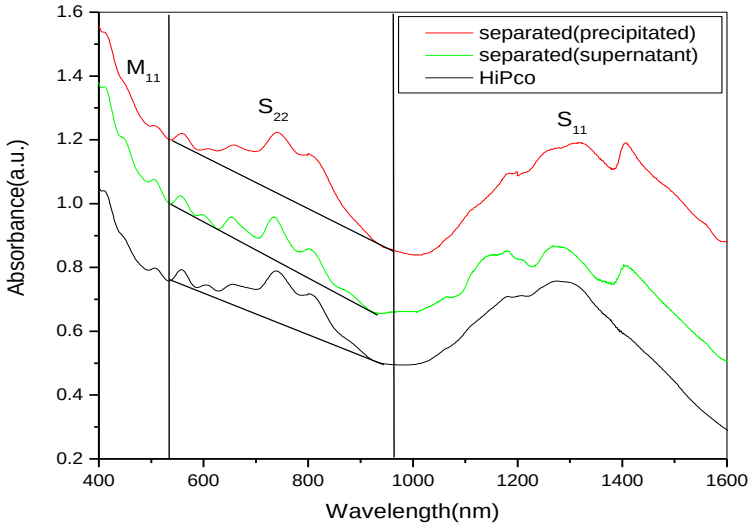

Figure 4. 5 UV-Vis-NIR spectra of the separated and as-received HiPco SWNTs.

The UV-Vis-NIR absorption[143] spectrum of the as-received HiPco SWNTs was also obtained as a reference. In our spectra (Fig. 4.5), the peaks appearing at 400-540 nm can be assigned to the M_{11} peak while those appearing at 540-1010 nm and 1010-1500 nm can be assigned to S_{22} and S_{11} respectively. The ratio of the absorption intensities of M_{11} and S_{22} was used as the indicator of the content ratio of *met*-SWNTs and *sem*-SWNTs because the S_{11} intensity is most susceptible to environmental perturbation. The intensity ratio of M_{11}/S_{22} (especially the obvious suppression of the intensity of the peaks from *met*- SWNTs at ~500nm) confirms that *met*-SWNTs are enriched in the supernatant solution (the M_{11} intensities is comparable while the enclosed area of the S_{22} from the

supernatant solution is much smaller than that of the as-received HiPco SWNTs) while *sem*-SWNTs are enriched in the precipitates, resulting from the multi-stage separation process.

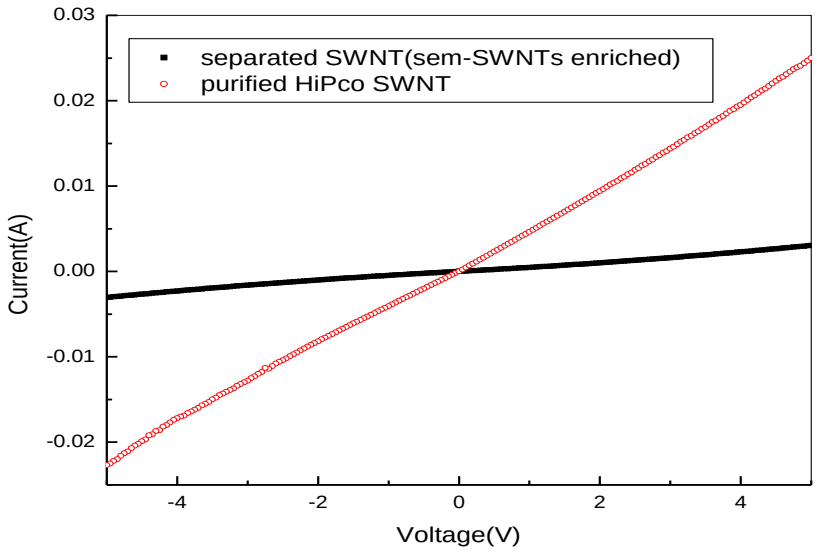

Figure 4. 6 Current-Voltage characteristic of SWNTs thin films.

The I-V characteristics were recorded by applying a voltage across thin films of SWNTs deposited from a chloroform solution. The thickness of the electrodes, the distance between the two electrodes and the overlapping length of the two electrodes were 60nm, 5μm and 9mm respectively. The I-V curves (Fig. 4.6) indicate that the conductivity decreased by a factor of 10 after separation. The conductivities of the network made from the as-received HiPco SWNTs and the *sem*-SWNTs enriched sample were 43 $S \cdot m^{-1}$ and 4.3 $S \cdot m^{-1}$ respectively. The area density of SWNTs, which is critical to the I-V characteristics of a network-type SWNTs film, has been confirmed to be comparable by the AFM images, in which almost the same coverage and thickness of the SWNTs networks made with separated/unseparated HiPco SWNTs can be seen. The decrease of the conductivity, which is a direct consequence of the enrichment of *sem*-

SWNTs in the precipitated sample, confirms the *met*-SWNTs selectivity of our synthesized compounds.

Further evidence of our pyrene electronic property selectivity comes from the stability of the network film conductivity with oxidation.[251] The extremely stable conductivity of *met*-SWNTs results from their constant electronic density of states near the Fermi level. In the case of a mixture of *met*- and *sem*-SWNTs, the existence of *sem*-SWNTs in the films makes the sheet resistance more sensitive to the adsorption of molecules mainly due to carrier doping.

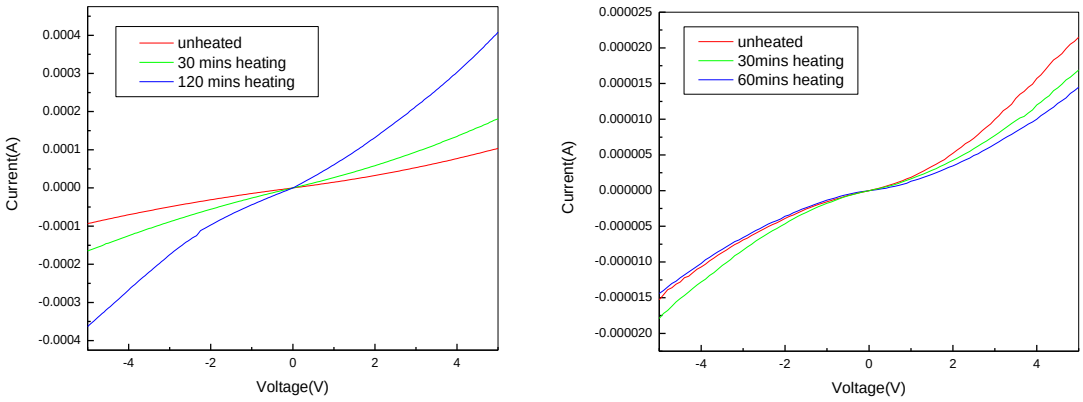

(a) (b)

Figure 4. 7 Response of conductive behavior of SWNT networks towards heating in air at temperature: 200℃ (a) precipitate (b) supernatant.

As shown in Figure 4.7, when heated in air at 200℃, the SWNTs in the precipitate show a rapid decrease in resistance and the resistance decrease continued for 120mins. The final resistance was 33% of the initial value at the voltage value of -1.0V. On the other hand, the resistance of the SWNTs in the supernatant solution was very stable and the variation was about 10% of the initial value at the voltage value of -1.0V and the resistance decrease reached its maximum in less than 60mins.

From the above discussion, we can conclude that all three pyrene derivatives are selective to *met*-SWNTs. Moreover, pa-18-C-6 is selective to smaller diameter *met*-SWNTs while other two are selective to larger diameter *met*-SWNTs. Strain force relaxation has been reported with smaller-diameter nanotube selectivity.[252] and we postulate that some kind of surface bond formation leading to strain force relaxation is involved in the pa-18-C-6 selectivity. We propose the structural rearrangement shown in Figure 4.8 and FTIR substantiates this selectivity mechanism.

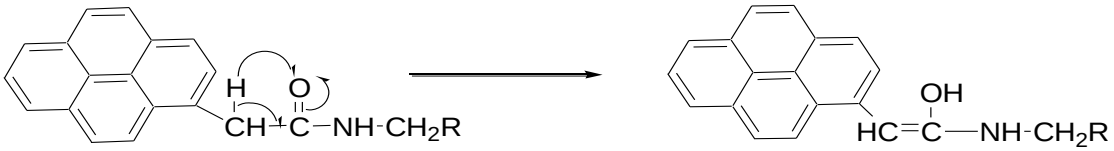

Figure 4. 8 Structural rearrangement of pa-18-C-6 in the presence of small diameter met-SWNTs.

In the ketone-to-enol rearrangement process, the SWNTs functions as a template and the resulting active -CH=C-OH group of pa-18-C-6 can be stabilized by adsorption on the sidewall of the smaller diameter *met*-SWNTs, whose strain force can also be partly released by weak surface bond formation. It seems that the direct attachment of the methylene group, which is involved in the rearrangement, to the pyrene moiety is beneficial for the rearrangement since the more delocalized conjugation can stabilize the resulting enol to some extent. Sonication and the warming up of the solvent during sonication may provide the energy necessary for the rearrangement. FT-IR spectra were obtained to confirm the proposed structural rearrangement.

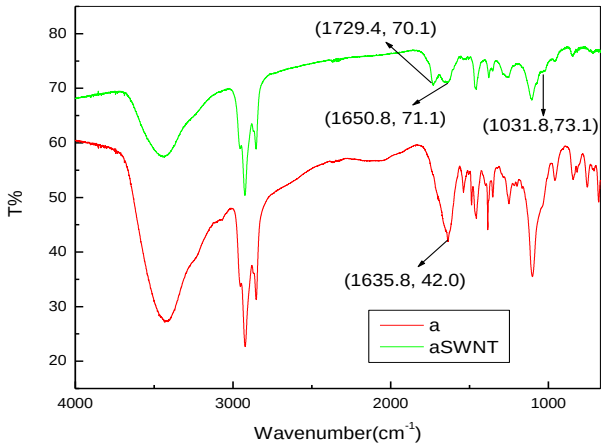

(a)

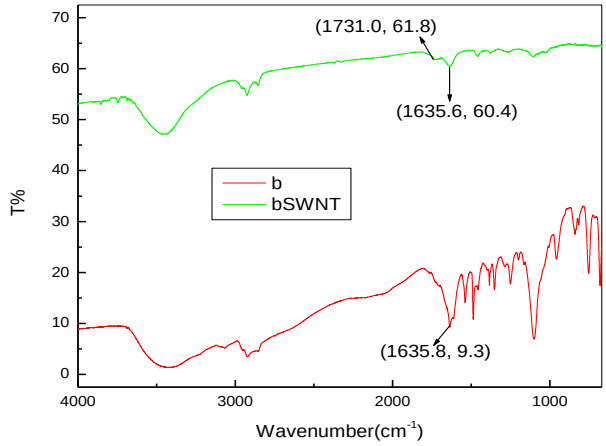

(b)

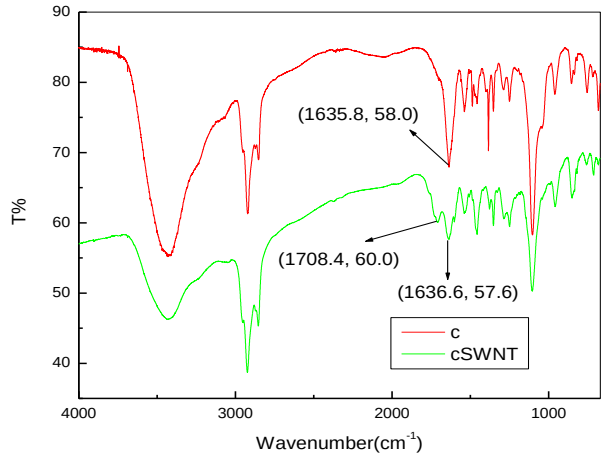

(c)

Figure 4. 9 FTIR spectra of the pyrene derivatives with / without SWNTs using different surfactants: (a) pa-18-C-6 (b) pb-18-C-6 (c) pc-18-C-6. (solvent used is chloroform.)

The spectra of pa-18-C-6, pb-18-C-6 and pc-18-C-6 are shown in Figs. 4.9 a, b, and c. The peaks appearing at about 1635cm^{-1} and 1700cm^{-1} are respectively attributed to amide group on the surfactant and carbonyl group on the SWNTs. In the case of pa-18-C-6 (Fig. 7a), the large blue shift of the amide peak in the presence of SWNTs, from about 1636cm^{-1} to 1650cm^{-1} indicates the presence of the C=C group, which are formed in the proposed structural rearrangement (Figure 4.8) since the peak at 1650cm^{-1} is its fingerprint. By comparison, the small shift of the amide peak locations in Figs. 4.9 b and 6c, which is in the range of the experimental error, suggests the mere physical interaction between SWNTs and pb-18-C-6 or pc-18-C-6. The presence of the peak at 1032cm^{-1}, which is the characteristic signal from C-O absorption, is another direct evidence of the structural rearrangement for pa-18-C-6 only.

For pb-18-C-6 and pc-18-C-6, we postulate the different electronic band structures of *met*-SWNTs and *sem*-SWNTs are responsible for our pyrene derivatives selectivity to *met*-SWNTs, in which some electron transfer[253] processes may be involved.

4.4 Conclusion

In conclusion, we have synthesized and characterized the SWNTs-property selection/separation behavior of a series of three pyrene derivatives. All three compounds are selective to *met*-SWNTs. Raman results indicate that two of the pyrene derivatives pb-18-C-6 and pc-18-C-6 are selective to large diameter *met*-SWNTs. On the contrary, the compound pa-18-C-6 is selective to small diameter *met*-SWNTs, which appears to be due to the ketone-to-enol rearrangement with this specific structure resulting in higher strain force relaxation with smaller diameter *met*-SWNTs. For their discrimination

between different semiconducting species, pb-18-C-6 is found to be selective to large diameter ones while pa-18-C-6 and pc-18-C-6 shows no selectivity.

Chapter 5 Diameter and Metallicity Selective Enrichment of Single-Walled Carbon Nanotubes using Polymethacrylates with Pendant Aromatic Functional Groups

5.1 Introduction

In this report, three novel polymethacrylates with different pendant aromatic functional groups, poly(2- naphthylmethacrylate) (PNMA), poly(methyl-methacrylate-*co*-fluorescein-*o*-acrylate) (PMMAFA) and poly(9-anthracenylmethyl methacrylate) (PAMMA) (Fig. 5.1) were investigated for their selectivity in SWNT separation. Compared with conjugated aromatic polymers, these polymers have a lower contact area between the pendant aromatic groups and the SWNTs sidewall so that it is easier to remove the separating agent after separation. The flexible polymethacrylate backbone assists SWNT solvation in common organic solvents whilst the large pendant aromatic structures have strong affinity to the SWNTs. The SWNTs studied were synthesized by the CoMoCAT process. Ultraviolet visible near infrared (UV-Vis-NIR) spectra and photoluminescence excitation maps (PLE) were used to measure the degree of *met*/*sem* dispersion and chiral species selectivity. The influence of the solvent on selectivity was explored. In addition, the change of the polymer fluorescence upon interaction with SWNTs was tracked. High enrichment of *sem*-SWNTs was confirmed in FET devices.

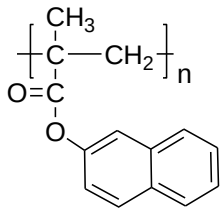

a.Poly(2-Naphthylmethacrylate)(PNMA)

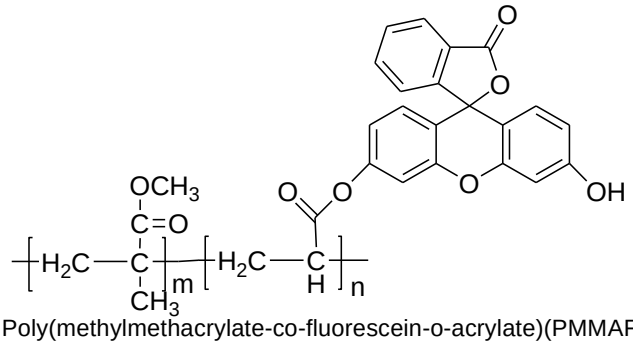

b.Poly(methylmethacrylate-co-fluorescein-o-acrylate)(PMMAFA)

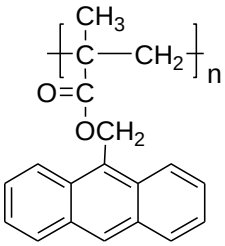

c.Poly(9-anthracenylmethyl methacrylate)(PAMMA)

Figure 5. 1 Structures of polymers used in this study.

5.2 Experimental section

5.2.1 Characterization Techniques.

For the supernatant scans of photoluminescence excitation (PLE) measurements for PMMAFA- and PAMMA-suspended nanotubes, due to the red-shift of the fluorescence band resulted from the formation of excimer at higher concentration, the solutions were diluted to avoid the excitation of the polymer in our interested wavelength region so that the unfavorable energy transfer can be eliminated.

The excitation wavelengths for the fluorescence spectra collection were 278nm, 269nm and 276nm for PNMA, PAMMA and PMMAFA respectively.

5.3 Results and discussion

5.3.1 UV-Vis-NIR spectra.

UV-Vis-NIR absorption spectra of post-separation suspended and precipitated SWNTs for all polymers are shown in Figure 5.2. Also shown are the absorbance spectra of the SWNTs dispersed in D_2O solution using the ionic SDBS surfactant, which is assumed to disperse SWNTs without any species preference.

(a)

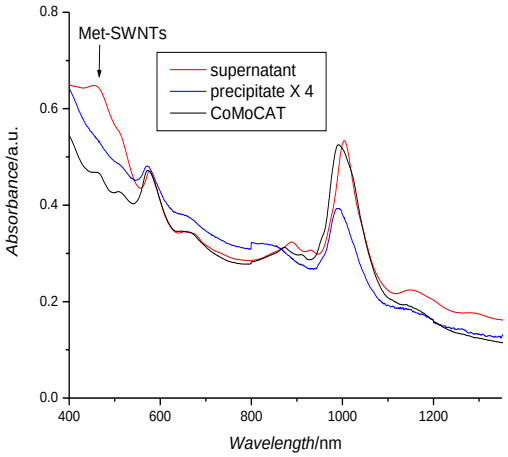

(b)

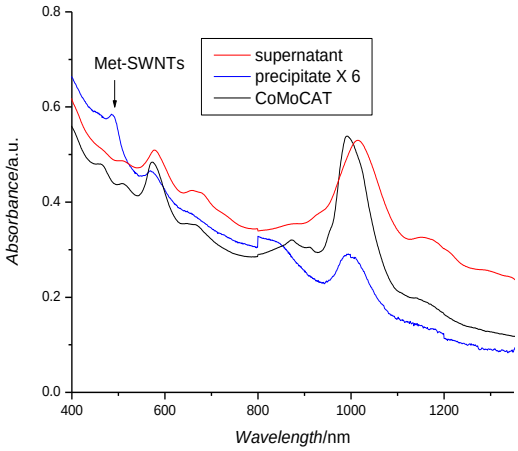

(c)

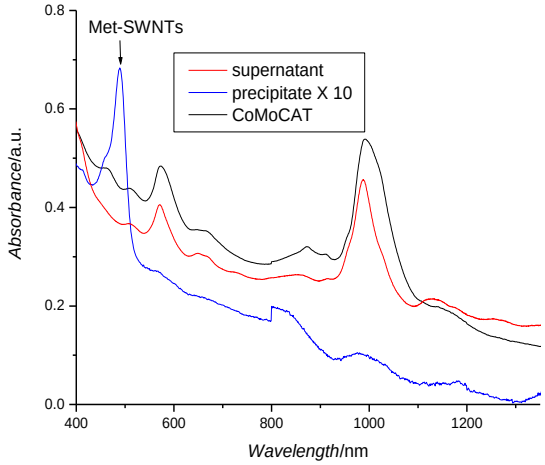

Figure 5. 2 UV-Vis-NIR absorbance spectra of chemically separated SWNTs. (a), (b), (c) CoMoCAT produced SWNTs in DMF with PNMA, PMMAFA and PAMMA respectively. (note: The black SWNT lines are spectra of the "as received" SWNTs dispersed in D_2O/SDBS solution.)

The optical absorbance spectra can tentatively be used to estimate the SWNT species content of the samples since the peak intensities are approximately proportional to the dispersed species concentrations. The spectra contain spectroscopic signatures of the interband electronic transitions corresponding to the M_{11} band of *met*-SWNTs and the S_{11} and S_{22} bands of *sem*-SWNTs.

All separations were performed with the same process parameters, including sonication power and time, concentration of polymer solution, and centrifugation conditions. Figure S1 shows the absorption spectra of the neat polymers. Only PAMMA has strong absorbance in the region that overlaps SWNT spectral features. PNMA and PMMAFA do not interfere with the optical spectroscopy and so were not removed from SWNTs suspended in the supernatant solution prior to spectroscopy (Fig 5.2a, b). For the separation agent PAMMA, SWNTs in the supernatant solutions (Fig 5.2c) were filtered from solution and thoroughly washed with toluene to remove polymer before resuspension in SDBS solution for characterization.

Figure 5.2a,b,c show the absorbance spectra of separated SWNTs (supernatant suspended, resuspended precipitate, and reference unseparated in SDBS solution) for each of the tested polymers. The CoMoCAT SWNTs have pronounced characteristic absorption bands from 400 to 510nm for metallic species and from 510 to 1350nm for semiconducting species. The bands at 800-1350nm and 510-800nm are due respectively to S_{11} and S_{22}. The sharp absorbances at about 576nm and 1000nm are due to the S_{22} and S_{11} interband transitions of the (6,5) nanotube species.[103,220,254] The M_{11}/S_{22} peak intensity ratio is used as a proxy for the relative content of *met*- and *sem*-SWNTs since S_{22} is less susceptible than S_{11} to environmental doping effects. The species content was roughly

estimated from the area enclosed by the "wiggles" in the spectra since subtraction of background of the SWNTs solution, whose intensity estimation can approximately be made[35] locally within each spectrum from the dips between the wiggles, is necessary.

Figure 5.2a shows that PNMA preferentially suspends *met*-SWNTs; the supernatant spectrum has a large M_{11} (~480nm) peak while the S_{22} band (~576nm) is dramatically suppressed with respect to the reference spectrum (as-received CoMoCAT SWNTs in SDBS solution). Correspondingly, the *met*-SWNTs feature is more suppressed in the PNMA precipitate spectrum than are the *sem*-SWNTs features. Similar qualitative analysis of the spectra in Figures 5.2b and 2c indicates that PMMAFA and PAMMA preferentially suspend *sem*-SWNTs, which is obviously corroborated by the strong increase in *met*-SWNT (~480nm) absorption in the precipitates.

Another obvious feature of the enriched supernatant solutions, especially for PNMA and PMMAFA (Fig. 5.2a, b), in contrast to the as-received SWNTs, is the red shift of the peak wavelengths, especially for the S_{11} peak at ~1000nm. For PAMMA separation (Fig. 5.2c), the polymer was removed prior to spectroscopy and a substantial blue shift of the peaks in the supernatant spectrum is evident; before PAMMA removal, a red shift of peak wavelengths in the supernatant solution is evident. The red shift might indicate large diameter selectivity or the influence of the dispersion media environment. From the photoluminescence results discussed below, the large diameter selectivity option can be eliminated.

5.3.2 Photoluminescence-Excitation (PLE).

Photoluminescence[255-257] excitation maps (Figure 5.3) were used to characterize the chiral index (*n,m*) distributions of semiconducting SWNTs in the washed precipitates

and in the supernatant solutions. As-received SWNTs dispersed in 1% SDBS solution in D_2O were also studied as a reference.

(a)

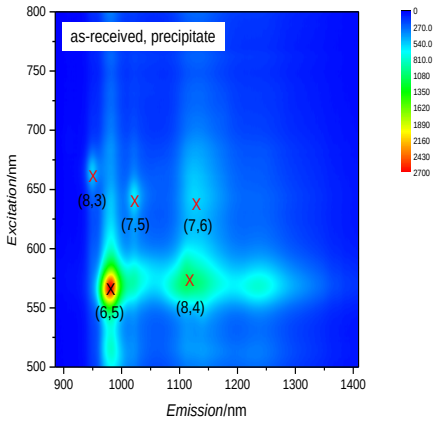

(b)

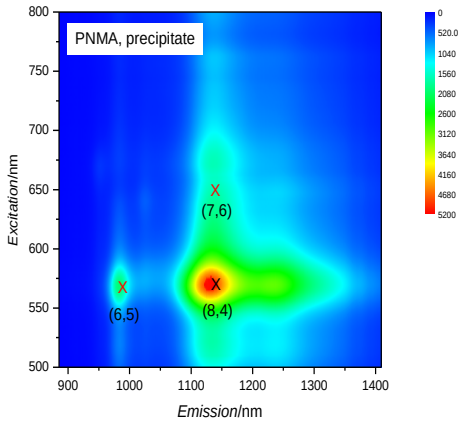

(c)

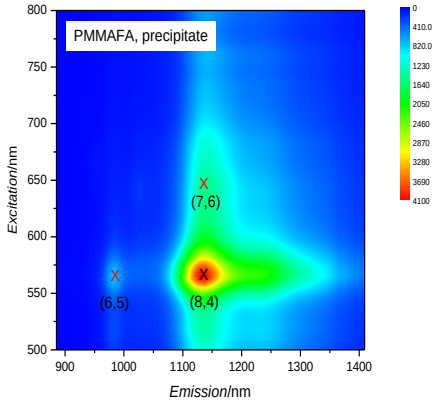

(d)

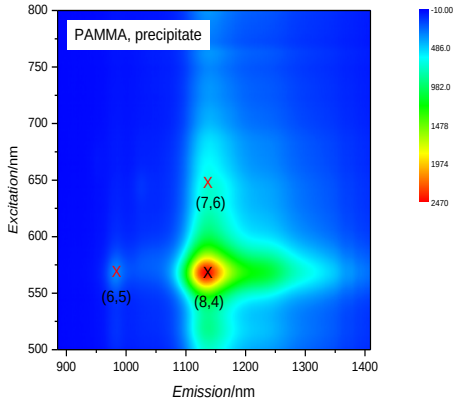

(e)

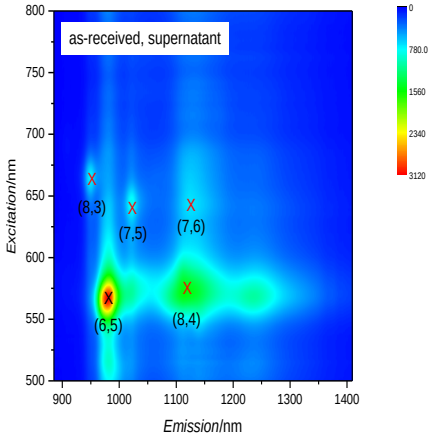

(f)

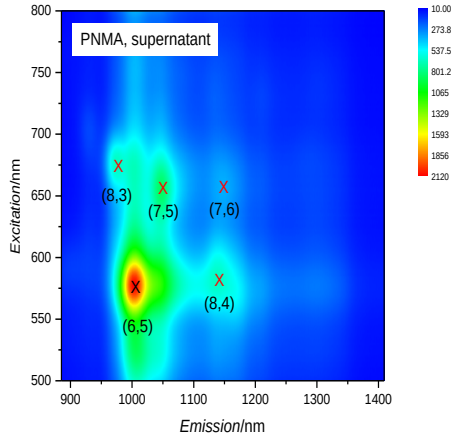

(g) (h)

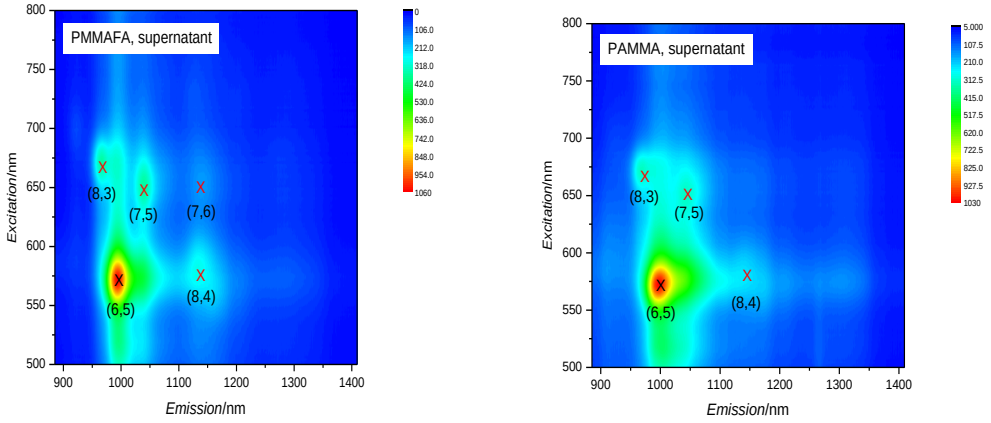

Figure 5. 3 PLE maps of SWNTs dispersed with SDBS solution (a), (e) and of SWNTs after chemical separation (b)-d, (f)-(h). (a), (e) As-received CoMoCAT SWNTs dispersed using SDBS solution with precipitate fraction (a) and supernatant fraction (e). (b-d) CoMoCAT SWNTs precipitates after separation in DMF with (b) PNMA (c) PMMAFA and (d) PAMMA. (f-h) CoMoCAT SWNTs in the supernatant solution after separation in DMF with (f) PNMA (g) PMMAFA and (h) PAMMA.

As-received CoMoCAT SWNTs (Fig 5.3a,e) are dominated by the (6,5) and (8,4) species. Also present with reasonably strong signals are the (8,3), (7,5) and (7,6) species. Fig 5.3a,e also indicate that SDBS shows no species selectivity. The polymer-separated precipitates (Fig 5.3b,c,d) exhibit similar modifications in their chiral distributions: the (6,5), (7,5) and (8,3) species PLE peaks are suppressed by all three polymers, indicating preferential suspension of these (with respect to (7,6) and (8,4)) in the supernatant solution. The preferentially suspended species (6,5), (8,3) and (7,5) are somewhat smaller (with d_{tube} = 0.757nm, 0.782nm and 0.829nm) than the precipitate species (8,4) and (7,6) (d_{tube} = 0.840nm and 0.895nm), which suggests a smaller size preference for dispersion by the polymers. Similar analysis of the PLE maps of the supernatant solution in Figures 5.3f, 5.3g and 5.3h confirms the preference for smaller diameter species of all tested polymers. The selection mechanism is not plain from this data. The polymers may prefer tubes in a specific diameter range because of favorable binding energy. However, since

the band gap E_{11} correlates closely (inversely) with the tube diameter, a preferential interaction between the polymers and SWNTs produced by a process related to the SWNTs' electronic structure is also compatible with our data. Whatever the underlying mechanism, it is apparent that the polymers prefer smaller diameter tubes. Consequently, the redshift observed in the PNMA- and PMMAFA-suspended SWNTs UV-Vis-NIR spectra (Fig. 5.2a, b – supernatant) should be attributed to the presence of unwashed polymer in the supernatant.

A subtle effect which could potentially confuse the interpretation of our PLE maps is the possibility of energy transfer from smaller tubes to larger tubes, which suppresses the small tube emission in favor of the larger tubes.[258] If this is present in our data, it alters the interpretation of peak height ratios within a single PLE map. This effect is presumably reproducible between maps provided that the sample processing conditions are comparable (as they are in this study) and so we are confident that changes in peak height ratios between different PLE maps are a reliable proxy for changes in the underlying species distributions.

It is evident from both the UV-Vis-NIR absorbance spectra and the PLE maps that the species selectivity differs noticeably for the different polymers. Specifically, PMMAFA and PAMMA preferentially disperse semiconducting SWNTs but PNMA preferentially disperses metallic SWNTs. All three polymers preferentially disperse smaller diameter species.

We tentatively ascribe the polymers' species selectivity to their diameter selectivity, which dominates the SWNTs wrapping. Diameter selectivity in our study may result from the different polymer conformation, which is also believed to be influenced by the

size and structure of the pendant functional groups as well as the solvent.[259-260] Solvent dependent characteristics of the species selectivity, which will be discussed below, corroborate our suggested mechanism. UV-Vis-NIR spectra and PLE maps were employed to characterize supernatant fraction of the separated SWNTs in different solvents, *i.e.*, CH_3CN and $CHCl_3$. The standing time after sonication was set to be 2 weeks and only the polymer PNMA was tested as its species selectivity in DMF is different as compared to the other two polymers.

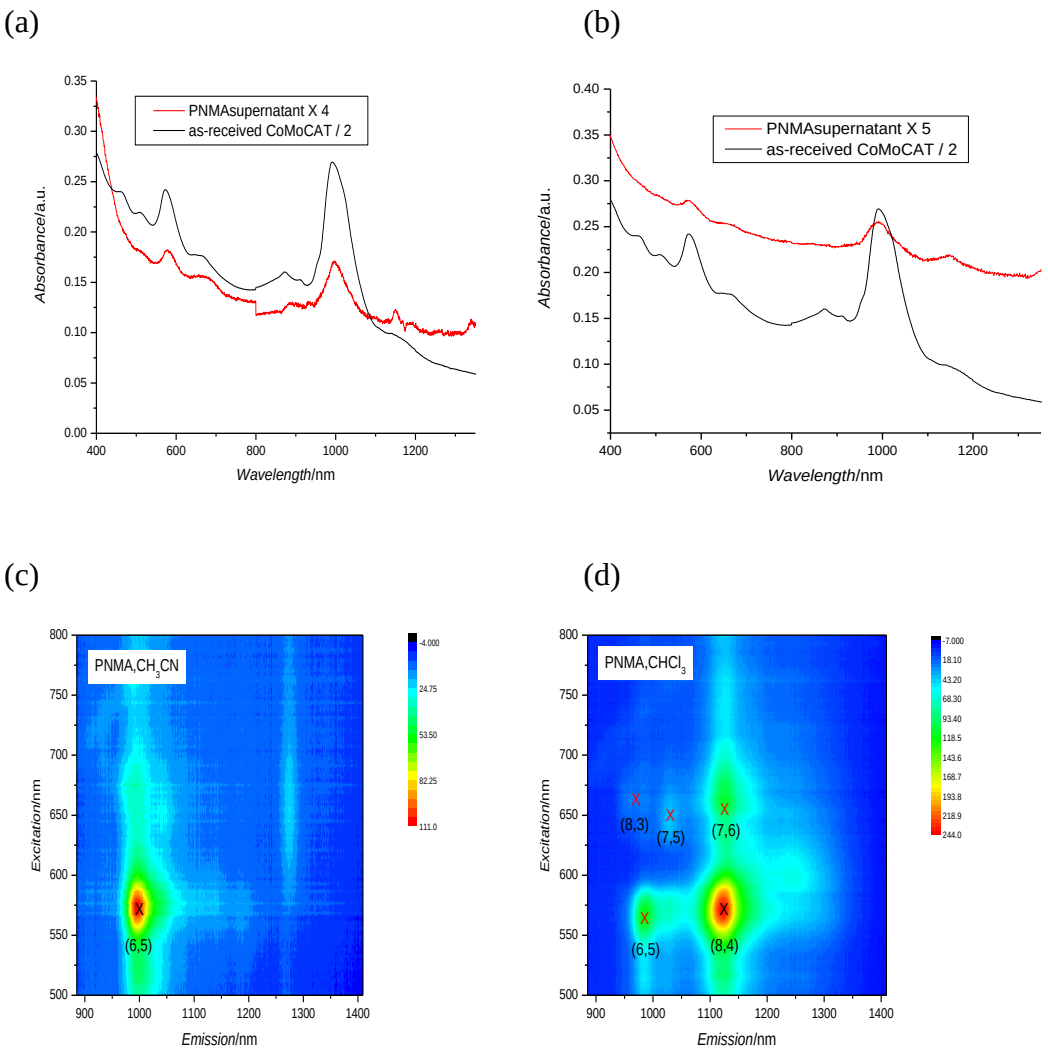

Figure 5. 4 Solvent effects on the species selectivity of PNMA. (a)(b) UV-Vis-NIR absorbance spectra of the SWNTs in the supernatant fraction using (a) CH_3CN (the concentration of PNMA in CH_3CN is ~0.5%, limited by its solubility) and (b) $CHCl_3$ as solvent. (c)(d) PLE maps of the

SWNTs in the supernatant fraction with solvents (c) CH_3CN and (d) $CHCl_3$. (note: The black SWNTs lines in (a-b) are spectra of the "as received" SWNTs dispersed in D_2O/SDBS solution.)

The absorption spectra (Figure 5.4a, b) indicate that PNMA is selective to semiconducting species in both CH_3CN and $CHCl_3$. However, the PLE maps (Figure 5.4c, d) suggest that PNMA is selective to smaller diameter species, mainly (6,5) in CH_3CN while larger diameter species, mainly (8,4) and (7,6) are preferred in $CHCl_3$. The different species selectivity of PNMA in various solvents is attributed to differing degrees of relaxation in the polymer conformation to the nanotube walls. The influence of the solvents on the conformation of PNMA was investigated using Hansen Solubility Parameters (HSP). Our prediction is made based on the group contribution method[261] starting from Poly(methyl methacrylate) (PMMA), which can be assumed as the precursor of PNMA, due to the availability of its HSP both theoretically and experimentally. To simplify the estimation, we assume the contributions of the naphthyl and methyl side groups to the HSP of the corresponding polymers, which in our case are PNMA and PMMA, to be additive.[261] We also neglect the difference between the HSP of polymers and their repeating units so that we can conveniently calculate the HSP of PNMA directly from the HSP of PMMA by replacing the contribution of methyl group with that of naphthyl group. The HSP of PMMA and the group contributions as well as the calculated HSP of PNMA is listed in table 5.1. The HSP of solvents[262] are listed in Table 5.2 and the affinity between solvent and PNMA is expressed as the distance R_a[262] between HSP of PNMA and those of solvents in Hansen space, which is calculated using

$$Ra^2 = 4(\delta_{D1}-\delta_{D2})^2 + (\delta_{P1}-\delta_{P2})^2 + (\delta_{H1}-\delta_{H2})^2$$

Table 5. 1 Hansen Solubility Parameters (unit: [$MPa^{1/2}$]) of polymers and groups contribution.

Polymer/ Functional Group	δ_D	δ_P	δ_H
PMMA	18.81	10.22	8.59
$-CH_3$	-0.9714	-1.6448	-0.7813
Napathyl	2.0876	-3.7727	-2.3123
PNMA	21.869	8.0921	7.059

Table 5. 2 Hansen Solubility Parameters of solvents and the expression of the distances between solvent and PNMA. (The units for the solubility parameters and Ra are [$MPa^{1/2}$].)

Solvent	δ_D	δ_P	δ_H	Ra^2
Acetonitrile	15.3	18.0	6.1	271.69
Dimethylformamide	17.4	13.7	11.3	129.32
Chloroform	17.8	3.1	5.7	92.99

The distance between PNMA and solvents is in the increasing order of Chloroform, DMF and Acetonitrile. The affinity of the PNMA to different solvents increases in the order CH_3CN, DMF and $CHCl_3$. $CHCl_3$ is the best solvent for PNMA and CH_3CN the poorest. The diameter of the SWNTs suspended by PNMA in different solvents increases in the same order: $CHCl_3$ suspends the larger diameter nanotubes. It seems that there is some direct relationship between PNMA's species selectivity and its affinities to solvents. In a poor solvent, the polymer conformation collapses to minimize the polymer exposure to the solvent. This would favor wrapping of the smaller diameter species (6,5) in CH_3CN compared with $CHCl_3$ or DMF. In a good solvent such as $CHCl_3$, the conformation of polymer is relaxed (*i.e.* looser) and larger diameter species such as (8,4) and (7,6) are thus preferentially suspended. The different behaviors of PNMA in different solvents suggest that its selectivity is explainable in part by a diameter preference which arises from the energetics of polymer conformation change when complexing with the SWNT. However, comparison of the metallicity selectivity of different polymers in DMF indicates that the side groups do play an important role during the wrapping process.

With naphthalene as the functional group, the polymer preferentially suspends metallic species while anthracene and fluorescein result in the polymers' selectivity to semiconducting species.

An interesting factor which is involved in the separation is light. In a control experiment, we repeat the experiments using the same setup of all experimental parameters except that, after sonication, we put the solutions in a dark area instead of a brightly lit area; in the "dark" experiments, no metallicity selectivity is observed in the UV-Vis-NIR spectra. We suggest that the presence of light will induce some dipole-dipole interaction between polymeric chromophores and SWNTs and it is this kind of dipole-dipole interaction that is responsible for the polymers' metallicity selectivity in DMF.[263-264] In experiments, photon induced dipole-dipole interaction will possibly result in energy transfer between the units on which the dipoles reside.[241]

5.3.3 Fluorescence spectra of polymers.

Energy transfer from polymeric chromophores to SWNTs can be characterized by the polymer fluorescence spectra.

(a) (b)

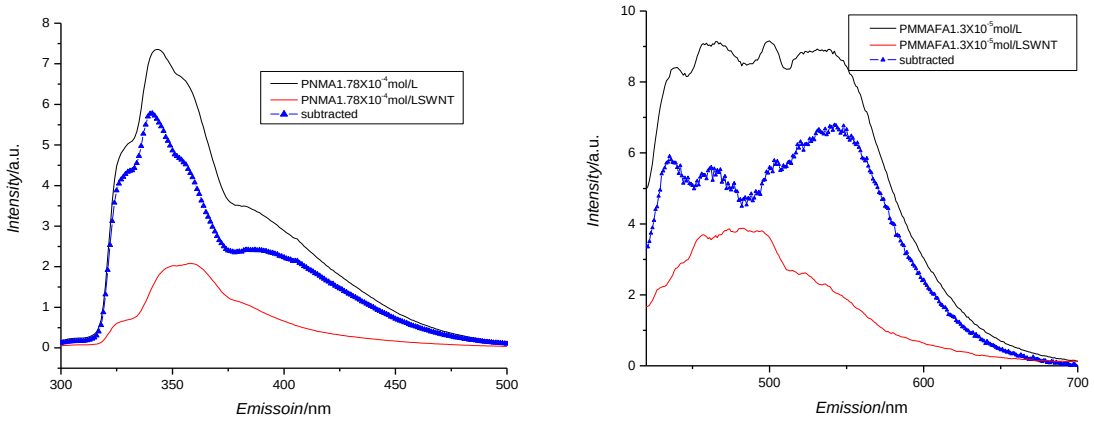

(c)

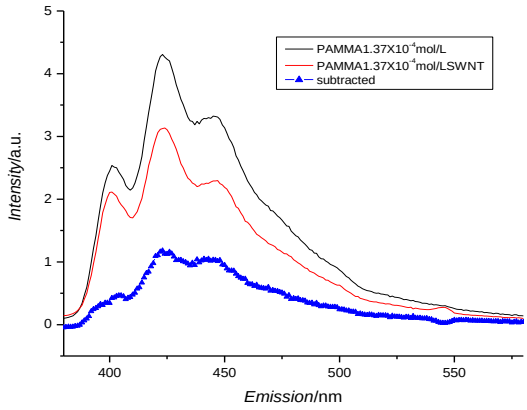

Figure 5. 5 Fluorescence spectra of PNMA and PAMMA in the presence/absence of SWNTs. (a) PNMA, (b) PMMAFA, (c) PAMMA. (note: The blue line is obtained by subtracting the red line from the black line.)

Fluorescence spectra of all polymers are shown in Figure 5.5a,b,c. To reduce the intermolecular interaction, low polymer concentration solutions were used in the fluorescence test. The separation process was repeated for all polymers in DMF and the fluorescence spectra of all polymers in the absence and presence of SWNTs were obtained. The concentrations of chromophores NMA, AMMA and FA were 1.78×10^{-4} mol/L, 1.37×10^{-4} mol/L and 1.3×10^{-5} mol/L respectively. During the spectra collection, all variable parameters were set to be the same so that the fluorescence intensities are comparable.

From Figures 5.5a,b,c, the lower intensities in the presence of SWNTs suggests strong quenching in the presence of SWNTs for all polymers. In all figures, the difference (suppressed fraction of the spectra) between the original and quenched spectra was represented by the blue line, which was obtained by subtraction of the spectra of polymers in the presence of SWNTs from those in the absence of SWNTs. The disproportionality between the suppressed intensity and the original spectra indicates that

it is unlikely to resolve the suppression by concentration variation since the chromophore concentration is in its linear range. This suggests the existence of some coupling interaction, such as energy transfer, between polymer and SWNTs. Further evidence of energy transfer can be observed in a typical PLE map of suspended SWNTs in the undiluted 0.1% PAMMA/DMF solution.

The different suppression tendency of the fluorescence for PNMA and PMMAFA/PAMMA suggests different interaction with SWNTs. For PNMA, the shorter wavelength emission is more obviously suppressed while suppression of longer wavelength emission is more prominent for PMMAFA/PAMMA. The necessary condition of spectral overlap[241] between the fluorescence spectra of polymeric chromophores and absorption spectra of SWNTs as well as the energy transfer will occur more readily in the energetically favorable direction determine the energy transfer tendency. It is their interplay determined the different fluorescence quenching styles for PNMA and PMMAFA/PAMMA, resulting in their diverse metallicity selectivity. One concern about the above argument is that the energy transfer is possibly resulted from rather than will result in the metallicity selectivity. Since we can observe the energy transfer immediately after sonication, we can eliminate the first possibility.

In our tested system, the interaction between SWNTs and aromatic functional groups is not limited to Van der Waals interaction, which is generated by thermal charge distribution fluctuations. On the contrary, the induced dipole-dipole interaction may get involved in the presence of light. In addition, the involvement of the polymer conformation change, which is enforced by the solvation in different solvents, complicated the situation. It is the interplay and relative magnitudes of all these kinds of

weak interaction that results in the polymers' unique metallicity and diameter selectivity. Other factors such as structural compatibility (simultaneous optimization of the effective contact area and atomic correlation between SWNTs and aromatic groups) or electronic interaction[234,265] cannot be completely excluded from the contribution to polymers' species discrimination and further investigation is required.

5.3.4 Electrical measurement.

To confirm the species enrichment, we fabricated short channel thin film FET devices using semiconductor enriched SWNTs and characterized the electrical properties of the nanoelectronics. The solution used in the device fabrication was obtained by dispersing in SDBS *sem*-SWNTs separated using PMMAFA. For the preparation of electronic devices, we prefer to use supernatant because precipitates normally contain many bundles which cannot be dispersed well into individual tubes.[266] Thin film FETs were fabricated by the drop-casting method. A gate bias was applied to the underlying Si substrate, which served as the gate electrode, to modulate the carrier concentration in the SWNTs network. The electrode configuration and typical device performance plots are shown in Figure 5.6.

(a)

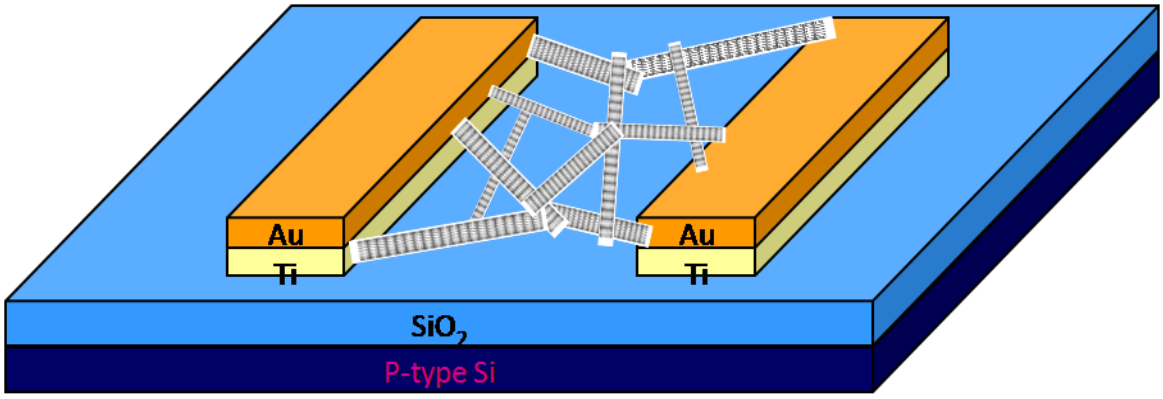

(b) (c)

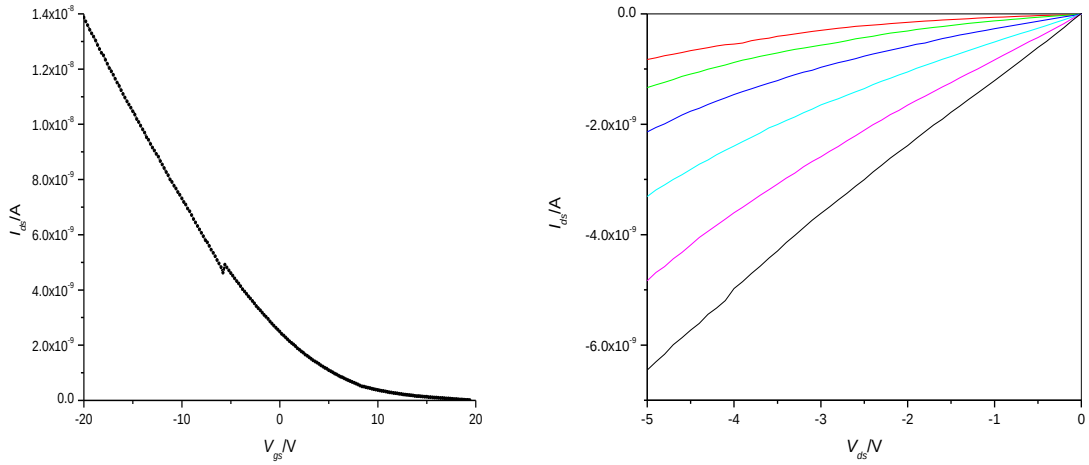

Figure 5. 6 FET fabricated with *sem*-enriched SWNTs as active channel using PMMAFA. (a) Device configuration; (b) Transfer characteristic (I_{ds}-V_{gs}) of a representative device at V_{ds}= 2 V; (c) Current-Voltage characteristics (I_{ds}-V_{ds}) of the device at V_{gs} ranging from -10 to 10 V with the step of 4 V from bottom to top.

At least 90% of the devices (9 of 10) exhibited good FET performance with on/off ratios of about 10^3 This is much superior to the performance of devices made from the as-received SWNTs (1 of 10 devices shows on/off ratio of ~10 and the rest <10), which confirms the enrichment of *sem*-SWNTs in the nanotube suspension. The relatively low on-state current may be limited by the low density of SWNTs in the channel, the lower current capacity of small diameter SWNTs (preferentially selected by PMMAFA) compared with larger diameter SWNTs and possibly high Schottky barriers and non-ohmic contacts.[73,267-268] The high (about 10^3) FET on/off ratio corroborates our other evidences of species selective enrichment. Further improvement in device performance can be anticipated by using larger diameter SWNTs or higher work function electrodes since on-state current can be substantially increased by lowering the Schottky barriers. The optimization of the electrode geometry and conditions for device fabrication will further improve the device performance.

The species selectivity is found to be quite sensitive to the polymer/solvent combinations. Different combinations show different discrimination between various SWNTs species, depending on their chiralities and diameters. Serial enrichment using multiple highly selective polymer/solvent combinations may provide higher purity and potentially even single species enrichment.

Our method is scalable, nondestructive, compatible with SWNTs of different sources, iteratively repeatable and affordable, and thus makes widespread application possible according to Mark C. Hersam's criteria.[87] Further improvement of FET device performance is anticipated through use of larger diameter SWNTs or higher work function electrodes as well as with optimization of electrode geometry and device fabrication conditions.

5.4 Conclusions

Three novel polymethacrylates, PNMA, PAMMA and PMMAFA, with pendant aromatic functional groups have been successfully employed in the separation of SWNTs according to their electronic properties (*met*-/*sem*-) and diameters and highly effective enrichment has been achieved. Optical absorbance spectra and photoluminescence excitation maps indicate that this family of polymers has strong selectivity towards certain SWNTs species with specific diameters and that the species selectivity is highly sensitive to the polymer/solvent combination. Specifically, in DMF, PMMAFA and PAMMA preferentially disperse semiconducting SWNTs while PNMA preferentially disperses metallic SWNTs. All three polymers preferentially disperse small diameter SWNTs in DMF. The selectivity of PNMA (to metallic species in DMF) is sensitive to the solvent employed. In CH_3CN, PNMA is selective to smaller diameter semiconducting

species while larger diameter semiconducting species are preferentially suspended in $CHCl_3$. The solvent effects on species selectivity suggest the mechanism of diameter selectivity, which results from a change of polymer conformation. The change of the polymer fluorescence in the presence of SWNTs was tracked and the involvement of photon in the enrichment process is identified and the photon induced dipole-dipole interaction is probably responsible for the metallicity selectivity in DMF. The diverse selective behavior of these polymers is resulted from the interplay between photon induced dipole-dipole interaction and polymer conformation change. Other kinds of weak interactions such as Van der Waals interaction as well as structural compatibility also cannot be excluded.

Successful fabrication of thin film FET devices with semiconductor enriched solution has been demonstrated. The reproducible on/off ratio of about 10^3 in these devices confirms the enrichment in semiconducting species.

Chapter 6 Separation of Single-Walled Carbon Nanotubes with Aromatic Group functionalized Polymethacrylates and Building Blocks Contribution to the Enrichmentment

6.1 Introduction

In our previous work (previous chapter),[269] we suggested another kind of weak interaction associated with resonant energy transfer between polymeric chromophores and SWNTs to influence SWNT species enrichment. We have proposed that the overlap of the polymer fluorescence wavelength with the absorption wavelength of particular nanotube species results in preferential energy transfer, resulting in dipole-dipole interaction, and consequently, the polymers' selectivity towards met- or semi-SWNTs. Two polymethacrylates, specifically poly(9-anthracenylmethyl methacrylate) (PAMMA) and poly(2-Naphthylmethacrylate) (PNMA), were studied (Fig 6.1).[269]

In this paper, two other polymethacrylates with different aromatic side groups (*i.e.* poly(benzyl methacrylate) (PBMA) and poly(methylmethacrylate)-co-(9-anthracenylmethyl acrylate) (PMMA-c-PAMA), Fig 6.1) were investigated for their selectivity to SWNT species. The pendant groups in these polymers are UV/vis-light absorbing chromophores. The size and content of these chromophores in the four polymers are different. The SWNTs investigated were produced by the CoMoCAT method. Using PBMA and PMMA-c-PAMA as dispersants of SWNTs in dimethylformamide (DMF), ultraviolet/visible/near infrared (UV-Vis-NIR) absorption spectra and photoluminescence excitation maps (PLE) were collected to characterize the degree of *met*-/*sem*- separation and species selectivity. The effect of solvent on semiconducting species suspension of PBMA and PMMA-c-PAMA was examined by PLE using two other solvents (acetonitrile and chloroform). The selectivities of the four polymethacrylates in Fig 6.1 were compared and the contribution of the side group

and main chain were analyzed using Group Contribution Theory. The influence on selectivity of the standing time of the SWNTs solution after sonication was also explored.

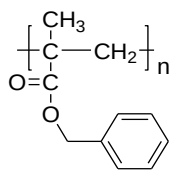

a.Poly(benzyl methacrylate)(PBMA)

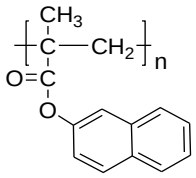

b.Poly(2-Naphthylmethacrylate)(PNMA)

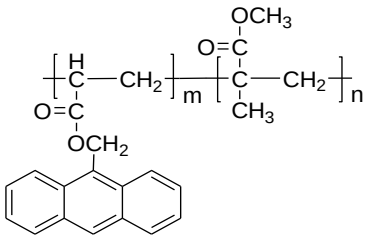

c.Poly((methylmethacrylate)-co-(9-anthracenylmethyl acrylate)) (PMMA-c-PAMA)

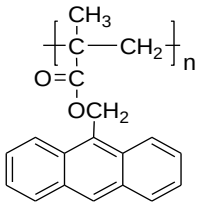

d.Poly(9-anthracenylmethyl methacrylate)(PAMMA)

Figure 6. 1 Structures of polymers used in this study.

6.2 Experimental section

6.2.1 Characterization Techniques.

Deuterated acetone was used as the solvent with tetramethylsilane (TMS) as the internal standard for ^{1}H NMR characterizations.

The excitation wavelengths of photoluminescence characterization for polymer solutions were 268 and 350nm for PBMA and PMMA-*c*-PAMA respectively.

6.3 Results and discussion

6.3.1 UV-Vis-NIR spectra.

UV-Vis-NIR absorption spectra of polymer suspended supernatant fraction and resuspended precipitate fraction with PBMA and PMMA-c-PAMA are shown in Figure 6.2a,b. To more clearly see the peaks, the background is removed from the raw UV-Vis-NIR data and shown in Figure 6.2c,d. The UV-Vis absorption and photoluminescence spectra of the neat polymers are also included (Figure 6.2e,f). (The results for polymers PNMA and PAMMA have been previously reported by us.[269] and were included in chapter 5) Also

included are the absorbance spectrum of the SDBS dispersed SWNTs, which was used as reference spectrum because SDBS is believed to disperse SWNTs without any species selectivity.

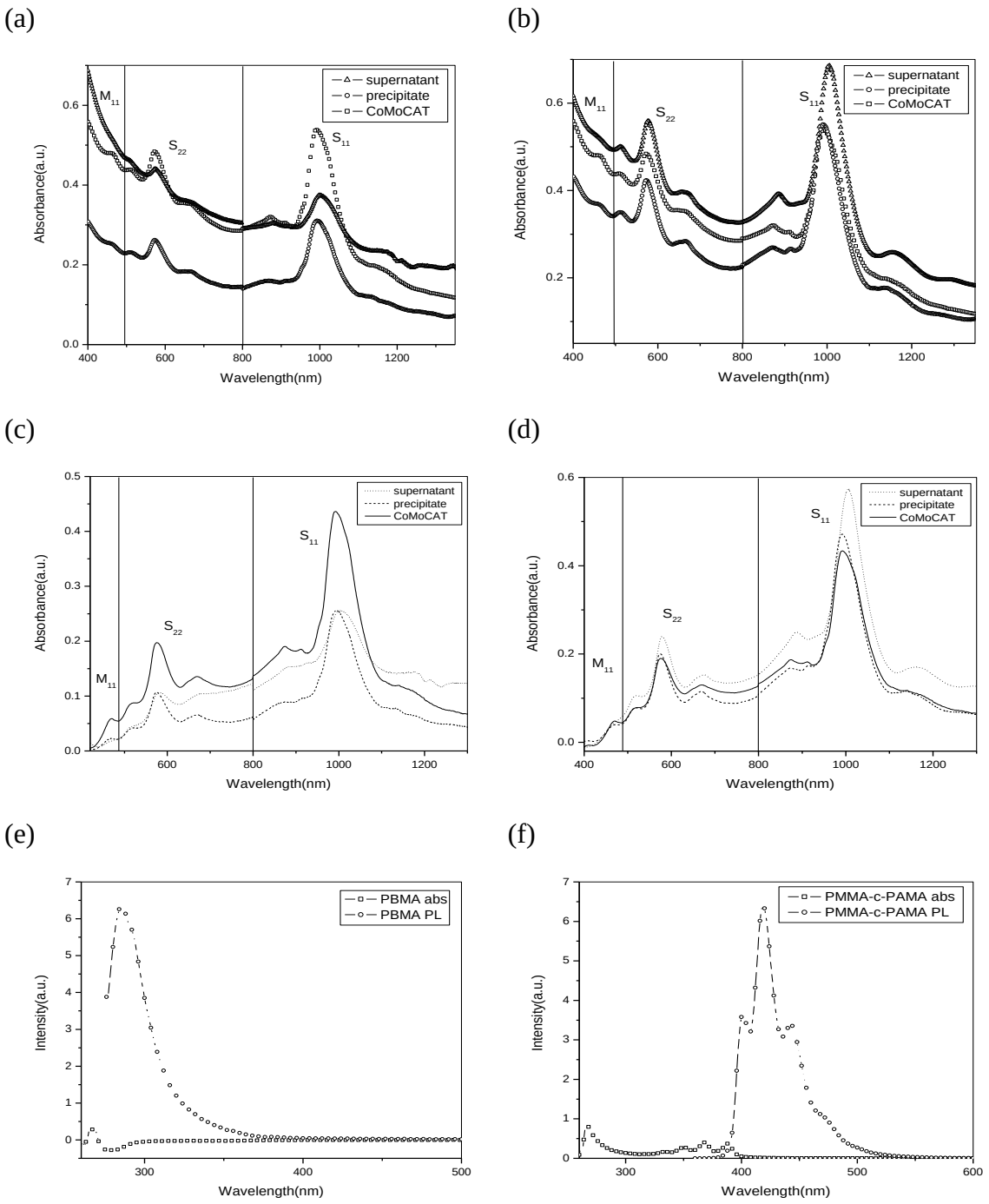

Figure 6. 2 UV-Vis-NIR absorbance spectra of chemically separated SWNTs. (a), (b) CoMoCAT produced SWNTs in DMF with PBMA and PMMA-c-PAMA respectively; (c), (d) background subtracted UV-Vis-NIR spectra of CoMoCAT produced SWNTs in DMF with PBMA and PMMA-c-PAMA respectively; (e), (f) UV-vis absorption (abs) and photoluminescence (PL) spectra of PBMA and PMMA-c-PAMA in DMF solution respectively.

The optical absorbance spectra were used for the assessment of the SWNT species abundance because the species' peak intensities above the background scale proportionally with their corresponding concentrations, regardless of whether the SWNTs are bundled or individually dispersed. The absorbance spectra exhibit absorption features due to the metallic M_{11} band as well as the semiconducting S_{11} and S_{22} bands.

All separations were carried out with the same experimental parameters such as sonication power and time, polymer solution concentration and centrifugation conditions. Absorption spectra of the neat polymers are shown in Figure 6.2e,f. PBMA and PMMA-c-PAMA do not affect the SWNT spectroscopic characteristics and so were not removed before spectroscopic scans of the SWNTs suspended in the supernatant solutions (Fig 6.2a, b, c, d).

Figure 6.2a,b show the absorbance spectra of the supernatant fraction and redispersed precipitate for PBMA and PMMA-c-PAMA as well as the unseparated SWNTs in SDBS solution. The CoMoCAT SWNTs exhibit prominent characteristic spectroscopic features from 400 to 510nm for metallic SWNTs and from 510 to 1350nm for semiconducting ones. The bands at 800-1350nm and 510-800nm correspond to S_{11} and S_{22} respectively.[103,220,254] The ratio of the peak intensity M_{11}/S_{22} is used for the estimation of the content ratio of *met*- to *sem*-SWNTs because S_{22} is more stable spectroscopically than S_{11} to environmental doping effects. The area enclosed above the baseline in the spectra is more relevant for calculating species concentration due to the presence of the SWNT solution background, which scales approximately exponentially with the transition energy.

Our previous results[269] in chapter 5 indicate that PNMA preferentially suspends *met*-SWNTs while PAMMA is selective to *sem*- SWNTs. However, no obvious metallicity selectivity was evident from comparison of the spectra of the supernatant and resuspended precipitates resulting from treatment with separation agents PBMA and PMMA-c-PAMA (Figure 6.2a, b). The background subtracted figures (Figure 6.2c,d) confirmed our above

conclusion. Both supernatant and precipitate are slightly enriched in semiconducting SWNTs as compared to the as-received CoMoCAT SWNTs although the degree of enrichment is a bit more obvious for supernatant suspended SWNTs. The species abundance may be resulted from some systematic error involved in sample preparation or data collection. Also, a parabolic background with "up" curvature will tend to suppress the different signature of an absorption peak, since the background has a more negative slope on the short-wavelength side of the peak than on the long-wavelength side. This could also contribute to the more obvious suppression of metallic features for supernatant suspended CoMoCAT SWNTs.

The selectivity difference among different polymers suggests that the aromatic functional groups play a critical role in the enrichment. Firstly, the absence of metallicity selectivity with the phenyl group in PBMA, in contrast to PNMA and PAMMA,[269] indicates that the size of the chromophores is quite critical. Secondly, the crucial role of the content of the aromatic groups in these copolymers may be suggested by the selectivity difference between PAMMA and PMMA-c-PAMA. Thirdly, the reversed metallicity selectivity for PNMA in contrast to PAMMA previously reported[1] brings out the significance of the side chromophores in the metallicity selectivity. We have postulated that selectivity is due to photon induced dipole-dipole interaction[269] which critically depends on the overlap of the polymer fluorescence wavelength with excitation wavelength of specific SWNT species. The above observed differences can be explained by our proposed mechanism regarding the metallicity selectivity.

As compared to the as-received SWNTs, another noteworthy feature of the suspended supernatant solutions is the red shift of the SWNTs' spectroscopic peak, especially for the S_{11} peak at ~1000nm. The red shift may suggest large diameter selectivity since the SWNT bandgap scales inversely with diameter. Alternatively, it may suggest the effects of the dispersion media.[241] The PLE results, to be discussed below, show that the red shift is not a

SWNT diameter selection effect so that the influence of the dispersion medium is the preferred explanation.

6.3.2 Photoluminescence-Excitation (PLE).

Photoluminescence[255-257] excitation maps (Figure 6.3) of semiconducting species in the resuspended precipitates as well as in the supernatant fraction were collected to characterize their chiral species (*n*,*m*) distributions. As-received SWNTs suspended with 1% SDBS/D_2O solution were also characterized as a reference. For the purpose of convenient comparison, species contents of various species suggested by PLE maps were estimated from their PLE signal intensities calibrated with their corresponding PLE quantum efficiency, neglecting the influence of microenvironment on the PL quantum efficiency of SWNT species. [270] The calculated species abundances are tabulated in table 6.1.

(a)

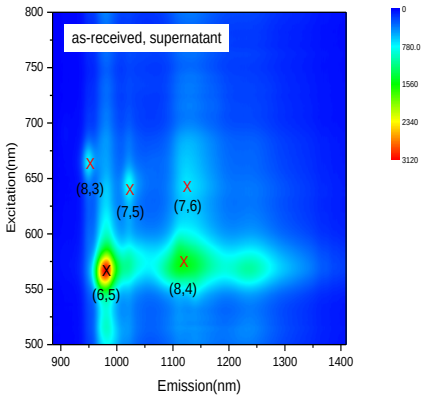

(b)

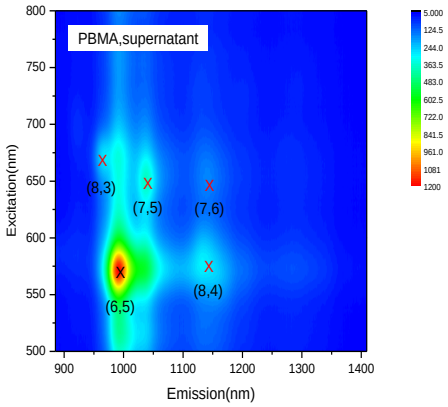

(c)

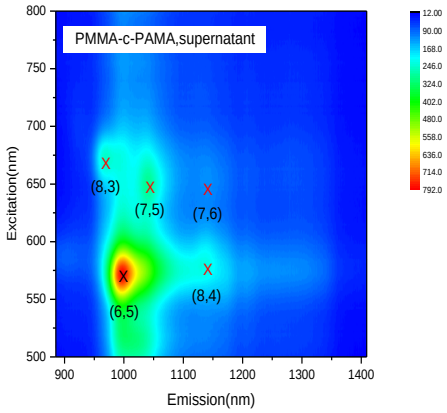

(d) (e)

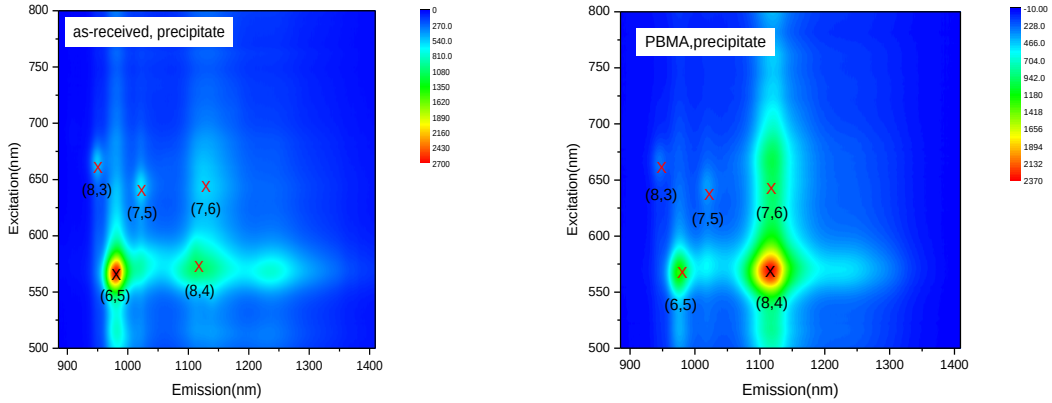

(f)

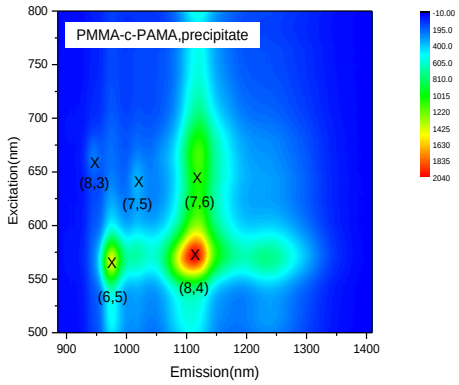

Figure 6. 3 PLE maps of SWNTs dispersed with SDBS solution (a), (d) and of SWNTs after chemical separation (b)-(c), (e)-(f). (a), (d) As-received CoMoCAT SWNTs dispersed using SDBS solution with supernatant fraction (a) and precipitate fraction (d). (b-c) CoMoCAT SWNTs in the supernatant solution after separation in DMF with (b) PBMA and (c) PMMA-c-PAMA. (e-f) CoMoCAT SWNTs precipitates after separation in DMF with (e) PBMA (f) PMMA-c-PAMA.

Table 6. 1 Tabulated values of the PLE peak intensities and calculated abundances for identified semiconducting species suspended by SDBS solution as well as supernatant and precipitate fraction separated with PBMA and PMMA-c-PAMA in DMF.

(n, m)	d_t[nm]	θ [°]	Calculated Intensity	SDBS		PBMA				PMMA-c-PAMA			
						supernatant		precipitate		supernatant		precipitate	
				Experimental Intensity	Species Abundance	Experimental Intensity	Species Abundance	Experimental Intensity	Species Abundance	Experimental Intensity	Species Abundance	Experimental Intensity	Species Abundance
(6,5)	0.75	27.02	0.67	3117	42.0%	1197	51.8%	1269	19.2%	1179	47.6%	1451	22.3%
(8,4)	0.83	19.19	0.46	1550	30.4%	297	18.7%	2362	52%	491	19.8%	2037	45.6%
(8,3)	0.78	15.40	2.13	768	3.3%	272	3.7%	274	1.3%	120	4.8%	241	1.2%
(7,5)	0.82	24.54	0.71	832	10.6%	380	15.5%	369	5.3%	417	16.8%	370	5.4%
(7,6)	0.89	27.47	0.47	717	13.8%	168	10.3%	1034	22.3%	268	10.8%	1171	25.6%

Typically, the as-received CoMoCAT SWNTs (Fig 6.3a,d and Table 6.1) are dominated by species (6,5) and (8,4). Other species such as (8,3), (7,5) and (7,6) are also detected. Fig 6.3a,d show quite similar species distributions and indicate that SDBS suspendswithout

species selectivity. The supernatant fraction of the SDBS suspension was selected for the reference SWNT species abundance calculation. The polymer-suspended SWNTs in the supernatant solutions (Fig 6.3b,c and Table 6.1) exhibit similar modifications of the SWNT chiral species distributions: the contents of species (6,5) and (7,5) are increased by both polymers; correspondingly, the species (8,4) and (7,6), which are diminished in the supernatant, are more prominent in the PLE maps of the redispersed precipitates (Figures 6.3e-3f and Table 6.1). This indicates preferential suspension of smaller diameter species by both polymers. The chiral selectivity is quite similar to our previous results with polymers PNMA and PAMMA, both of which selectively suspend species (6,5), (7,5) and (8,3).[269]

It has been reported that polymers may selectively suspend tubes with specific diameters dictated by the matching of nanotube diameter with the cavity size of polymer in its helical wrapping configuration.[271] Alternatively, the preferential wrapping of SWNTs by polymers may result from a process determined by the SWNTs' band structure since the band gap E_{11} is approximately inversely proportional to the tube diameter. Whatever the driving force, it is apparent that the polymers prefer tubes with smaller diameters. As a result, the redshift presented in the UV-Vis-NIR spectra (Fig. 6.2a, b–supernatant) for PBMA- and PMMA-c-PAMA- suspended SWNTs should be ascribed to modification of the SWNT electronic structure or other modification of the SWNT photon absorption physics when complexed with polymer.

6.3.3 Solvent effect.

UV-Vis-NIR absorbance spectra and the PLE maps indicate that different polymers have different species selectivities. Specifically, PAMMA preferentially disperses semiconducting SWNTs and PNMA selectively suspend metallic SWNTs[269] while PBMA and PMMA-c-PAMA show no metallicity selectivity. Smaller diameter species are preferred by all four polymers.

Diameter selectivity of all polymers may result from the different degree of swelling of the polymer chain in different solvents of varying solvating power; the polymer size in solution is dependent on the size and structure of the aromatic side groups as well as the solvent.[259-260]

Due to the limited dispersion efficiency of these polymers, the UV-Vis-NIR spectra were not well resolved and PLE maps were used to characterize the polymer suspended SWNTs in the supernatant fraction in CH_3CN and $CHCl_3$ solvents as well as in DMF (Fig. 6.4). Standing time was set to 2 weeks in all the tests. Also, quantitative species abundances were extracted from the PLE maps of SWNTs suspended by the polymers in $CHCl_3$ (Table 6.2). PLE maps of SWNTs suspended by polymers in CH_3CN were excluded from this analysis because no species other than (6,5) could be clearly identified (Fig. 6.4) due to the high background/signal ratio resulting from poor dispersion.

(a) (b)

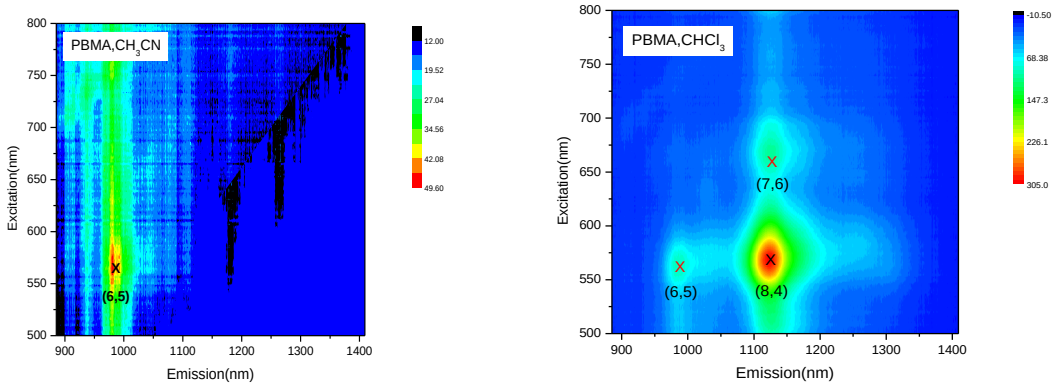

(c) (d)

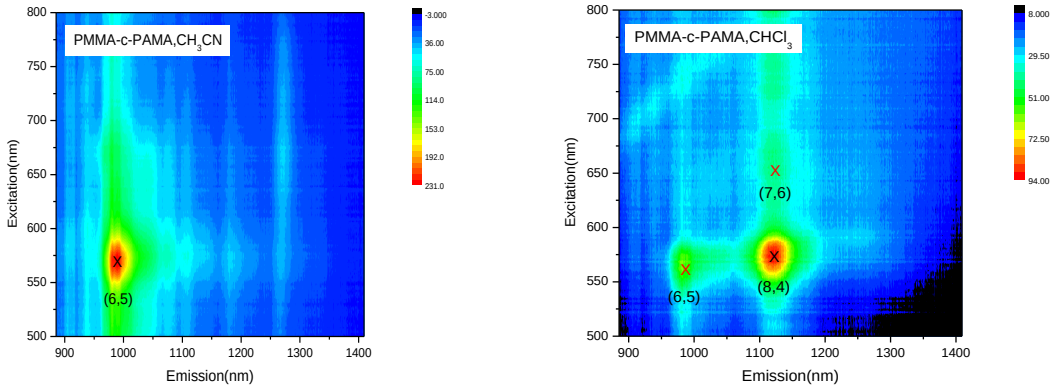

(e) (f)

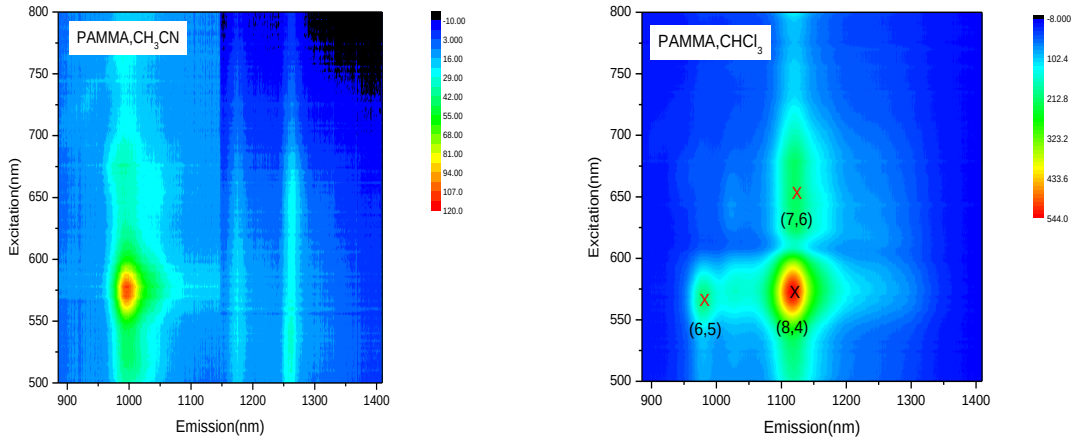

Figure 6. 4 Solvent effects on the species selectivity of PBMA, PNMA, PMMA-c-PAMA and PAMMA. (a-b) PLE maps of the SWNTs in the supernatant fraction using PBMA with solvents (a) CH_3CN and (b) $CHCl_3$. (c-d) PLE maps of the SWNTs in the supernatant fraction using PMMA-c-PAMA with solvents (c) CH_3CN and (d) $CHCl_3$. (e-f) PLE maps of the SWNTs in the supernatant fraction using PAMMA with solvents (e) CH_3CN and (f) $CHCl_3$.

Table 6. 2 Tabulated values of the PLE peak intensities and calculated abundances for identified semiconducting species suspended with PBMA, PMMA-c-PAMA and PAMMA in chloroform.

(n,m)	d_t[nm]	θ [°]	Calculated Intensity	PBMA		PMMA-c-PAMA		PAMMA	
				Experimental Intensity	Species Abundance	Experimental Intensity	Species Abundance	Experimental Intensity	Species Abundance
(6,5)	0.75	27.02	0.67	93	13.5%	64	24.4%	206	15.7%
(8,4)	0.83	19.19	0.46	304	64.2%	94	51.8%	541	60.2%
(8,3)	0.78	15.40	2.13	not available	not available	not available	not available	not available	not available
(7,5)	0.82	24.54	0.71	not available	not available	not available	not available	not available	not available
(7,6)	0.89	27.47	0.47	108	22.3%	44	23.9%	221	24.1%

The PLE maps (Figure 6.4a, b, c, d, e, f and Table 6.2) suggest that for all polymers, PBMA, PMMA-c-PAMA and PAMMA, small diameter species (6,5) is preferred in CH_3CN while species with larger diameters such as (8,4) and (7,6) are selectively suspended in $CHCl_3$. (The solvent effect on PNMA has been previously investigated[269] and shows the same diameter trend.) The different selective behavior of this class of polymer, regardless of the different side functional groups, in different solvents is ascribed to the different degree of relaxation of the polymer chain upon dissolution in different solvents. Hansen Solubility Parameters (HSP) was employed to investigate the solvent effects on the polymeric conformation. The prediction was made using the group contribution method.[261] Poly(methyl methacrylate) (PMMA), which is regarded as the precursor of the tested polymers, was chosen as the starting point for the calculation because its HSPs are available both

experimentally and theoretically. To simplify the calculation, additive contributions of the methyl groups and various chromophore groups to the HSP of the buildup polymers, which in our case are the tested polymers and PMMA, was assumed.[261] We also neglect the difference between the HSPs of the repeating building blocks and the buildup polymers so that replacement of the methyl group contribution with that of the aromatic functional groups would permit estimation of the HSP of the tested polymers from that of PMMA. The HSP of PMMA and its component contributions as well as the estimated HSPs of our employed polymers are listed in Tables 6.3, 6.5 and 6.7. The HSPs of the solvents[262] are listed in Table 6.4, 6.6 and 6.8. The affinities between the solvents and polymers was estimated with the distance R_a [262] between the HSPs of the polymers and the solvents in Hansen space using the expression

$$Ra^2 = 4(\delta_{D1}-\delta_{D2})^2 + (\delta_{P1}-\delta_{P2})^2 + (\delta_{H1}-\delta_{H2})^2$$

where δ_D, δ_P and δ_H are respectively the dispersion Hansen solubility parameter, polar Hansen solubility parameter, and the hydrogen-bonding Hansen solubility parameter. Subscripts 1 and 2 represent the substance 1 and substance 2, *i.e.* polymer and solvent.

Table 6. 3 Calculation of the Hansen Solubility Parameters (unit: $MPa^{1/2}$) for polymer PBMA.

Polymer/ Functional Group	δ_D	δ_P	δ_H
PMMA	18.81	10.22	8.59
$-CH_3$	-0.9714	-1.6448	-0.7813
Benzyl	1.703	-5.0243	-2.2816
PBMA	21.4844	6.8405	7.0897

Table 6. 4 Hansen Solubility Parameters of solvents and the expression of the distances between solvent and PBMA. (The units for the solubility parameters and Ra are $MPa^{1/2}$.)

Solvent	δ_D	δ_P	δ_H	R_a^2
Acetonitrile	15.3	18.0	6.1	163.76
Dimethylformamide	17.4	13.7	11.3	81.46
Chloroform	17.8	3.1	5.7	29.5

Table 6. 5 Calculation of the Hansen Solubility Parameters (unit: $MPa^{1/2}$) for polymer PMMA-c-PAMA.

Polymer/ Functional Group	δ_D	δ_P	δ_H
PMMA	18.81	10.22	8.59
$-CH_3$	-0.9714	-1.6448	-0.7813
Anthracenylmethyl	3.4591	-7.2061	-3.3024
PMMA-c-PAMA	20.0566	9.3162	8.1885

Table 6. 6 Hansen Solubility Parameters of solvents and the expression of the distances between solvent and PMMA-c-PAMA. (The units for the solubility parameters and Ra are $MPa^{1/2}$.)

Solvent	δ_D	δ_P	δ_H	R_a^2
Acetonitrile	15.3	18.0	6.1	102.39
Dimethylformamide	17.4	13.7	11.3	35.96
Chloroform	17.8	3.1	5.7	49.93

Table 6. 7 Calculation of the Hansen Solubility Parameters (unit: $MPa^{1/2}$) for polymer PAMMA.

Polymer/ Functional Group	δ_D	δ_P	δ_H
PMMA	18.81	10.22	8.59
$-CH_3$	-0.9714	-1.6448	-0.7813
anthracenylmethyl	3.4591	-7.2061	-3.3024
PAMMA	23.2405	4.6587	6.0689

Table 6. 8 Hansen Solubility Parameters of solvents and the expression of the distances between solvent and PAMMA. (The units for the solubility parameters and Ra are $MPa^{1/2}$.)

Solvent	δ_D	δ_P	δ_H	R_a^2
Acetonitrile	15.3	18.0	6.1	241.04
Dimethylformamide	17.4	13.7	11.3	143.22
Chloroform	17.8	3.1	5.7	32.16

The distance between the polymer and the employed solvents in Hansen space is in the increasing sequence of Chloroform, DMF and Acetonitrile for all tested polymers except PMMA-c-PAMA. For the latter, the contribution to HSP of methyl and anthracenylmethyl groups was mole-fraction averaged over all the repeating units and we ascribed this abnormal behavior of PMMA-c-PAMA to the overestimation/underestimation of the averaging method of the functional groups. The polymer/solvents affinity decreases in the order $CHCl_3$, DMF and CH_3CN. In different solvents, the diameter of the suspended species by all tested polymers decreases in the same order: larger diameter species are selectively suspended in

$CHCl_3$ and smaller diameter species are preferred in CH_3CN. It is obvious that there is some straightforward relationship between polymers' species selectivity and its solvophilic property. In order to minimize its exposure to the solvent, the polymer shrinks in a poor solvent. This would result in the selective wrapping of the smaller diameter species (6,5) in CH_3CN as contrast to $CHCl_3$ or DMF. In the good solvent ($CHCl_3$), the tendency is reversed and larger diameter species, *i.e.* (8,4) and (7,6) are selected. The solvent dependent characteristics of all these three polymers are consistent with our reported results with polymer PNMA.[269]

The uniform behavior of the solvent dependent diameter selectivity for all polymers suggests the dominant role of the polymeric conformation on the diameter selectivity although the side groups are involved in determining the affinity between polymers and solvents, as listed in the above table.

The different species selective behaviors of various polymers in DMF suggest that the aromatic functional groups do play some decisive role with respect to the metallicity selectivity. With naphthalene/anthracene as the side group, the polymer will selectively suspend certain SWNTs species with specific electronic properties. However, no obvious metallicity selectivity can be observed for PBMA and PMMA-c-PAMA, due possibly to the small aromatic functional groups (phenyl) and low loading of the anthracenyl groups in PMMA-c-PAMA.(The anthracenylmethyl to methyl ratio of PMMA-c-PAMA (Fig. 6.1c) was determined by its ^{1}H NMR spectra to be 3:10.)

In our previous experiments, the involvement of light in the separation was identified and the role of the photon induced dipole-dipole interaction as the driven force for metallicity selectivity was suggested for this class of polymer. With this mechanism, the requirements for selectivity are two-fold: firstly, the overlap of the polymer fluorescence with the specific nanotube species absorption[269] and secondly, the energy transfer of polymer fluorescence to

specific nanotube species with overlapping absorption. The diverse behavior regarding metallicity selectivity with the employed polymers can be interpreted with such criteria.

6.3.4 Fluorescence spectra of polymers.

Energy transfer from the aromatic functional groups of the polymers to SWNTs can be explored with polymer fluorescence spectra. Fluorescence spectra of polymer PMMA-c-PAMA are shown in Figure 6.5a while those of polymers PNMA and PAMMA have been reported previously.[269] The polymer PBMA was excluded from this investigation because it shows no fluorescence in our interested wavelength region (Figure 6.2e). This means that there will be no spectral overlap between polymer fluorescence of PBMA and SWNTs absorption and no energy transfer will occur. Low concentration solutions were employed in the test in order to reduce intermolecular interactions. The fluorescence spectra of 1.5×10^{-3} mol/L PMMA-c-PAMA in DMF were collected in the presence and in the absence of SWNTs. (The concentration of polymer was represented by the concentration of the corresponding aromatic chromophores.) To make the fluorescence intensity comparable, all variable experimental parameters were set consistently during the spectra collection with different polymers.

(a) (b)

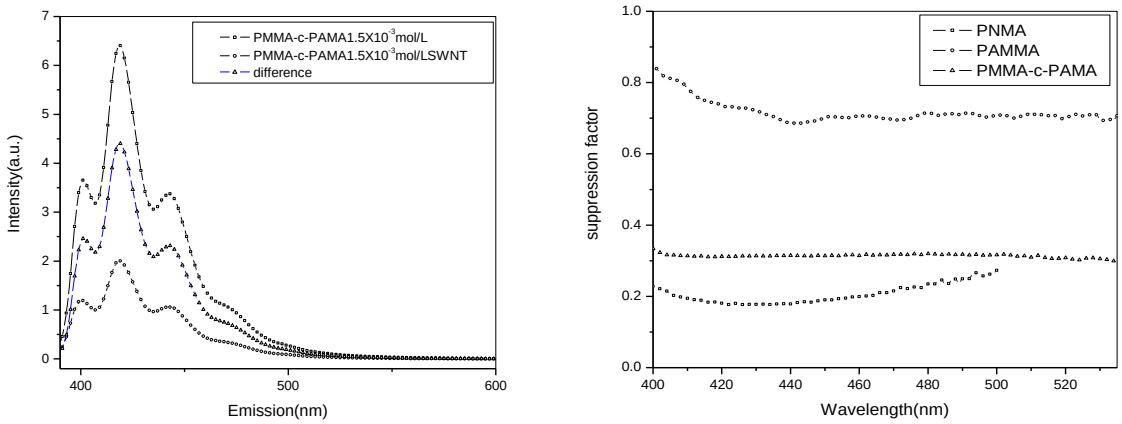

Figure 6. 5 (a) Fluorescence spectra of PMMA-c-PAMA in the presence and in the absence of SWNTs. (b) suppression factor of fluorescence signal intensities for all three polymers.

From Figure 6.5a, the intensity difference of the spectra, represented by the triangle curve suggests strong quenching by SWNTs. For the sake of convenient comparison, the wavelength-dependent suppression factor defined as the ratio of PLE intensity in the presence of SWNTs to its intensity in the absence of SWNTs at various wavelengths for all three polymers were calculated (Figure 6.5b). The suppression factors of PNMA and PAMMA are significantly more variable with wavelength than is that of PMMA-c-PAMA.

The non-constant reduction in polymer fluorescence for PNMA and PAMMA in the presence of SWNTs is hypothesized to be due to energy transfer to selected SWNT species resulting from dipole-dipole interaction. The constant proportionality for PMMA-c-PAMA suggests that there will possibly be no selective dipole-dipole interaction between this copolymer and *met*- or *sem*- SWNTs, which is substantiated by our experimental results. Moreover, the distinction between radiative and non-radiative energy transfer suggests that non-radiative transfer,[241] which is a consequence of the dipole-dipole interaction, is more likely to be responsible for the observed metallicity selectivity for PNMA and PAMMA.[269]

Our previous results[269] indicate that for PNMA and PAMMA, the variation in fractional suppression of the polymer photoluminescence with emission wavelength indicates that it is unlikely to interpret the photoluminescence suppression by the variation in chromophore concentration or absorption/emission cross section because the concentration of the chromophore is in its spectroscopic linear range. This corroborates our proposal of existence of some kind of coupling interaction, specifically energy transfer, between polymeric chromophore and SWNTs.

The different suppression tendency of the fluorescence for PNMA and PAMMA also suggests different interaction with SWNTs. It is the interplay of the spectral overlap and the tendency of energy transfer in energetically more favorable direction that determines the different photoluminescence suppression behaviors for PNMA and PAMMA, resulting in

their distinct metallicity selectivity. Tentatively, the polymers' metallicity selectivity is ascribed to different fluorescence quenching styles, associated with which is the underlying preferential dipole-dipole interaction.

In our tested system, the induced dipole-dipole interaction may, in some situations, be present with reasonable strength in the presence of light despite the existence of van der Waals interaction and π-π stacking interaction between SWNTs and aromatic side groups. The presence of such kind of interaction ultimately results in the polymers' diverse metallicity selectivity. Moreover, the different degree of polymer conformation relaxation induced by the solvent solvation complicates the interpretation. The polymers' unique diameter and metallicity selective behavior is due to the interplay and relative scales of all involved interactions. Other factors such as electronic interaction,[234,265] as well as structural compatibility may also contribute to the polymers' species discrimination. The effects of polymer backbone on the effective mapping and structural correlation between SWNTs and aromatic functional groups (involved π-π stacking interaction) may also need to be taken into consideration. For instance, the short "arm" between the polymer backbone and the anthracene groups makes its maximum contact with SWNT sidewall and optimum orientation unlikely. During the wrapping process, this type of strain effect between the polymer backbone and chromophore groups, which accompanies the attachment of functional groups onto the SWNT sidewall, may also alter their selectivity.

6.3.5 Standing time dependence.

Standing time has been identified as another factor which will influence the polymers' species selectivity. UV-Vis-NIR spectra and PLE maps were used to characterize different batches of separated SWNTs at different standing times after sonication. Only the polymer PNMA was selected for this investigation as its metallic species suspension decrease with standing time can be conveniently observed with UV-vis-NIR spectroscopy.

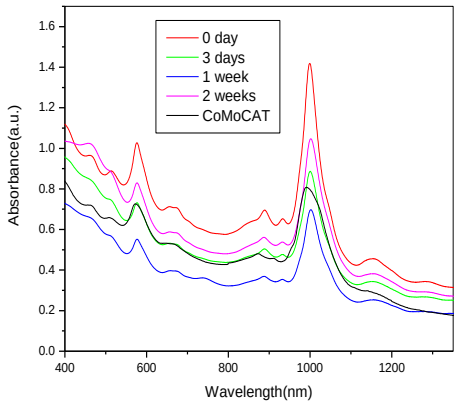

Figure 6. 6 Standing time dependence characterization by UV-Vis-NIR absorbance spectra of CoMoCAT produced SWNTs. standing periods of 0day, 3days, 1week, 2weeks for the supernatant solution with PNMA in DMF.

It is clear from the absorption spectra (Figure 6.6) that the standing time is a critical factor for high efficiency enrichment. The degree of enrichment varied with differing standing periods of 0 day, 3 days, 1 week, and 2 weeks, with longer standing time resulting in higher selectivity by PNMA. However, PLE maps of the supernatant solution at different standing times show no change with increasing standing time. (PLE maps are not shown here because they are quite similar to the map of the SWNT solution prepared with 2 weeks standing.)

The tendency of metallicity selectivity improvement with increasing standing time for this polymer can be interpreted as evidence that mapping of side functional groups onto the nanotubes after sonication is necessary for the mixture to form the lowest energy wrapping states. The adjustment of the polymer backbone conformation is anticipated to be associated with the adsorption/desorption mapping throughout the process. Concisely, strong sonication results in random mapping of the aromatic functional groups onto SWNT sidewalls as well as random wrapping of segments of polymer backbones around different SWNT species, both of which suppress differential selectivity. As a result, no metallicity selectivity can be observed soon after sonication. However, due to their structural similarity, SWNTs' affinity to the aromatic side groups (π-π stacking interaction) is higher as compared with that to the polymer

backbone. It can be anticipated that a lower energy conformation can be achieved by the polymer molecules adopting a "backbone outside and functional groups inside" conformation to wrap the SWNTs, provided the standing time is long enough. Diameter selectivity is the direct consequence of induced long range wrapping of the polymer chain around SWNTs, which seems to be relatively fast from our PLE maps at different standing times. On the other hand, the presence of light will induce interaction between chromophores on the polymeric side aromatic groups and SWNTs species with specific electronic properties. Longer standing time is required for the observation of metallicity selectivity for our specific system, possibly due to the weak character of the driving force responsible for metallicity selective mapping. The situation is further complicated by the strong pi-pi interaction of of SWNT sidewall with the side aromatic functional groups of the polymer, which results in relatively stable initial non-selective random wrappings which require time for mapping adjustment to lower-energy states which are more selective.

6.4 Conclusions

Four polymethacrylates with different aromatic side groups (PBMA, PNMA, PMMA-c-PAMA and PAMMA) have been employed here and in our previous study[269] (Chapter 5) in the electronic properties (*met*-/*sem*-) and diameter based species selection of SWNTs. Effective enrichment has been achieved. UV-Vis-NIR absorbance spectra and photoluminescence excitation maps suggest that these polymers have strong preferentiality to certain SWNTs species and the species selectivity depends on the polymer/solvent combination. In DMF, we previously showed that PAMMA preferentially disperses semiconducting SWNTs and PNMA selectively suspends metallic SWNTs while PBMA and PMMA-c-PAMA are shown in this paper to have no metallicity selectivity. All four polymers selectively suspend species with smaller diameters. Their selective behavior is quite sensitive to the solvent employed and highly similar tendency in diameter preference is observed upon

change of solvents. For all four polymers in CH_3CN, PLE spectra show that the semiconducting species suspended are mainly of smaller diameters while in $CHCl_3$, extracted semiconducting species are mainly of larger diameters. The parallel relationship between the diameters of the extracted species and the affinity between the polymers and solvents substantiate our argument that the uniform behavior of the solvent dependent diameter selectivity results from the conformation relaxation of polymer chain in solvents, which is believed to be mainly determined by the polymer backbone although the side groups do make some non-negligible contribution. On the contrary, the different species selective behaviors of various polymers in DMF suggest that the aromatic functional groups play some decisive role with respect to the metallicity selectivity. Both aromatic ring size and loading of the chromophores are essential factors. We propose that photon induced coupling is potentially responsible for their discrimination between *met*- and *sem*- SWNTs. Other factors, *i.e.* structural compatibility (simultaneous optimization of the effective mapping and structural correlation between SWNTs and aromatic functional groups) or electronic interaction,[234,265] *etc.* cannot be totally excluded from the contribution to polymers' species selective behavior and further study is required. Nevertheless, these polymethacrylates with pendant aromatic side groups facilitate the dissection of the contribution to chiral selectivity from the side chain and main chain constituents. Systematic study of the various chemical units' contribution to the separation effect is thus possible with rationally designed polymer structure. Standing time of the SWNTs solution after sonication is identified as another critical factor for the species enrichment.

Chapter 7 Resonance Energy Transfer (RET) induced Intermolecular Pairing Force: a Tunable Weak Interaction and its Application in SWNT Separation

7.1 Introduction

Resonance energy transfer (RET),[272] as a well established intermolecular interaction, has been the topic of tremendous investigation due to its fundamental nature, ranging from working as the prototype for test of the foundations of quantum mechanics and measurement theory to assisting in elucidation of the underlying mechanism by exemplified dynamics. The application of RET in optoelectronic device to adjust the desired wavelength for optimal energy conversion as well as in protein structure and conformation elucidation has been widely explored.[272] However, rare experimental attention has been paid to the intermolecular pairing force associated with RET. Theoretical investigation indicated that the application of a constant or time-varying radiation field will cause a shift in the energy levels of atomic or molecular systems and the existence of such kind of interaction was inconclusively suggested by sporadic experimental results.[273-274] To the best of our knowledge, however, no effort has been devoted to verify the existence of and make use of RET induced intermolecular pairing force.[274] In our previous experimental, some polymer shows different species selectivity behaviour in the presence and absence of optical illumination.[269] This illumination responsive selectivity was tentatively ascribed to the RET induced intermolecular pairing force. However, the involvement of RET in the process was not clearly demonstrated and deficient theoretical verification calls for further study.

In this report, two conjugated polymers[242] (Figure 7.1) with distinct optical properties were employed in SWNTs separation. The effect of illumination on the separation was investigated and the role of RET induced intermolecular pairing force in the species

enrichment was identified. With polymer's optical emission spectra overlap the intrinsic interband absorption features of SWNTs species, the polymer's selectivity was tuned with the RET induced intermolecular pairing force. The existence of such kind of interaction was thus successfully verified and our research is the first experimental demonstration of the application of RET induced intermolecular pairing force. Moreover, molecular quantum electrodynamics (MQE) theoretical calculation suggested that the RET induced intermolecular weak interaction scales with the illumination irradiance under certain circumstance.[274] This suggested the tunability of the interaction upon change of external experimental setups.

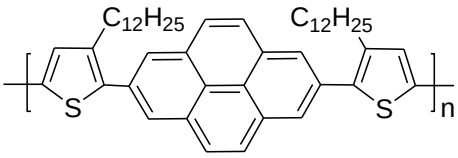

PPyrBT

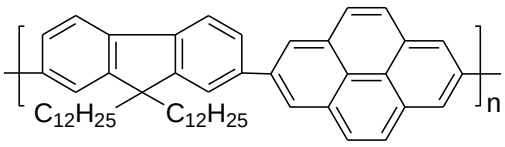

PFluPyr

Figure 7. 1 Structures of polymers used in this study.

7.2 Experimental section

7.2.1 SWNTs separation with polymers.

For the investigation of the photon-induced RET, All sample preparation and data collection was repeated after 3 months' standing in ambient indoor illumination (25 W incandescent lamp).

UV-Vis-NIR absorbance spectra of SWNTs suspended in the supernatant solution by PPyrBT was obtained from the clean SWNTs powders, which were resuspended in 1% SDBS/D_2O solution after polymer removal by thorough washing with THF.

7.2.2 Characterization Techniques.

For the collection of photoluminescence excitation (PLE) maps, fast scan was performed with 4nm excitation wavelength interval to minimize the effect of the RET/cascaded RET induced intermolecular pairing force on the signal strength of SWNT species.

7.3 Results

7.3.1 Photoluminescence-Excitation (PLE).

Photoluminescence excitation maps (Figure 7.2) were used to characterize the distributions of chiral species (n,m) of polymer suspended semiconducting chiral species as well as to investigate the RET between the conjugated polymers and SWNT species. As-received CoMoCAT SWNTs which were suspended in 1% SDBS solution in D_2O were also studied as a reference. For the sake of convenience and accuracy, the relative contents of the identified semiconducting species calculated from the PLE maps of both SDBS and polymers (PFluPyr & PPyrBT) suspended SWNTs were summarized in Table 7.1. The species contents were estimated from the PLE signal of various species calibrated with their corresponding PLE quantum efficiency by assuming that the reported PL quantum efficiencies can be applied to our system.[270]

(a)

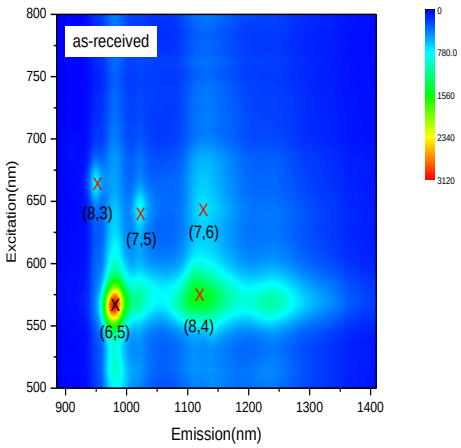

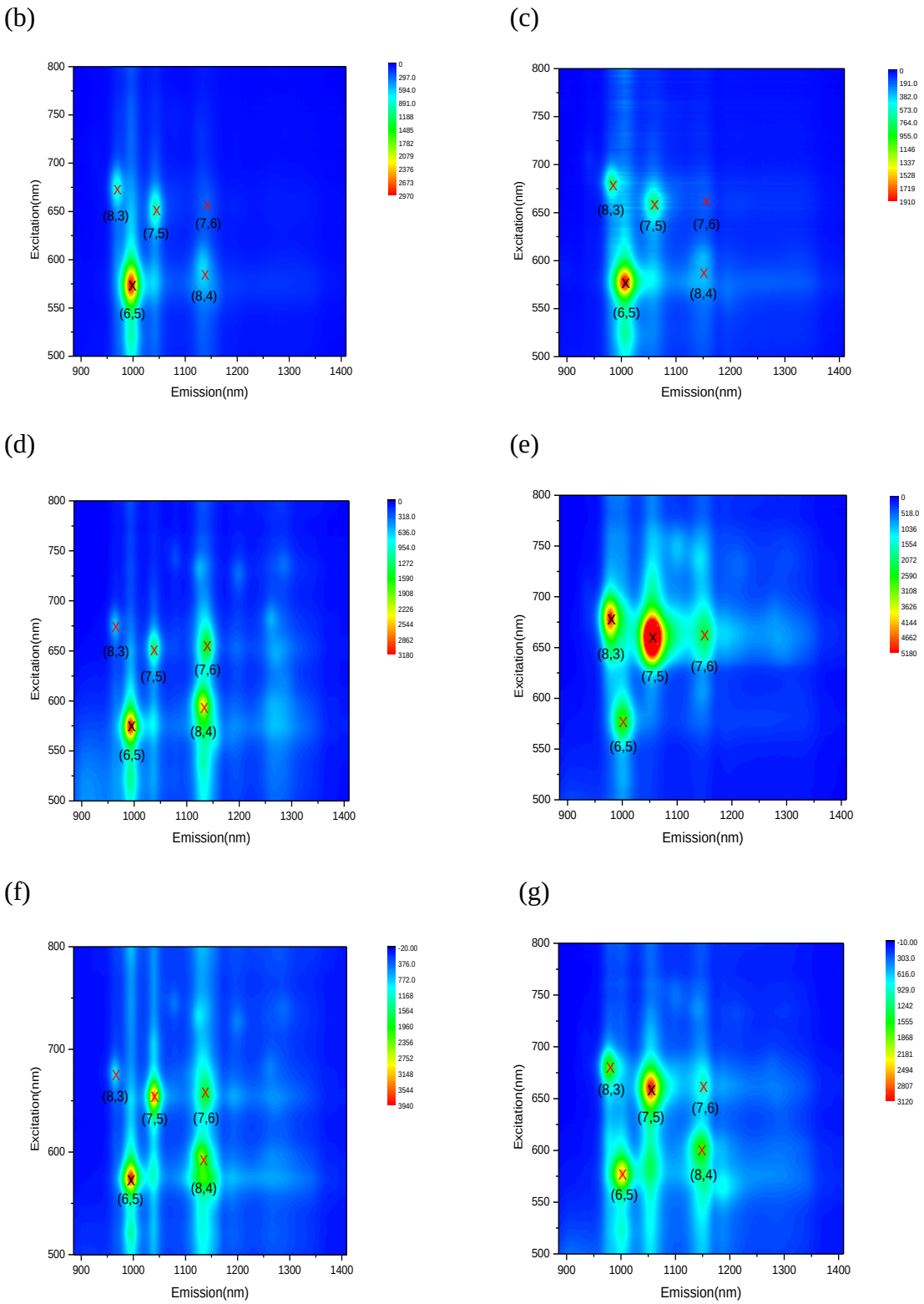

Figure 7. 2 PLE maps of SWNTs suspended with SDBS solution (a) and of SWNTs after chemical separation (b)-(e). (a) As-received CoMoCAT SWNTs dispersed using SDBS solution. (b-e) CoMoCAT SWNTs suspended with PFluPyr and PPyrBT with different standing time under room illumination. (b) PFluPyr suspended with immediate scan. (c) PPyrBT suspended with immediate scan. (d) PFluPyr suspended with three months standing under room illumination. (e) PPyrBT suspended with three months standing under room illumination. (f) PPyrBT suspended with three months standing in dark area. (g) Immediate successive scan of solution (e).

Table 7. 1 Tabulated values of the PLE peak intensities and calculated abundances for identified semiconducting species suspended with PFluPyr and PPyrBT with different standing time under room illumination/in dark area.

(n, m)	d_t[nm]	θ [°]	λ_{22}	Calculated Intensity	SDBS		PFluPyr				PPyrBT			
					Experimental Intensity	Species Abundance	Immediate scan		3months standing under illumination		Immediate scan		3months standing under illumination	
							Experimental Intensity	Species Abundance	Experimental Intensity	Species Abundance	Experimental Intensity	Species Abundance	Experimental Intensity	Species Abundance
(6,5)	0.75	27.02	566	0.67	3117	42.0%	2963	53.8%	3170	30.9%	1906	51.7%	2888	22.9%
(8,4)	0.83	19.19	589	0.46	1550	30.4%	645	17.1%	2349	33.3%	364	14.4%	Not available	Not available
(8,3)	0.78	15.40	665	2.13	768	3.3%	870	5.0%	645	2.0%	793	6.8%	5165	12.9%
(7,5)	0.82	24.54	645	0.71	832	10.6%	975	16.7%	1259	11.6%	763	19.6%	5173	38.7%
(7,6)	0.89	27.47	648	0.47	717	13.8%	288	7.5%	1602	22.2%	196	7.6%	2264	25.6%

(n,m)	d_t[nm]	θ [°]	λ_{22}	Calculated Intensity	PPyrBT			
					3months standing (dark area)		3months standing under illumination(successive scan)	
					Experimental Intensity	Species Abundance	Experimental Intensity	Species Abundance
(6,5)	0.75	27.02	566	0.67	3921	28.4%	2536	25.4%
(8,4)	0.83	19.19	589	0.46	2475	26.1%	1740	25.4%
(8,3)	0.78	15.40	665	2.13	944	2.2%	1823	5.8%
(7,5)	0.82	24.54	645	0.71	3470	23.8%	3119	29.5%
(7,6)	0.89	27.47	648	0.47	1886	19.5%	971	13.9%

As-received CoMoCAT SWNTs (Fig 7.2a and Table 7.1) are dominated by chiral species (6,5) and (8,4). Species (8,3), (7,5) and (7,6) are also present with obvious signals. The PLE maps of the SWNTs in the supernatant solution upon immediate scan (Fig 7.2b,c and Table 7.1) suggest that both polymers preferentially suspended chiral species (6,5), (7,5) and (8,3) provided that the standing time is not long enough for polymer conformation relaxation. To some extent, the extracted species are smaller (with d_{tube} = 0.75nm, 0.82nm and 0.78nm respectively) than the remaining species (8,4) and (7,6) (d_{tube} = 0.83nm and 0.89nm), which suggests a smaller size selectivity for both polymers.

Our previous publications suggests that the interplay of various weak interactions such as Van der Waals interaction, π-π stacking interaction and RET induced intermolecular pairing force, etc, necessitates relative long standing time to bring out the if existed RET induced intermolecular pairing force as the decisive factor for SWNT species enrichment.[269,275] As a natural following, we intentionally put the sample under room illumination for three months before we repeated the centrifugation as well as PLE scan and the resulted PLE maps are also included in Figure 7.2(d,e). With three months standing under

room illumination, substantial changes of the species distribution can be observed from the PLE maps. In the case of PFluPyr, (8,4) and (7,6) were selectively suspended upon three months standing under room irradiation as contrast to its selectivity to smaller diameter species suggested by immediate scan. More interestingly, with PPyrBT as the separating agent, (7,5), (8,3) and (8,4) are dramatically enriched under room illumination. The different species selective behaviours before/after three months standing suggests that some weak interaction will slowly modify the equilibrium process, adsorption/desorption of the polymers onto/from the sidewall of SWNTs, of the mixture so that more stable stacking state can be established. The change of selective behaviour of PFluPyr is presumably resulted from the interplay of Van der Waals interaction and π-π stacking interaction while in the case of PPyrBT, it is the RET induced intermolecular pairing force that plays the leading role so that E_{22} dependent species enrichment behaviour (with the detailed mechanism discussed in the discussion section) can be observed. In the following discussion, we will focus on the behaviour of PPyrBT since E_{22} dependent species enrichment can only be observed for PPyrBT, in which RET induced intermolecular pairing force is responsible. It is the RET induced intermolecular pairing force that is more fruitful and shows more significant potential for future application.

One concern about above discussion is that the signal intensity change of SWNT species in PLE map (Figure 7.2e) was possibly resulted from the fluctuation of species' absorption/emission cross section due to the variation of their micro environment resulted from polymeric adsorption/desorption or conformation change. To eliminate this possibility, we employed UV-Vis-NIR absorbance spectrum and Resonance Raman Scattering (RRS) Spectra to characterize the clean SWNTs powder and the discussion of the result was included in the following section. The removal of the polymer was achieved by thorough wash with THF and facilitated by the RET induced intermolecular pairing force.

In order to confirm the crucial contribution of the illumination to PPyrBT's selectivity, control experiment was conducted in parallel. Freshly prepared SWNT suspension with PPyrBT solution was placed in dark area for three months before centrifugation and PLE scan was performed. The resulted PLE map was included in Figure 7.2f. With three months standing in dark area, different species distribution (Figure 7.2f and table 7.1) was resulted as compared to the case with exposure to room illumination (Figure 7.2e and table 7.1). S_{22} dependent species selectivity in which (8,3), (7,5) and(7,6) are preferentially suspended can be observed under room illumination while (7,5), (8,4) and (7,6) are selectively suspended instead with dark area standing. The PPyrBT's behaviour in dark area indicates a diameter selectivity since the suspended species are somewhat larger than the remaining species (6,5) and (8,3).

The modification of illumination (RET induced intermolecular pairing force) on the species abundance was also confirmed by the distinct PLE maps upon immediately successive PLE scans. After collection of the PLE map (Figure 7.2e), successive PLE scan was immediately conducted and the resulted PLE map was included in Figure 7.2g. Prominent difference between Figure 7.2e and Figure 7.2g can be observed. The different species distribution was attributed to RET induced intermolecular pairing force since the existence of such kind of intertube interaction will inevitably facilitate SWNTs aggregation. Consequently, modification of the PLE intensity of various species can be observed because the PLE efficiency of SWNT species strongly depends on whether they are individually suspended or bundled. The most prominent difference (Figure 7.2e Vs. Figure 7.2g) is the brought out of species (8,4) after the initial PLE scan. Due to its trivial species content, (8,4) can hardly be detected in the first scan and its role in RET process can thus be neglected. Since RET will inevitably results in the aggregation of species (6,5), (8,3), (7,5) and (7,6) which are anticipated to be involved in the RET process, their species contents determined

from PLE measurement will be dramatically suppressed. Consequently, species (8,4) was brought out in the immediate successive scan.

7.3.2 UV-Vis-NIR and Resonance Raman Scattering (RRS) spectra.

UV-Vis-NIR absorption spectrum of post-separation suspended SWNTs for PPyrBT is shown in Figure 7.3. Also included is the absorbance spectrum of the SWNTs suspended in D_2O solution with ionic surfactant SDBS, which shows no preferentiality to any SWNT species.

(a) (b)

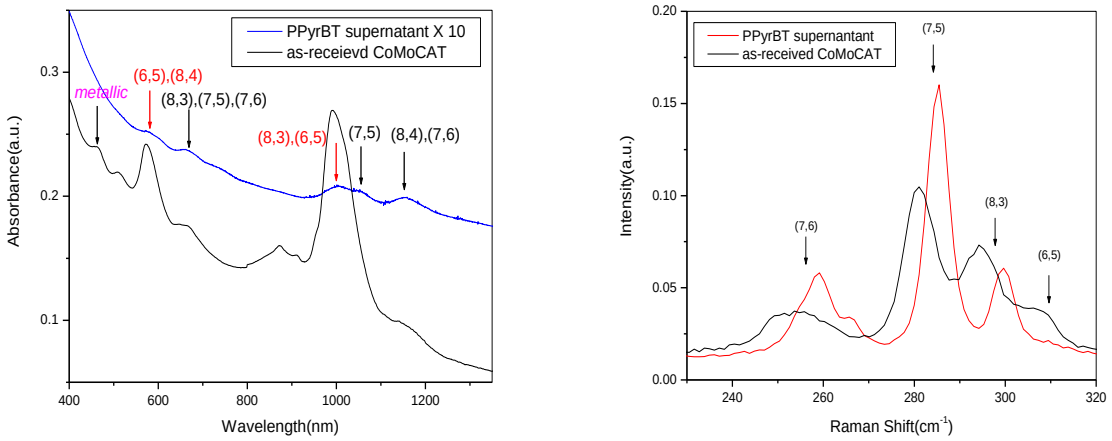

Figure 7. 3 UV-Vis-NIR absorbance spectrum and Resonance Raman Scattering (RSS) spectra of PPyrBT's suspended CoMoCAT SWNTs and as-received CoMoCAT SWNTs. (a) UV-Vis-NIR absorbance spectrum of supernatant fraction of PPyrBT enriched CoMoCAT SWNTs redispersed in SDBS/D_2O solution. (note: The black SWNT lines are spectra of the "as received" SWNTs suspended in SDBS/D_2O solution.) (b) With a 633 nm laser, RRS Raman spectra of PPyrBT suspended CoMoCAT SWNTs after polymer removal and as received CoMoCAT SWNT.

With the peak intensities proportional to species concentrations, optical absorbance spectra can be used as a proxy for the estimation of the contents of different SWNT species. Spectroscopic features of the interband electronic transitions arising from M_{11} band of metallic SWNTs as well as E_{11} and E_{22} bands of semiconducting SWNTs was covered in the optical absorbance spectra.

Figure 7.3a includes the optical absorbance spectra of reference unseparated SWNTs in SDBS solution as well as polymer suspended SWNTs, which were collected upon polymer

removal and resuspended in SDBS/D_2O solution. CoMoCAT SWNTs have prominent intrinsic absorption features from 400 to 510nm for metallic species and from 510 to 1350nm for semiconducting species. The absorbance features at 800-1350nm and 510-800nm correspond to S_{11} and S_{22} interband transitions respectively.[103,220,254] The sharp absorbances at about 576nm and 1000nm are the characteristic absorbance features of the E_{22} and E_{11} interband transitions of tube (6,5). The relative content of the metallic SWNTs and the semiconducting SWNTs was estimated from the M_{11}/S_{22} peak intensity ratio because S_{22} absorbance feature is more stable upon environmental doping.

Figure 7.3a shows that (6,5) content dramatically decreased in the PPyrBT suspended SWNTs, this confirms the above conclusion from PLE map analysis, which suggest the preferential suspension of (8,3), (7,5) and (7,6). In the absorbance spectra, the peaks were tentatively assigned to different chiral species. The ratio of the species peak intensities is qualitatively in good agreement with the species distribution suggested by PLE maps. This corroborate our PLE analysis and eliminate the possibility that the signal intensity change of SWNT species in PLE map is due to the fluctuation of SWNT species' absorption/emission cross section due to the variation of their micro environment.

Moreover, the *met*-SWNTs feature (at around 460nm) is more dramatically suppressed in the spectrum of PPyrBT suspended SWNTs than are the *sem*-SWNTs features, which suggests the PPyrBT's selectivity towards semiconducting species.

The comparison between RRS spectra, taken using a 633nm laser, of PPyrBT suspended CoMOCAT and as-received CoMoCAT was schemed in Figure 7.3b. With 633 nm excitation, our interested species can all be effectively probed.[244,248] The species abundance indicated by the RRS spectra is in good qualitative agreement with the species distribution suggested by PLE maps and UV-Vis-NIR absorbance spectra.

7.3.3 Electrical measurement.

To independently assess the PPyrBT's selectivity to semiconducting species, we fabricated short channel thin film FET devices using the semiconductor enriched SWNTs and investigated their electrical properties. PPyrBT-separated semiconductor enriched SWNTs (supernatant fraction) resuspended in SDBS/D_2O solution after polymer removal were used for device fabrication. Drop-casting method was employed for the fabrication of thin film FETs. To the underlying Si substrate which functioned as the gate electrode was applied a gate bias to modulate the charge carrier concentration in the SWNTs network. The electrode configuration and a typical device performance as well as AFM image of the SWNT network of the test device are shown in Figure 7.4.

(a)

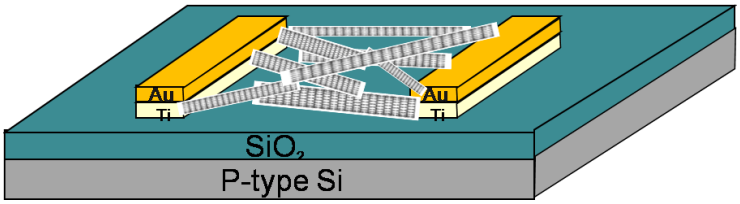

(b)

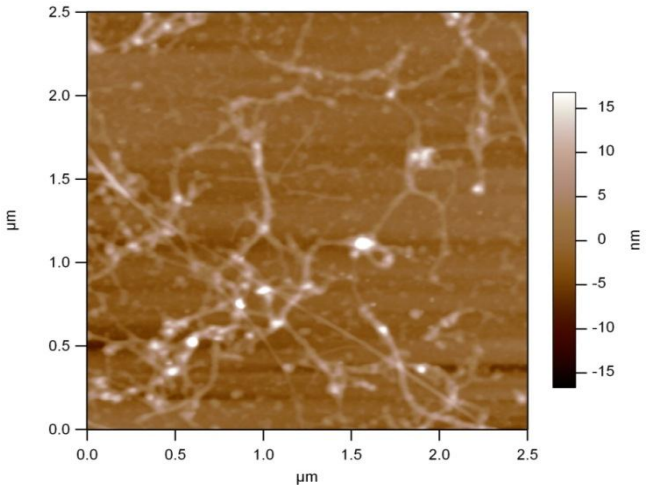

(c) (d)

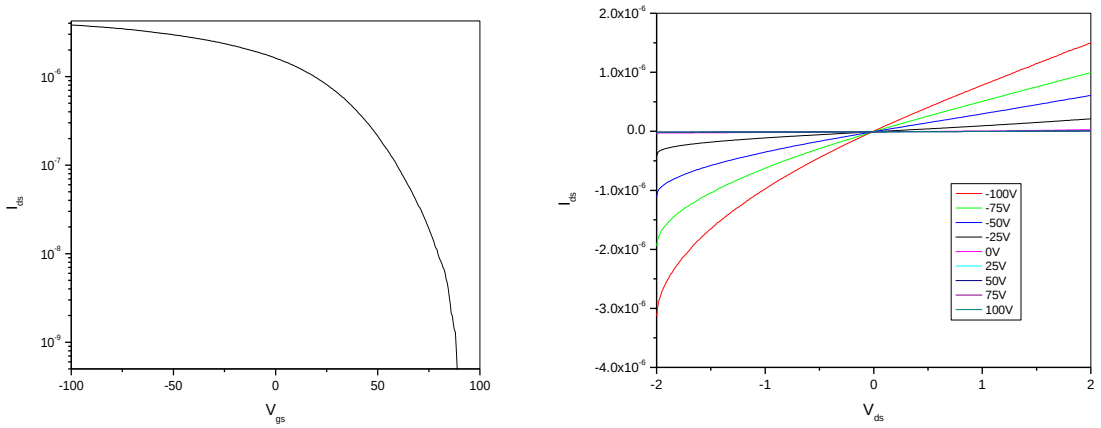

Figure 7. 4 FET fabricated with enriched semiconducting SWNTs as active channel using PPyrBT. (a) Device configuration; (b) AFM image of the SWNT network in the channel; (c) Transfer characteristic (I_{ds}-V_{gs}) of a representative device at V_{ds}= 2 V; (d) Current-Voltage characteristics (I_{ds}-V_{ds}) of the device at V_{gs} ranging from -100 to 100 V with the step of 25 V from bottom to top.

The devices exhibited good FET characteristics with on/off ratio of about 10^4, this confirms the enrichment of semiconducting SWNTs as compared to the performance of FET devices fabricated with the as-received SWNTs (most devices shows on/off ratio of <10, as shown in our previous publication). Moreover, the improvement of the on-state current of the devices (with respect to the device performance indicated in our previous publications) are presumably result from the content decrease of smallest diameter species (6,5) with lower on-current carrying capacity due to the higher Schottky barriers and non-ohmic contacts.[73,267-268] The high (about 10^4) FET on/off ratio substantiates our conclusion drawn from UV-Vis-NIR absorbance spectra.

7.4 Theory

In the context of molecular quantum electrodynamics, the interaction energy between two molecules with distinct electronic band structures was calculated and comprehensively understood, both in the absence and in the presence of irradiation.[273-274] It was suggested that the intermolecular interaction beyond the orbital overlap is resulted from the exchange of real or virtual photons between them. Typically, in the near zone limit where the intermolecular

distances are small compared to longest wavelengths of absorption or fluorescence, the intermolecular coupling is essentially instantaneous. The intermolecular interaction energies between two free rotating molecules in their ground states can be expressed by the following expression, which is the Van der Waals-London dispersion energy.[274]

$$\Delta E_{\text{NZ}} = -\frac{3}{64\pi^2\varepsilon_0{}^2R^6}\alpha(A;0)\alpha(B;0)\hat{E} \quad (1)$$

Where $\alpha(\varepsilon,0)$ (ε = A, B) is the static isotropic electric dipole polarizability of molecules ε; ε_0 and R stand for vacuum permittivity and intermolecular separation respectively while the scaled energy is

$$\hat{E} = \frac{2E^AE^B}{E^A+E^B} \quad (2)$$

With E^{ε} (ε = A, B) denoting the lowest energy transition in molecules ε.

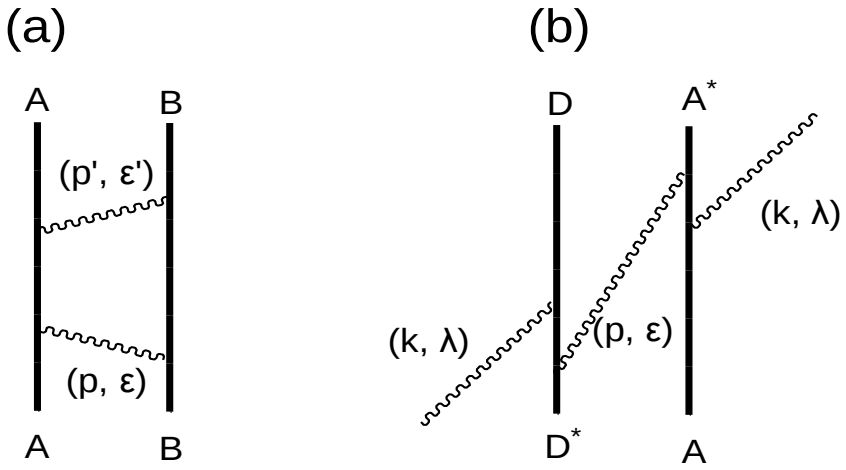

Figure 7. 5 Representative Feynman diagrams with time progresses upward used for related calculations. (a) One of the twelve time-ordered graphs used for the calculation of ground state dispersion potential; (b) One of the twenty four time-ordered graphs used for the calculation of RET induced intermolecular energy shift in a radiation field.

The Feynman diagram used to calculate the ground state intermolecular interaction is schemed in Figure 7.5a.

The expression for the radiation induced intermolecular dispersion energy has also been derived in the context of related *molecular quantum electrodynamics* theory.[273-274] However, some revision is needed before the theory can be adopted in our experimental phenomenon

interpretation. The detailed elucidation of the derivation of the radiation induced intermolecular dispersion force will not be included. The most obvious difference is that RET is unidirectional (from donor PPyrBT to acceptor SWNT species) rather than the usually assumed bidirectional behaviours of RET. In parallel with the situation of above discussion regarding two free rotating molecules in their ground states, near zone limit expression with molecular and pair orientational averaging is listed below.[273-274]

$$< \Delta E_{NZ} >= -\frac{11Ik^2}{120\pi\varepsilon_0{}^2R}\alpha(D;k)\alpha(A;k) \quad (3)$$

Where the $\alpha(\varepsilon,k)$ (ε = D, A) is molecular dynamic polarizability and I stands for illumination irradiance. R, k and ε_0 stand for intermolecular separation, wave vector of the illumination and vacuum permittivity respectively. The derivation of above equation was based on the assumption of laser illumination (with high irradiance I) so that the irradiance decrease due to absorption can be neglected. For the purpose of convenience, we will also neglect the irradiance decrease due to polymer absorption in the following section so that the above equation can be applied.

The above expressions were derived following similar calculation outlined in the related *molecular quantum electrodynamics* textbook in the fourth order optical process approximation by neglecting the molecular vibrations.[273-274] It can be anticipated that with the inclusion of molecular vibration, modification of the expression is necessary. Coupling of the intrinsic electronic states of the acceptor to states in the donors is essential for energy transfer process;[272] the near zone limit should thus be expressed as:

$$< \Delta E_{NZ} >= -\frac{11I^{1/2}\hbar^{1/2}k^{7/2}k'^{1/2}}{240\sqrt{2}\pi^{5/2}\varepsilon_0{}^2R}\alpha(D;k)\alpha(A;k') \quad (4)$$

since the involvement of molecular internal conversion/surrounding solvent molecules will assist in the energy dissipation so that for acceptor A, it was in an intrinsic electronic excited state corresponding to pumping from photon k' rather than k. It is the intrinsic electronic

excited states that will be coupled to the states in the donor. From this point of view, the wave vector of the donor (k) in the equation corresponds to its emission wavelength rather than its absorption wavelength. Due to the universally existed Stokes shift, emission wavelength of donor always differs from its absorption wavelength. In this case, the illumination irradiance I ($n\hbar c^2k/V = n\hbar c^2k^4/8\pi^3$) in the equation should thus be replaced by $\hbar c^2k^{7/2}k'^{1/2}/8\pi^3$ and the near zone limit, with approximation $k \approx k'$ for the purpose of simplifying the calculation, can be expressed as:

$$< \Delta E_{NZ} >= -\frac{11\hbar c k^{11/2} k'^{1/2}}{960\pi^4 \varepsilon_0^2 R}\alpha(D;k)\alpha(A;k') \quad (5)$$

Although the nature of the attraction energy between two particles (SWNT species and conjugated polymer) is the same as that between two molecules, integration of all the interaction between molecules from two particles will result in a totally different dependence of force on distance.[276] As an approximation, we will use equation (1) since no exact Van der Waals-London dispersion energy between SWNTs and conjugated polymers are available. Comparing with the above Van der Waals-London dispersion energy, which has inverse sixth power dependence and a much more rapid falloff, radiation induced intermolecular dispersion force can be appreciable for a large number of pairs as in a molecular assembly. Another method by which $<\Delta E_{NZ}>$ may be increased in magnitude is if the frequency of the incident laser is tuned to near resonance with a molecular transition frequency, thereby resonantly enhancing the dynamic polarizability.[273-274] In the case of RET as expressed by equation (5), two fold resonances were involved and the induced intermolecular interaction was thus further enhanced.

7.5 Discussion

The well-known involvement of all kinds of weak interaction, such as Van der Waals interaction, π-π stacking interaction and RET induced intermolecular pairing force, etc. is

responsible for the diverse SWNT species selective behaviours of various molecules or polymers. In our case with PPyrBT as the dispersant, the presence of the RET induced intermolecular pairing force is responsible for the change of the species selective behaviour upon three months' room illumination. The significant role of RET induced intermolecular pairing force for PPyrBT's selectivity was substantiated by its different selective behaviours in the presence and absence of illumination. As a contrast, no such kind of E_{22} dependent species selectivity can be observed for dispersant PFluPyr, which is presumably due to the trivial role the RET induced intermolecular pairing force played with respect to Van der Waals interaction and π-π stacking interaction. The existence of RET between polymer PPyrBT and SWNTs is verified by the PLE map which was shown in Figure 7.6b. Also included is the PLE map of the SWNTs suspension with dispersing agent PFluPyr (Figure 7.6a). The emission range was set to be from 950nm to 1200nm for the purpose of convenient comparison. This can ensure the coverage of PLE signals of presented species. The excitation wavelength starts at 300nm and ends at 800 to ensure all possible excitation of polymers and SWNTs. The interval between successive excitation wavelengths was set to be 4nm to facilitate a fast scan.

(a) (b)

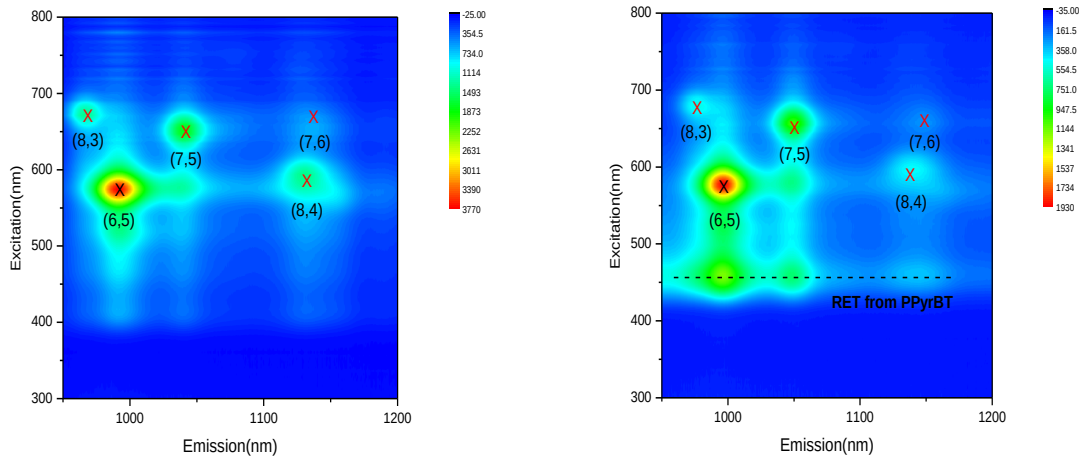

(c)

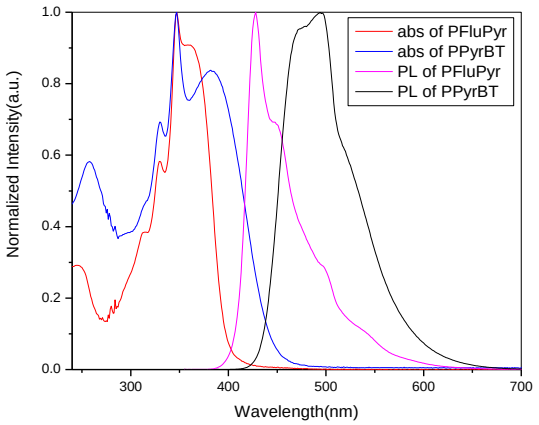

(d)

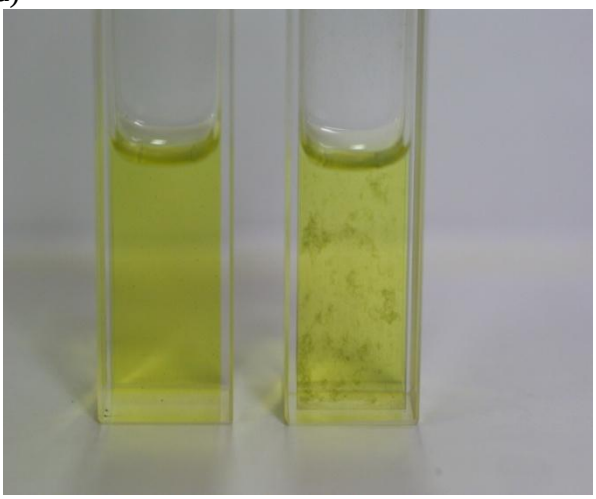

Figure 7. 6 (a,b) PLE maps of PFluPyr and PPyrBT suspended SWNTs with fast scan. (a) PFluPyr; (b) PPyrBT; (c) UV-vis absorption (abs) and photoluminescence (PL) spectra of PFluPyr and PPyrBT in THF solution; (d) picture of PPyrBT suspended SWNTs solution after PLE scan (cuvette on the right side) along with the solution from the same batch under room illumination for the same period of time (cuvette on the left side).

The existence of RET between PPyrBT and SWNT species is manifested in the PLE map (Figure 7.6b), which is indicated by the dashed line corresponding to PPyrBT excitation and SWNT emission. Associated with the RET process between PPyrBT and SWNT species was inevitably the RET induced intermolecular pairing force, which will drag them together. It is the RET induced intermolecular pairing force that is responsible for PPyrBT's SWNT species selectivity dependent on SWNTs' E_{22} energy as well as its preferentiality towards semiconducting species. However, no obvious RET from PFluPyr to SWNT species can be observed from the PLE map. This can explain the different illumination responsive behaviours of PPyrBT and PFluPyr as well as the distinct selective behaviour of PPyrBT in the presence of illumination against that in the dark area.

It is also worth pointing out that, in our system, it is the polymers that in the vicinity of SWNT species that will assist in SWNTs' solvation. In this regard, it is reasonable to confine our following discussion to the near zone limit where $kR<<1$ for all kinds of weak interaction.[272-274] In the near zone limit, nonradiative RET mechanism dominates and Förster

theory can be applied. The fluorescent behaviour of the conjugated polymer in the absence and presence of SWNTs (Figure S1 in supporting information) suggested that this is a reasonable starting point since fluorescence of polymer is more prominent suppressed beyond the spectra overlap region as contrast to the suppression in the overlap region. The following Förster equation defines the essential elements which are essential for the RET efficiency (*E*).[272]

$$k_{RET} = \frac{1}{\tau_D^0}\left[\frac{R_0}{r}\right]^6 \tag{6}$$

With

$$R_0^6 = (8.79 \times 10^{23})k^2 n^{-4} \Phi_d J_{da} \tag{7}$$

in which τ_D^0 is the lifetime of the donor in the absence of transfer; R_0 is the donor-acceptor distance (Å) when the efficiency of RET is 50%; Φ_d is the quantum efficiency of the donor; k^2 is the Förster orientation factor; n is the refractive index of the solvent (which is generally assumed to be isotropic); and J_{da} is the overlap of the donor emission spectrum with the absorption spectrum of the acceptor. The Förster equation suggests that both donor-acceptor distance and the spectra overlap of donor emission with acceptor absorption are quite critical for nonradiative RET.[272]

For the purpose of qualitative analysis, the absorption and photoluminescence spectra of both polymers are included in Figure 7.6. It follows from the Förster equation (7) that the exciton energy on PPyrBT is more likely to be transferred to PLE covered SWNT species than that of exciton energy on PFluPyr since PPyrBT's photoluminescence red-shifted dramatically as compared to PFluPyr so that the overlap of PPyrBT emission and SWNTs absorption, *i.e.* J_{da}, is more prominent. Our argument is probably strengthened in the case of SWNTs suspension since higher concentration solutions were used for SWNTs dispersion. Red-shift of the photoluminescence can be anticipated due to the presence of excimer/aggregation formation.[241] The PLE maps of SWNTs suspensions confirmed this

qualitative argument. Although radiative RET will also inevitably contribute to the PPyrBT-excitaion SWNT-emission PLE signal, it does not contradict above argument.[241,272-274] The intermolecular pairing force associated with RET process is responsible for different illumination responsive behaviours of PPyrBT and PFluPyr. The distinct selective behaviours of PPyrBT in the presence of illumination against that in the dark area is also explainable with RET induced intermolecular pairing force taken into consideration.

Detailed analysis of the PLE maps 6b also suggests that the PPyrBT's discrimination between (7,5) and (6,5) is resulted from their distinct dynamic polarizability although RET from PPyrBT to both (7,5) and (6,5) is possible.

The existence of significant RET induced intermolecular pairing force was also verified by the agglomeration of SWNTs upon PLE scan. Obvious precipitation can frequently be observed even with short period of exposure to illumination. Figure 7.6d shows the picture of the SWNTs sediment upon a fast PLE scan along with the control solution under room illumination with the same standing time. The SWNT precipitation is quite obvious and is presumably resulted from RET/cascaded RET induced intermolecular pairing force between different SWNT species. SWNT aggregation will certainly be substantially facilitated by the universally existed Van der Waals-London dispersion energy, which has inverse sixth power dependence and a much more rapid falloff. This photon assisted precipitation was indeed intentionally employed in PPyrBT's removal in order to collect neat SWNTs powder from the supernatant suspension. However, with low irradiance under room illumination, long standing time is needed to observe the effect of RET induced intermolecular pairing force due to the slow conformational dynamics limited by the rigid polymer backbone. As a contrast, for flexible polymer, much shorter standing time is enough for the observation of such effect.[275] The standing time dependent behaviour is conceptually understandable. Since the RET induced intermolecular dispersion energy with its magnitude expressed above will be

generated upon the completion of the whole cycle of the RET process, from polymer excitation to SWNT deactivation, continuous illumination with enough time is needed for the completion of enough cycles of the RET process so that the species selectivity resulted from the associated attractive force can be observed. The involvement of Van der Waals interaction and π-π stacking interaction will surely elongate the standing time needed for the observation of the selectivity. It is interesting to note that the polymer-SWNT separation and Förster orientation factor, owing to the existence of significant RET induced intermolecular pairing force, more probably keep changing during the illuminative standing.[272] However, the effect of RET induced intermolecular pairing force is overall attractive and will draw polymer and SWNTs together as long as their separation is beyond the orbital overlap, which is true for most cases of non-covalent functionalization. Once the polymer-SWNT is scaled down to the orbital overlap, the interactions are overall a repulsive character, resulting from the interplay of exchange interaction, Pauling exclusion and charge transfer effects, *etc*.[274]

7.6 Conclusions

Two conjugated polymers with distinct optical properties were employed in the selective suspension of CoMoCAT SWNT species. Their different illumination responsive behaviour verified the involvement of RET induced intermolecular pairing force, which is a tuneable interaction with its magnitude scales with an external stimuli parameter, *i.e.*, illumination irradiance *(I)*. The distinct species selectivity behaviour of PPyrBT in the presence of illumination against that in the absence of illumination suggests the significant role of this kind of weak interaction as contrast to Van der Waals interaction and π-π stacking interaction. This suggest a facile technique to alter the intermolecular interaction between molecules/polymers and SWNT species so as to modify their selective behaviour towards specific species. The species selectivity driven by this novel technique is interband transition (E_{ii}) energies dependent. Many fluorescent molecules/polymers with appropriate optical

properties are thus suggested to be the potential candidates for SWNTs separation. It is the first time that RET induced intermolecular pairing force was verified and applied. Also, with RET induced intermolecular pairing force taken into account, reasonable interpretation of the conflicting data after some kind of optical process can be made since the weak interaction, if presented, is strong enough to induce SWNTs aggregation so that PLE signal of the involved species will be dramatically suppressed. Moreover, since the derivation of the expression of RET induced intermolecular pairing force was not confined to SWNT and conjugated polymer, the above conclusion can be applied to whatever entities as long as they are electronically neutral and photon-induced RET can happen between them. The significant RET induced intermolecular pairing force thus makes direct manipulation of molecules/particles possible and suggests its future application in molecular engineering.

Chapter 8 Conclusions & Recommendations

8.1 Conclusions

In this thesis, the experimental results enable the following conclusions to be made:

Amide-functionalized pyrene derivatives are effective in separation of HiPco SWNTs according to their electronic properties.

Three similar amide-functionalized pyrene derivatives with different alkyl chain lengths between the amide groups and pyrene moieties have been successfully synthesized and effectively employed in the separation of HiPco SWNTs according to their electronic structures (metallic/semiconducting) and diameters. All three derivatives are selective to metallic SWNTs with pb-18-C-6 and pc-18-C-6 selective to large diameter (D>1nm) metallic SWNTs while the third compound, pa-18-C-6, selective to small diameter (D<1.03nm) ones due to the ketone-to-enol rearrangement. The rearrangement was corroborated by Fourier Transform Infrared spectroscopy data. For their discrimination between different semiconducting species, the results indicate pb-18-C-6 is selective to large diameter ones while pa-18-C-6 and pc-18-C-6 show no selectivity. The selectivity for metallic SWNTs in the solution is confirmed by a 10-fold decline in thin-film SWNTs network resistivity (from 43 $S \cdot m^{-1}$ to 4.3 $S \cdot m^{-1}$) after depletion of metallic SWNTs by a four-pass selection procedure using pa-18-C-6 and pc-18-C-6 surfactants alternately. Further, the lower thermal stability of the network resistivity of the precipitate SWNTs and higher thermal stability of the network resistivity of the supernatant SWNTs corroborated the above conclusion.

Polymethacrylates with Pendant Aromatic Functional Groups are quite efficient in selection of certain species of CoMoCAT SWNTs.

Three polymethacrylates, PNMA, PAMMA and PMMAFA, with pendant aromatic functional groups have been demonstrated to be pretty efficient in the separation of SWNTs

according to their electronic properties (*met*-/*sem*-) and diameters. These polymers have strong selectivity towards certain SWNTs species with specific electronic properties and diameters. The species selectivity depends dramatically on the polymer/solvent combination. In DMF, PMMAFA and PAMMA preferentially disperse semiconducting SWNTs while PNMA preferentially disperses metallic SWNTs. All three polymers preferentially disperse small diameter SWNTs in DMF. The selectivity of PNMA (to metallic species in DMF) is sensitive to the solvent employed. In CH_3CN, PNMA is selective to smaller diameter semiconducting species while larger diameter semiconducting species are preferentially suspended in $CHCl_3$. The solvent effects suggest the mechanism of diameter selectivity, which results from a change of polymer conformation. The change of the polymer fluorescence in the presence of SWNTs was tracked and the involvement of photon in the enrichment process is identified and the photon induced dipole-dipole interaction is probably responsible for the metallicity selectivity in DMF. The diverse selective behavior of these polymers is resulted from the interplay between photon induced dipole-dipole interaction and polymer conformation change.

Different Building Blocks' Contribution to the Enrichmentment of CoMoCAT Single-Walled Carbon Nanotubes with Aromatic Group functionalized Polymethacrylates is substantiated.

Systematic study of separation of SWNTs with aromatic group functionalized Polymethacrylates (PBMA, PNMA, PMMA-c-PAMM and PAMMA) confirmed that the species selectivity is highly sensitive to the polymer/solvent combination. In DMF, PAMMA were found preferentially disperses semiconducting SWNTs and PNMA preferentially disperses metallic SWNTs while PBMA and PMMA-c-PAMA show no metallicity selectivity. All four polymers preferentially disperse smaller diameter species. Their selectivity is quite sensitive to the used solvent and highly similar tendency can be observed

upon change of solvents. In CH_3CN, they are selective to smaller diameter semiconducting species while larger diameter semiconducting species are preferentially suspended in $CHCl_3$. This corroborated our argument that the uniform behavior of the solvent dependent diameter selectivity is resulted from the polymer conformation in solvents. On the contrary, the comparison of the species selectivity of different polymers in DMF indicates that the side groups play some decisive role with respect to the metallicity selectivity. The diversity of their behavior is explainable with our proposed mechanism. Photon induced coupling is potentially responsible for their discrimination between *met*- and *sem*- SWNTs.

The Role of RET (resonance energy transfer) induced intermolecular pairing force has been identified.

Two conjugated polymers with distinct optical properties were employed in SWNT species enrichment. The involvement of RET induced intermolecular pairing force was brought out by their different illumination responsive behaviours. The magnitude of this kind of weak interaction scales with an external stimuli parameter, *i.e.*, illumination irradiance *(I)* and thus tuneable. This suggest a facile technique to modify molecules/polymers' selectivity towards some specific SWNT species by altering the corresponding intermolecular interaction. The species selectivity driven by this novel technique is dependent on SWNT interband transition (E_{ii}) energies as well as dispersant's fluorescent properties. Many fluorescent molecules/polymers with appropriate fluorescent properties are thus suggested to be potential separating agents towards certain species.

8.2 Recommendations

As a natural following, extensions to this work can be considered for investigation based on our previous mechanism understanding.

1. Polymers with distinct optical properties (especially their fluorescence properties) are probably appropriate candidates for certain SWNT species enrichment. This is due to the fact that the electronic/optical features of aromatic molecules/units strongly dependent on their conjugation area. The increase of the size of the aromatic groups will shift the molecules/polymers' preferentiality towards SWNT species with higher interband transition energies provided that the RET induced intermolecular pairing force plays the leading role during the selective suspension of SWNT species. Optical filter and light source with continuous wavelength emission may be necessary for the investigation in order to control the wavelength of the illumination. This will be beneficial for the identification of the effective wavelength regarding SWNTs species enrichment.

2. Polymers with high absorption coefficients such as Poly[9,9-di-(2'-ethylhexyl)fluorenyl-2,7-diyl] (UV absorbance$_{240nm}$ 0.271, $\lambda_{max378nm}$ 0.864), Poly[(4,4'-hexafluoroisopropylidene)diphthalic anhydride-*alt*-ethidium bromide] (UV absorbance$_{278nm}$ 1.3085, $\lambda_{max731nm}$ 0.0324) and Poly(pyromellitic dianhydride-*alt*-ethidium bromide) (UV absorbance$_{282nm}$ 1.1084, $\lambda_{max844nm}$ 0.0400) are probably appropriate candidates for the investigation of role of the photon-induced interaction, the involvement of which has been identified in our previous study. Optical filter and light source with continuous wavelength emission will also be needed for the investigation in order to control the wavelength of the illumination. Higher absorption coefficient of the polymers ensures the efficient usage of the illumination.

3. The influence of the type (electron-withdrawing/electron-donating) and number of the substitution groups on the separation effects of dispersing surfactants can be investigated by molecular structural modification. This is due to the fact that the electronic/optical properties of the substituted aromatic fluorescent functional groups can be effectively tailed by rational molecular structural design. The adjustment the optical absorption/emission wavelength of

the surfactants will surely influence the magnitude of the RET between the polymer and different SWNTs species. As a consequence, the affinity of polymer functionalized with different side groups towards various SWNT species will be different. Among the potential functional groups which will be the effective for modifying the polymer's electronic/optical properties are CN, NO_2, OR and NR, etc. The former two are electron withdrawing groups and are anticipated to shift the absorption/emission towards short wavelength region while the last two are strong electron donating functional groups which are expected to be effective for red-shift of the polymer's absorption/emission features.

4. Alternatively, various photophysical properties of fluorescent molecules/polymers are suggested to be effective for the modification of their species selective behavior. For example, appropriate quencher may be employed to suppress the molecular/polymeric emission so as to tune their species selective behaviors. This is due to the fact that RET is only one possible deactivation pathway of the excited molecules/polymers and the increase of other deactivating channel will certainly suppress the probability of excitonic relaxation via RET. As a result, the RET induced intermolecular pairing force will decrease and different selective behavior can be observed. Change of the solvent may be another effective approach to tune the relative magnitude of various photophysical processes so as to modify the molecules/polymer's species selectivity. Heavy atom effect as well as intersystem crossing resulted from spin-orbit coupling may be involved. Solvent effects on species selectivities share the same rationale as fluorescence quencher in terms of providing additional relaxation channel for the excited molecules/polymers.

5. Great care should be taken for the investigation of effects of illumination irradiance (I) on species selectivity. The involvement of the cascaded RET makes the control and prediction of the selective dispersion difficult or even impossible. Molecules/polymers' selective suspension towards certain SWNT species will possibly be spoiled in the presence of

cascaded RET between the suspended SWNT species and unpreferred species since cascaded RET will also induce intermolecular pairing force between the involved SWNTs species so as to result in their aggregation. One possible solution to this issue is the introduction of some preferential quencher. The ideal situation is that if we can find some quencher which will be effective for quenching the photoluminescence from SWNT species rather that from the molecules/polymers so that we can intentionally increase the illumination irradiance (*I*) to improve the intermolecular pairing force between molecules/polymers and the preferred SWNTs species while the cascaded RET and the associated detrimental SWNT aggregation suppressed.

6. Polymers with smaller conjugated functional groups such as Poly(styrene sulfonic acid), sodium salt, Poly(2-naphthylmethacrylate), Poly(9-anthracenylmethyl methacrylate) may be suitable for the investigation of the relative magnitudes and interplay of different kinds of involved weak interactions such as electrostatic interaction, Van der Waals interaction, π-π stacking interaction and RET induced intermolecular pairing force, *etc*. Whether the RET induced intermolecular pairing force under high illumination irradiance (*I*) is comparable to the electrostatic interaction associated with ionic surfactants are not clear at this moment and need further investigation.

Reference:

(1) White, C. T.; Todorov, T. N. *Nature* **1998**, *393*, 240.

(2) Quinn, B. M.; Lemay, S. G. *Advanced Materials* **2006**, *18*, 855.

(3) Pop, E.; Mann, D.; Wang, Q.; Goodson, K.; Dai, H. J. *Nano Letters* **2006**, *6*, 96.

(4) Yu, M. F.; Lourie, O.; Dyer, M. J.; Moloni, K.; Kelly, T. F.; Ruoff, R. S. *Science* **2000**, *287*, 637.

(5) Pan, Z. W.; Xie, S. S.; Lu, L.; Chang, B. H.; Sun, L. F.; Zhou, W. Y.; Wang, G.; Zhang, D. L. *Applied Physics Letters* **1999**, *74*, 3152.

(6) Poncharal, P.; Wang, Z. L.; Ugarte, D.; de Heer, W. A. *Science* **1999**, *283*, 1513.

(7) Walters, D. A.; Ericson, L. M.; Casavant, M. J.; Liu, J.; Colbert, D. T.; Smith, K. A.; Smalley, R. E. *Applied Physics Letters* **1999**, *74*, 3803.

(8) Artukovic, E.; Kaempgen, M.; Hecht, D. S.; Roth, S.; GrUner, G. *Nano Letters* **2005**, *5*, 757.

(9) Takenobu, T.; Takahashi, T.; Kanbara, T.; Tsukagoshi, K.; Aoyagi, Y.; Iwasa, Y. *Applied Physics Letters* **2006**, *88*.

(10) Durkop, T.; Getty, S. A.; Cobas, E.; Fuhrer, M. S. *Nano Letters* **2004**, *4*, 35.

(11) Bradley, K.; Gabriel, J. C. P.; Gruner, G. *Nano Letters* **2003**, *3*, 1353.

(12) Cao, Q.; Kim, H. S.; Pimparkar, N.; Kulkarni, J. P.; Wang, C. J.; Shim, M.; Roy, K.; Alam, M. A.; Rogers, J. A. *Nature* **2008**, *454*, 495.

(13) Zhou, Y. X.; Gaur, A.; Hur, S. H.; Kocabas, C.; Meitl, M. A.; Shim, M.; Rogers, J. A. *Nano Letters* **2004**, *4*, 2031.

(14) Cao, Q.; Rogers, J. A. *Advanced Materials* **2009**, *21*, 29.

(15) Yao, Z.; Kane, C. L.; Dekker, C. *Physical Review Letters* **2000**, *84*, 2941.

(16) Avouris, P. *Accounts of Chemical Research* **2002**, *35*, 1026.

(17) Saito, R.; Fujita, M.; Dresselhaus, G.; Dresselhaus, M. S. *Applied Physics Letters* **1992**, *60*, 2204.

(18) Li, Y. M.; Mann, D.; Rolandi, M.; Kim, W.; Ural, A.; Hung, S.; Javey, A.; Cao, J.; Wang, D. W.; Yenilmez, E.; Wang, Q.; Gibbons, J. F.; Nishi, Y.; Dai, H. J. *Nano Letters* **2004**, *4*, 317.

(19) Yang, C. M.; Park, J. S.; An, K. H.; Lim, S. C.; Seo, K.; Kim, B.; Park, K. A.; Han, S.; Park, C. Y.; Lee, Y. H. *Journal of Physical Chemistry B* **2005**, *109*, 19242.

(20) Huang, H. J.; Maruyama, R.; Noda, K.; Kajiura, H.; Kadono, K. *Journal of Physical Chemistry B* **2006**, *110*, 7316.

(21) Krupke, R.; Hennrich, F.; von Lohneysen, H.; Kappes, M. M. *Science* **2003**, *301*, 344.

(22) Zheng, M.; Jagota, A.; Strano, M. S.; Santos, A. P.; Barone, P.; Chou, S. G.; Diner, B. A.; Dresselhaus, M. S.; McLean, R. S.; Onoa, G. B.; Samsonidze, G. G.; Semke, E. D.; Usrey, M.; Walls, D. J. *Science* **2003**, *302*, 1545.

(23) Zheng, M.; Semke, E. D. *Journal of the American Chemical Society* **2007**, *129*, 6084.

(24) Strano, M. S.; Zheng, M.; Jagota, A.; Onoa, G. B.; Heller, D. A.; Barone, P. W.; Usrey, M. L. *Nano Letters* **2004**, *4*, 543.

(25) Lustig, S. R.; Jagota, A.; Khripin, C.; Zheng, M. *Journal of Physical Chemistry B* **2005**, *109*, 2559.

(26) Arnold, M. S.; Green, A. A.; Hulvat, J. F.; Stupp, S. I.; Hersam, M. C. *Nature Nanotechnology* **2006**, *1*, 60.

(27) Nair, N.; Kim, W. J.; Braatz, R. D.; Strano, M. S. *Langmuir* **2008**, *24*, 1790.
(28) Strano, M. S.; Dyke, C. A.; Usrey, M. L.; Barone, P. W.; Allen, M. J.; Shan, H. W.; Kittrell, C.; Hauge, R. H.; Tour, J. M.; Smalley, R. E. *Science* **2003**, *301*, 1519.
(29) Menard-Moyon, C.; Izard, N.; Doris, E.; Mioskowski, C. *Journal of the American Chemical Society* **2006**, *128*, 6552.
(30) An, L.; Fu, Q. A.; Lu, C. G.; Liu, J. *Journal of the American Chemical Society* **2004**, *126*, 10520.
(31) Kim, W. J.; Usrey, M. L.; Strano, M. S. *Chemistry of Materials* **2007**, *19*, 1571.
(32) Hemraj-Benny, T.; Wong, S. S. *Chemistry of Materials* **2006**, *18*, 4827.
(33) Maeda, Y.; Kimura, S.; Kanda, M.; Hirashima, Y.; Hasegawa, T.; Wakahara, T.; Lian, Y. F.; Nakahodo, T.; Tsuchiya, T.; Akasaka, T.; Lu, J.; Zhang, X. W.; Gao, Z. X.; Yu, Y. P.; Nagase, S.; Kazaoui, S.; Minami, N.; Shimizu, T.; Tokumoto, H.; Saito, R. *Journal of the American Chemical Society* **2005**, *127*, 10287.
(34) Chattopadhyay, D.; Galeska, L.; Papadimitrakopoulos, F. *Journal of the American Chemical Society* **2003**, *125*, 3370.
(35) Chen, Z. H.; Du, X.; Du, M. H.; Rancken, C. D.; Cheng, H. P.; Rinzler, A. G. *Nano Letters* **2003**, *3*, 1245.
(36) Li, H. P.; Zhou, B.; Lin, Y.; Gu, L. R.; Wang, W.; Fernando, K. A. S.; Kumar, S.; Allard, L. F.; Sun, Y. P. *Journal of the American Chemical Society* **2004**, *126*, 1014.
(37) Zhang, Z. B.; Zhang, S. L. *Journal of the American Chemical Society* **2007**, *129*, 666.
(38) Ju, S. Y.; Doll, J.; Sharma, I.; Papadimitrakopoulos, F. *Nature Nanotechnology* **2008**, *3*, 356.
(39) Chen, R. J.; Zhang, Y. G.; Wang, D. W.; Dai, H. J. *Journal of the American Chemical Society* **2001**, *123*, 3838.
(40) Georgakilas, V.; Kordatos, K.; Prato, M.; Guldi, D. M.; Holzinger, M.; Hirsch, A. *Journal of the American Chemical Society* **2002**, *124*, 760.
(41) Fernando, K. A. S.; Lin, Y.; Wang, W.; Kumar, S.; Zhou, B.; Xie, S. Y.; Cureton, L. T.; Sun, Y. P. *Journal of the American Chemical Society* **2004**, *126*, 10234.
(42) So, H. M.; Kim, B. K.; Park, D. W.; Kim, B. S.; Kim, J. J.; Kong, K. J.; Chang, H. J.; Lee, J. O. *Journal of the American Chemical Society* **2007**, *129*, 4866.
(43) LeMieux, M. C.; Roberts, M.; Barman, S.; Jin, Y. W.; Kim, J. M.; Bao, Z. N. *Science* **2008**, *321*, 101.
(44) Wang, W.; Fernando, K. A. S.; Lin, Y.; Meziani, M. J.; Veca, L. M.; Cao, L.; Zhang, P.; Kimani, M. M.; Sun, Y. P. *Journal of the American Chemical Society* **2008**, *130*, 1415.
(45) Pan, X. Y.; Cai, Q. J.; Li, C. M.; Zhang, Q.; Chan-Park, M. B. *Nanotechnology* **2009**, *20*.
(46) Nish, A.; Hwang, J. Y.; Doig, J.; Nicholas, R. J. *Nature Nanotechnology* **2007**, *2*, 640.
(47) Hwang, J. Y.; Nish, A.; Doig, J.; Douven, S.; Chen, C. W.; Chen, L. C.; Nicholas, R. J. *Journal of the American Chemical Society* **2008**, *130*, 3543.
(48) Chen, F. M.; Wang, B.; Chen, Y.; Li, L. J. *Nano Letters* **2007**, *7*, 3013.
(49) Iijima, S. *Nature* **1991**, *354*, 56.
(50) Biro, L. P.; Horvath, Z. E.; Szalmas, L.; Kertesz, K.; Weber, F.; Juhasz, G.; Radnoczi, G.; Gyulai, J. *Chemical Physics Letters* **2003**, *372*, 399.
(51) Burstein, E. *Journal of the Franklin Institute-Engineering and Applied Mathematics* **2003**, *340*, 221.
(52) Iijima, S.; Ichihashi, T. *Nature* **1993**, *363*, 603.

(53) Hamada, N.; Sawada, S.; Oshiyama, A. *Physical Review Letters* **1992**, *68*, 1579.

(54) Murakami, Y.; Miyauchi, Y.; Chiashi, S.; Maruyama, S. *Chemical Physics Letters* **2003**, *377*, 49.

(55) Kim, S. N.; Rusling, J. F.; Papadimitrakopoulos, F. *Advanced Materials* **2007**, *19*, 3214.

(56) Belin, T.; Epron, F. *Materials Science and Engineering B-Solid State Materials for Advanced Technology* **2005**, *119*, 105.

(57) Charlier, J. C. *Accounts of Chemical Research* **2002**, *35*, 1063.

(58) Wildoer, J. W. G.; Venema, L. C.; Rinzler, A. G.; Smalley, R. E.; Dekker, C. *Nature* **1998**, *391*, 59.

(59) Jorio, A.; Saito, R.; Hafner, J. H.; Lieber, C. M.; Hunter, M.; McClure, T.; Dresselhaus, G.; Dresselhaus, M. S. *Physical Review Letters* **2001**, *86*, 1118.

(60) Ouyang, M.; Huang, J. L.; Lieber, C. M. *Accounts of Chemical Research* **2002**, *35*, 1018.

(61) Samsonidze, G. G.; Gruneis, A.; Saito, R.; Jorio, A.; Souza, A. G.; Dresselhaus, G.; Dresselhaus, M. S. *Physical Review B* **2004**, *69*.

(62) Chiang, I. W.; Brinson, B. E.; Huang, A. Y.; Willis, P. A.; Bronikowski, M. J.; Margrave, J. L.; Smalley, R. E.; Hauge, R. H. *Journal of Physical Chemistry B* **2001**, *105*, 8297.

(63) Barros, E. B.; Jorio, A.; Samsonidze, G. G.; Capaz, R. B.; Souza, A. G.; Mendes, J.; Dresselhaus, G.; Dresselhaus, M. S. *Physics Reports-Review Section of Physics Letters* **2006**, *431*, 261.

(64) Niyogi, S.; Hamon, M. A.; Hu, H.; Zhao, B.; Bhowmik, P.; Sen, R.; Itkis, M. E.; Haddon, R. C. *Accounts of Chemical Research* **2002**, *35*, 1105.

(65) Dai, H. J. *Accounts of Chemical Research* **2002**, *35*, 1035.

(66) Peierl, R. F. *Quantum Theory of Solids* **1955**, 108.

(67) Fisher, D. S.; Lee, P. A. *Physical Review B* **1981**, *23*, 6851.

(68) Buttiker, M.; Imry, Y.; Landauer, R.; Pinhas, S. *Physical Review B* **1985**, *31*, 6207.

(69) Büttiker, M. *Physical Review Letters* **1986**, *57*, 1761.

(70) R. Saito, G. D., and M.S. Dresselhaus *Physical Properties of Carbon Nanotubes* **1998**.

(71) Yao, Z.; Kane, C. L.; Dekker, C. *Physical Review Letters* **2000**, *84*, 2941.

(72) Tans, S. J.; Devoret, M. H.; Dai, H. J.; Thess, A.; Smalley, R. E.; Geerligs, L. J.; Dekker, C. *Nature* **1997**, *386*, 474.

(73) Javey, A.; Guo, J.; Wang, Q.; Lundstrom, M.; Dai, H. J. *Nature* **2003**, *424*, 654.

(74) Mann, D.; Javey, A.; Kong, J.; Wang, Q.; Dai, H. J. *Nano Letters* **2003**, *3*, 1541.

(75) Kane, C. L.; Mele, E. J.; Lee, R. S.; Fischer, J. E.; Petit, P.; Dai, H.; Thess, A.; Smalley, R. E.; Verschueren, A. R. M.; Tans, S. J.; Dekker, C. *Europhysics Letters* **1998**, *41*, 683.

(76) Woods, L. M.; Mahan, G. D. *Physical Review B* **2000**, *61*, 10651.

(77) Bockrath, M.; Liang, W. J.; Bozovic, D.; Hafner, J. H.; Lieber, C. M.; Tinkham, M.; Park, H. K. *Science* **2001**, *291*, 283.

(78) Shockley, W.; Pearson, G. L. *Physical Review* **1948**, *74*, 232.

(79) Tans, S. J.; Verschueren, A. R. M.; Dekker, C. *Nature* **1998**, *393*, 49.

(80) A. Thess, R. L., P. Nikolaev, et al. *Science* **1996**, *273*, 483.

(81) Martel, R.; Derycke, V.; Lavoie, C.; Appenzeller, J.; Chan, K. K.; Tersoff, J.; Avouris, P. *Physical Review Letters* **2001**, *87*.

(82) Bachtold, A.; Hadley, P.; Nakanishi, T.; Dekker, C. *Science* **2001**, *294*, 1317.

(83) Appenzeller, J.; Knoch, J.; Derycke, V.; Martel, R.; Wind, S.; Avouris, P. *Physical Review Letters* **2002**, *89*.

(84) Javey, A.; Kim, H.; Brink, M.; Wang, Q.; Ural, A.; Guo, J.; McIntyre, P.; McEuen, P.; Lundstrom, M.; Dai, H. J. *Nature Materials* **2002**, *1*, 241.

(85) Maruyama, S.; Kojima, R.; Miyauchi, Y.; Chiashi, S.; Kohno, M. *Chemical Physics Letters* **2002**, *360*, 229.

(86) Cao, H.; Wang, Q.; Wang, D. W.; Dai, H. J. *Small* **2005**, *1*, 138.

(87) Hersam, M. C. *Nature Nanotechnology* **2008**, *3*, 387.

(88) Krupke, R.; Hennrich, F. *Advanced Engineering Materials* **2005**, *7*, 111.

(89) Gruner, G. *Journal of Materials Chemistry* **2006**, *16*, 3533.

(90) Song, Y. I.; Yang, C. M.; Kim, D. Y.; Kanoh, H.; Kaneko, K. *Journal of Colloid and Interface Science* **2008**, *318*, 365.

(91) Tenent, R. C.; Barnes, T. M.; Bergeson, J. D.; Ferguson, A. J.; To, B.; Gedvilas, L. M.; Heben, M. J.; Blackburn, J. L. *Advanced Materials* **2009**, *21*, 3210.

(92) Hu, H.; Larson, R. G. *Journal of Physical Chemistry B* **2006**, *110*, 7090.

(93) Small, W. R.; Walton, C. D.; Loos, J.; Panhuis, M. I. H. *Journal of Physical Chemistry B* **2006**, *110*, 13029.

(94) Zhang, M. N.; Su, L.; Mao, L. Q. *Carbon* **2006**, *44*, 276.

(95) Zhang, Q. H.; Vichchulada, P.; Lay, M. D. *Journal of Physical Chemistry C* **2010**, *114*, 16292.

(96) Barman, S. N.; LeMieux, M. C.; Baek, J.; Rivera, R.; Bao, Z. N. *Acs Applied Materials & Interfaces* **2010**, *2*, 2672.

(97) Dresselhaus, M. S.; Dresselhaus, G.; Saito, R. *Physical Review B* **1992**, *45*, 6234.

(98) Mintmire, J. W.; Dunlap, B. I.; White, C. T. *Physical Review Letters* **1992**, *68*, 631.

(99) Sfeir, M. Y.; Beetz, T.; Wang, F.; Huang, L. M.; Huang, X. M. H.; Huang, M. Y.; Hone, J.; O'Brien, S.; Misewich, J. A.; Heinz, T. F.; Wu, L. J.; Zhu, Y. M.; Brus, L. E. *Science* **2006**, *312*, 554.

(100) Pedersen, T. G. *Physical Review B* **2003**, *67*, 073401.

(101) Perebeinos, V.; Tersoff, J.; Avouris, P. *Physical Review Letters* **2004**, *92*, 257402.

(102) Brar, V. W.; Samsonidze, G. G.; Dresselhaus, M. S.; Dresselhaus, G.; Saito, R.; Swan, A. K.; Ünlü, M. S.; Goldberg, B. B.; Souza Filho, A. G.; Jorio, A. *Physical Review B* **2002**, *66*, 155418.

(103) Bachilo, S. M.; Strano, M. S.; Kittrell, C.; Hauge, R. H.; Smalley, R. E.; Weisman, R. B. *Science* **2002**, *298*, 2361.

(104) Lefebvre, J.; Fraser, J. M.; Finnie, P.; Homma, Y. *Physical Review B* **2004**, *69*, 075403.

(105) Kane, C. L.; Mele, E. J. *Physical Review Letters* **2003**, *90*, 207401.

(106) Kataura, H.; Kumazawa, Y.; Maniwa, Y.; Umezu, I.; Suzuki, S.; Ohtsuka, Y.; Achiba, Y. *Synthetic Metals* **1999**, *103*, 2555.

(107) Hagen, A.; Hertel, T. *Nano Letters* **2003**, *3*, 383.

(108) Bachilo, S. M.; Balzano, L.; Herrera, J. E.; Pompeo, F.; Resasco, D. E.; Weisman, R. B. *Journal of the American Chemical Society* **2003**, *125*, 11186.

(109) Dresselhaus, M. S.; Dresselhaus, G.; Saito, R.; Jorio, A. *Annual Review of Physical Chemistry* **2007**, *58*, 719.

(110) Kamada, Y.; Naka, M.; Nagasawa, N.; Li, Z. M.; Tang, Z. K. *Physica B-Condensed Matter* **2002**, *323*, 239.

(111) Zhang, Y.; Iijima, S. *Physical Review Letters* **1999**, *82*, 3472.

(112) Freitag, M.; Martin, Y.; Misewich, J. A.; Martel, R.; Avouris, P. H. *Nano Letters* **2003**, *3*, 1067.

(113) Misewich, J. A.; Martel, R.; Avouris, P.; Tsang, J. C.; Heinze, S.; Tersoff, J. *Science* **2003**, *300*, 783.

(114) Freitag, M.; Perebeinos, V.; Chen, J.; Stein, A.; Tsang, J. C.; Misewich, J. A.; Martel, R.; Avouris, P. *Nano Letters* **2004**, *4*, 1063.

(115) Freitag, M.; Chen, J.; Tersoff, J.; Tsang, J. C.; Fu, Q.; Liu, J.; Avouris, P. *Physical Review Letters* **2004**, *93*.

(116) Liu, J.; Rinzler, A. G.; Dai, H. J.; Hafner, J. H.; Bradley, R. K.; Boul, P. J.; Lu, A.; Iverson, T.; Shelimov, K.; Huffman, C. B.; Rodriguez-Macias, F.; Shon, Y. S.; Lee, T. R.; Colbert, D. T.; Smalley, R. E. *Science* **1998**, *280*, 1253.

(117) Mawhinney, D. B.; Naumenko, V.; Kuznetsova, A.; Yates, J. T.; Liu, J.; Smalley, R. E. *Journal of the American Chemical Society* **2000**, *122*, 2383.

(118) Mawhinney, D. B.; Naumenko, V.; Kuznetsova, A.; Yates, J. T.; Liu, J.; Smalley, R. E. *Chemical Physics Letters* **2000**, *324*, 213.

(119) Hamon, M. A.; Chen, J.; Hu, H.; Chen, Y. S.; Itkis, M. E.; Rao, A. M.; Eklund, P. C.; Haddon, R. C. *Advanced Materials* **1999**, *11*, 834.

(120) Zhao, B.; Hu, H.; Haddon, R. C. *Advanced Functional Materials* **2004**, *14*, 71.

(121) Pompeo, F.; Resasco, D. E. *Nano Letters* **2002**, *2*, 369.

(122) Delgado, J. L.; de la Cruz, P.; Urbina, A.; Navarrete, J. T. L.; Casado, J.; Langa, F. *Carbon* **2007**, *45*, 2250.

(123) Wu, W.; Zhu, H. R.; Fan, L. Z.; Yang, S. H. *Chemistry-a European Journal* **2008**, *14*, 5981.

(124) Giordani, S.; Colomer, J. F.; Cattaruzza, F.; Alfonsi, J.; Meneghetti, M.; Prato, M.; Bonifazi, D. *Carbon* **2009**, *47*, 578.

(125) Katz, E.; Willner, I. *Chemphyschem* **2004**, *5*, 1085.

(126) He, P.; Urban, M. W. *Biomacromolecules* **2005**, *6*, 2455.

(127) Baker, S. E.; Cai, W.; Lasseter, T. L.; Weidkamp, K. P.; Hamers, R. J. *Nano Letters* **2002**, *2*, 1413.

(128) Gu, L. R.; Elkin, T.; Jiang, X. P.; Li, H. P.; Lin, Y.; Qu, L. W.; Tzeng, T. R. J.; Joseph, R.; Sun, Y. P. *Chemical Communications* **2005**, 874.

(129) Ju, S. Y.; Papadimitrakopoulos, F. *Journal of the American Chemical Society* **2008**, *130*, 655.

(130) Sheeney-Haj-Khia, L.; Basnar, B.; Willner, I. *Angewandte Chemie-International Edition* **2005**, *44*, 78.

(131) Patolsky, F.; Weizmann, Y.; Willner, I. *Angewandte Chemie-International Edition* **2004**, *43*, 2113.

(132) Li, H. P.; Martin, R. B.; Harruff, B. A.; Carino, R. A.; Allard, L. F.; Sun, Y. P. *Advanced Materials* **2004**, *16*, 896.

(133) Baskaran, D.; Mays, J. W.; Zhang, X. P.; Bratcher, M. S. *Journal of the American Chemical Society* **2005**, *127*, 6916.

(134) Cosnier, S.; Holzinger, M. *Electrochimica Acta* **2008**, *53*, 3948.

(135) Mickelson, E. T.; Huffman, C. B.; Rinzler, A. G.; Smalley, R. E.; Hauge, R. H.; Margrave, J. L. *Chemical Physics Letters* **1998**, *296*, 188.

(136) Mickelson, E. T.; Chiang, I. W.; Zimmerman, J. L.; Boul, P. J.; Lozano, J.; Liu, J.; Smalley, R. E.; Hauge, R. H.; Margrave, J. L. *Journal of Physical Chemistry B* **1999**, *103*, 4318.

(137) Bettinger, H. F.; Kudin, K. N.; Scuseria, G. E. *Journal of the American Chemical Society* **2001**, *123*, 12849.

(138) Boul, P. J.; Liu, J.; Mickelson, E. T.; Huffman, C. B.; Ericson, L. M.; Chiang, I. W.; Smith, K. A.; Colbert, D. T.; Hauge, R. H.; Margrave, J. L.; Smalley, R. E. *Chemical Physics Letters* **1999**, *310*, 367.

(139) Peng, H. Q.; Gu, Z. N.; Yang, J. P.; Zimmerman, J. L.; Willis, P. A.; Bronikowski, M. J.; Smalley, R. E.; Hauge, R. H.; Margrave, J. L. *Nano Letters* **2001**, *1*, 625.

(140) Bahr, J. L.; Yang, J. P.; Kosynkin, D. V.; Bronikowski, M. J.; Smalley, R. E.; Tour, J. M. *Journal of the American Chemical Society* **2001**, *123*, 6536.

(141) Allongue, P.; Delamar, M.; Desbat, B.; Fagebaume, O.; Hitmi, R.; Pinson, J.; Saveant, J. M. *Journal of the American Chemical Society* **1997**, *119*, 201.

(142) Bahr, J. L.; Tour, J. M. *Chemistry of Materials* **2001**, *13*, 3823.

(143) Chen, J.; Hamon, M. A.; Hu, H.; Chen, Y. S.; Rao, A. M.; Eklund, P. C.; Haddon, R. C. *Science* **1998**, *282*, 95.

(144) Holzinger, M.; Vostrowsky, O.; Hirsch, A.; Hennrich, F.; Kappes, M.; Weiss, R.; Jellen, F. *Angewandte Chemie-International Edition* **2001**, *40*, 4002.

(145) Maggini, M.; Scorrano, G.; Prato, M. *Journal of the American Chemical Society* **1993**, *115*, 9798.

(146) Prato, M.; Maggini, M. *Accounts of Chemical Research* **1998**, *31*, 519.

(147) Wang, H. *Current Opinion in Colloid & Interface Science* **2009**, *14*, 364.

(148) Vaisman, L.; Wagner, H. D.; Marom, G. *Advances in Colloid and Interface Science* **2006**, *128*, 37.

(149) Britz, D. A.; Khlobystov, A. N. *Chemical Society Reviews* **2006**, *35*, 637.

(150) Bahr, J. L.; Tour, J. M. *Journal of Materials Chemistry* **2002**, *12*, 1952.

(151) Singh, P.; Campidelli, S.; Giordani, S.; Bonifazi, D.; Bianco, A.; Prato, M. *Chemical Society Reviews* **2009**, *38*, 2214.

(152) Chen, Y.; Haddon, R. C.; Fang, S.; Rao, A. M.; Lee, W. H.; Dickey, E. C.; Grulke, E. A.; Pendergrass, J. C.; Chavan, A.; Haley, B. E.; Smalley, R. E. *Journal of Materials Research* **1998**, *13*, 2423.

(153) Hamon, M. A.; Itkis, M. E.; Niyogi, S.; Alvaraez, T.; Kuper, C.; Menon, M.; Haddon, R. C. *Journal of the American Chemical Society* **2001**, *123*, 11292.

(154) Haddon, R. C. *Science* **1993**, *261*, 1545.

(155) Kong, J.; Franklin, N. R.; Zhou, C. W.; Chapline, M. G.; Peng, S.; Cho, K. J.; Dai, H. J. *Science* **2000**, *287*, 622.

(156) Collins, P. G.; Bradley, K.; Ishigami, M.; Zettl, A. *Science* **2000**, *287*, 1801.

(157) Chang, H.; Lee, J. D.; Lee, S. M.; Lee, Y. H. *Applied Physics Letters* **2001**, *79*, 3863.

(158) Peng, S.; Cho, K. J. *Nanotechnology* **2000**, *11*, 57.

(159) Jhi, S. H.; Louie, S. G.; Cohen, M. L. *Physical Review Letters* **2000**, *85*, 1710.

(160) Chen, R. F., N.; Kong, J.; Cao, J.; Tombler, T.; et al. *Appl. Phys. Lett.* **2001**, *79*, 2258.

(161) Sumanasekera, G. U.; Adu, C. K. W.; Fang, S.; Eklund, P. C. *Physical Review Letters* **2000**, *85*, 1096.

(162) Kittel, C. *Quantum Theory of Solids, Wiley: New York* **1963**.

(163) O'Connell, M. J.; Boul, P.; Ericson, L. M.; Huffman, C.; Wang, Y. H.; Haroz, E.; Kuper, C.; Tour, J.; Ausman, K. D.; Smalley, R. E. *Chemical Physics Letters* **2001**, *342*, 265.

(164) Star, A.; Stoddart, J. F.; Steuerman, D.; Diehl, M.; Boukai, A.; Wong, E. W.; Yang, X.; Chung, S. W.; Choi, H.; Heath, J. R. *Angewandte Chemie-International Edition* **2001**, *40*, 1721.

(165) Steuerman, D. W.; Star, A.; Narizzano, R.; Choi, H.; Ries, R. S.; Nicolini, C.; Stoddart, J. F.; Heath, J. R. *Journal of Physical Chemistry B* **2002**, *106*, 3124.

(166) Star, A.; Liu, Y.; Grant, K.; Ridvan, L.; Stoddart, J. F.; Steuerman, D. W.; Diehl, M. R.; Boukai, A.; Heath, J. R. *Macromolecules* **2003**, *36*, 553.

(167) Star, A.; Stoddart, J. F. *Macromolecules* **2002**, *35*, 7516.

(168) Guo, Z. J.; Sadler, P. J.; Tsang, S. C. *Advanced Materials* **1998**, *10*, 701.

(169) Gao, H. J.; Kong, Y. *Annual Review of Materials Research* **2004**, *34*, 123.

(170) Dieckmann, G. R.; Dalton, A. B.; Johnson, P. A.; Razal, J.; Chen, J.; Giordano, G. M.; Munoz, E.; Musselman, I. H.; Baughman, R. H.; Draper, R. K. *Journal of the American Chemical Society* **2003**, *125*, 1770.

(171) Zorbas, V.; Ortiz-Acevedo, A.; Dalton, A. B.; Yoshida, M. M.; Dieckmann, G. R.; Draper, R. K.; Baughman, R. H.; Jose-Yacaman, M.; Musselman, I. H. *Journal of the American Chemical Society* **2004**, *126*, 7222.

(172) Star, A.; Steuerman, D. W.; Heath, J. R.; Stoddart, J. F. *Angewandte Chemie-International Edition* **2002**, *41*, 2508.

(173) Stobinski, L.; Tomasik, P.; Lii, C. Y.; Chan, H. H.; Lin, H. M.; Liu, H. L.; Kao, C. T.; Lu, K. S. *Carbohydrate Polymers* **2003**, *51*, 311.

(174) Lii, C. Y.; Stobinski, L.; Tomasik, P.; Liao, C. D. *Carbohydrate Polymers* **2003**, *51*, 93.

(175) Duclaux, L.; Metenier, K.; Salvetat, J. P.; Lauginie, P.; Bonnamy, S.; Beguin, F. *Molecular Crystals and Liquid Crystals* **2000**, *340*, 769.

(176) Chen, G.; Furtado, C. A.; Kim, U. J.; Eklund, P. C. *Physical Review B* **2005**, *72*.

(177) Shim, M.; Javey, A.; Kam, N. W. S.; Dai, H. J. *Journal of the American Chemical Society* **2001**, *123*, 11512.

(178) Lu, J. P. *Physical Review Letters* **1997**, *79*, 1297.

(179) Garg, A.; Han, J.; Sinnott, S. B. *Physical Review Letters* **1998**, *81*, 2260.

(180) Ebbesen, T. W.; Lezec, H. J.; Hiura, H.; Bennett, J. W.; Ghaemi, H. F.; Thio, T. *Nature* **1996**, *382*, 54.

(181) Wong, E. W.; Sheehan, P. E.; Lieber, C. M. *Science* **1997**, *277*, 1971.

(182) JIAN PING LU, J. H. *International Journal of High Speed Electronics and Systems* **1998**, *9*, 101.

(183) Hone, J.; Batlogg, B.; Benes, Z.; Johnson, A. T.; Fischer, J. E. *Science* **2000**, *289*, 1730.

(184) Yi, W.; Lu, L.; Dian-lin, Z.; Pan, Z. W.; Xie, S. S. *Physical Review B* **1999**, *59*, R9015.

(185) Hone, J.; Whitney, M.; Piskoti, C.; Zettl, A. *Physical Review B* **1999**, *59*, R2514.

(186) Baumgartner, G.; Carrard, M.; Zuppiroli, L.; Bacsa, W.; de Heer, W. A.; Forró, L. *Physical Review B* **1997**, *55*, 6704.

(187) Lu, J. P. *Physical Review Letters* **1995**, *74*, 1123.

(188) Saito, R.; Fujita, M.; Dresselhaus, G.; Dresselhaus, M. S. *Physical Review B* **1992**, *46*, 1804.

(189) Schonenberger, C.; Bachtold, A.; Strunk, C.; Salvetat, J. P.; Forro, L. *Applied Physics a-Materials Science & Processing* **1999**, *69*, 283.

(190) Terrones, M. *International Materials Reviews* **2004**, *49*, 325.

(191) Dai, H. J. In *Carbon Nanotubes* 2001; Vol. 80, p 29.

(192) Liu, J.; Fan, S. S.; Dai, H. J. *Mrs Bulletin* **2004**, *29*, 244.

(193) Mann, D. *CRC Press Taylor & Francis Group(eBook) Carbon Nanotubes Properties and Applications* **2006**, 31.

(194) Thess, A.; Lee, R.; Nikolaev, P.; Dai, H. J.; Petit, P.; Robert, J.; Xu, C. H.; Lee, Y. H.; Kim, S. G.; Rinzler, A. G.; Colbert, D. T.; Scuseria, G. E.; Tomanek, D.; Fischer, J. E.; Smalley, R. E. *Science* **1996**, *273*, 483.

(195) Bethune, D. S.; Kiang, C. H.; Devries, M. S.; Gorman, G.; Savoy, R.; Vazquez, J.; Beyers, R. *Nature* **1993**, *363*, 605.

(196) Farhat, S.; de La Chapelle, M. L.; Loiseau, A.; Scott, C. D.; Lefrant, S.; Journet, C.; Bernier, P. *Journal of Chemical Physics* **2001**, *115*, 6752.

(197) Waldorff, E. I.; Waas, A. M.; Friedmann, P. P.; Keidar, M. *Journal of Applied Physics* **2004**, *95*, 2749.

(198) Journet, C.; Maser, W. K.; Bernier, P.; Loiseau, A.; delaChapelle, M. L.; Lefrant, S.; Deniard, P.; Lee, R.; Fischer, J. E. *Nature* **1997**, *388*, 756.

(199) Endo, M.; Takeuchi, K.; Igarashi, S.; Kobori, K.; Shiraishi, M.; Kroto, H. W. *Journal of Physics and Chemistry of Solids* **1993**, *54*, 1841.

(200) Height, M. J.; Howard, J. B.; Tester, J. W.; Sande, J. B. V. *Carbon* **2004**, *42*, 2295.

(201) Fan, S. S.; Chapline, M. G.; Franklin, N. R.; Tombler, T. W.; Cassell, A. M.; Dai, H. J. *Science* **1999**, *283*, 512.

(202) Dervishi, E.; Li, Z. R.; Xu, Y.; Saini, V.; Biris, A. R.; Lupu, D.; Biris, A. S. *Particulate Science and Technology* **2009**, *27*, 107.

(203) Terranova, M. L.; Sessa, V.; Rossi, M. *Chemical Vapor Deposition* **2006**, *12*, 315.

(204) Zhou, W. Y.; Bai, X. D.; Wang, E. G.; Xie, S. S. *Advanced Materials* **2009**, *21*, 4565.

(205) Choi, H. C.; Kim, W.; Wang, D. W.; Dai, H. J. *Journal of Physical Chemistry B* **2002**, *106*, 12361.

(206) Li, Y. M.; Kim, W.; Zhang, Y. G.; Rolandi, M.; Wang, D. W.; Dai, H. J. *Journal of Physical Chemistry B* **2001**, *105*, 11424.

(207) Kitiyanan, B.; Alvarez, W. E.; Harwell, J. H.; Resasco, D. E. *Chemical Physics Letters* **2000**, *317*, 497.

(208) Herrera, J. E.; Resasco, D. E. *Journal of Catalysis* **2004**, *221*, 354.

(209) Alvarez, W. E.; Kitiyanan, B.; Borgna, A.; Resasco, D. E. *Carbon* **2001**, *39*, 547.

(210) Resasco, D. E.; Alvarez, W. E.; Pompeo, F.; Balzano, L.; Herrera, J. E.; Kitiyanan, B.; Borgna, A. *Journal of Nanoparticle Research* **2002**, *4*, 131.

(211) Meyyappan, M.; Delzeit, L.; Cassell, A.; Hash, D. *Plasma Sources Science & Technology* **2003**, *12*, 205.

(212) Kato, T.; Jeong, G. H.; Hirata, T.; Hatakeyama, R.; Tohji, K.; Motomiya, K. *Chemical Physics Letters* **2003**, *381*, 422.

(213) Mahan, A. H.; Alleman, J. L.; Heben, M. J.; Parilla, P. A.; Jones, K. M.; Dillon, A. C. *Applied Physics Letters* **2002**, *81*, 4061.

(214) Peng, H. Q.; Alemany, L. B.; Margrave, J. L.; Khabashesku, V. N. *Journal of the American Chemical Society* **2003**, *125*, 15174.

(215) Campidelli, S.; Sooambar, C.; Diz, E. L.; Ehli, C.; Guldi, D. M.; Prato, M. *Journal of the American Chemical Society* **2006**, *128*, 12544.

(216) Dresselhaus, M. S.; Dresselhaus, G.; Jorio, A.; Souza, A. G.; Saito, R. *Carbon* **2002**, *40*, 2043.

(217) Dresselhaus, M. S.; Dresselhaus, G.; Saito, R.; Jorio, A. *Physics Reports-Review Section of Physics Letters* **2005**, *409*, 47.

(218) Jorio, A.; Pimenta, M. A.; Souza, A. G.; Saito, R.; Dresselhaus, G.; Dresselhaus, M. S. *New Journal of Physics* **2003**, *5*.

(219) Fantini, C.; Jorio, A.; Santos, A. P.; Peressinotto, V. S. T.; Pimenta, M. A. *Chemical Physics Letters* **2007**, *439*, 138.

(220) O'Connell, M. J.; Bachilo, S. M.; Huffman, C. B.; Moore, V. C.; Strano, M. S.; Haroz, E. H.; Rialon, K. L.; Boul, P. J.; Noon, W. H.; Kittrell, C.; Ma, J. P.; Hauge, R. H.; Weisman, R. B.; Smalley, R. E. *Science* **2002**, *297*, 593.

(221) Burghard, M. *Surface Science Reports* **2005**, *58*, 1.

(222) Kim, U. J.; Furtado, C. A.; Liu, X. M.; Chen, G. G.; Eklund, P. C. *Journal of the American Chemical Society* **2005**, *127*, 15437.

(223) Weisman, R. B. *Springer eBook (Applied physics of carbon nanotubes)* **2005**, 20.

(224) Billinge, S. J. L.; Levin, I. *Science* **2007**, *316*, 561.

(225) Giordani, S.; Bergin, S. D.; Nicolosi, V.; Lebedkin, S.; Kappes, M. M.; Blau, W. J.; Coleman, J. N. *Journal of Physical Chemistry B* **2006**, *110*, 15708.

(226) Odom, T. W.; Huang, J. L.; Kim, P.; Lieber, C. M. *Nature* **1998**, *391*, 62.

(227) Accorsi, G.; Armaroli, N.; Parisini, A.; Meneghetti, M.; Marega, R.; Prato, M.; Bonifazi, D. *Advanced Functional Materials* **2007**, *17*, 2975.

(228) Hashimoto, A.; Suenaga, K.; Gloter, A.; Urita, K.; Iijima, S. *Nature* **2004**, *430*, 870.

(229) Lee, D. S.; Kim, D. W.; Kim, H. S.; Lee, S. W.; Jhang, S. H.; Park, Y. W.; Campbell, E. E. B. *Applied Physics A: Materials Science and Processing* **2005**, *80*, 5.

(230) Lutz, T.; Donovan, K. J. *Carbon* **2005**, *43*, 2508.

(231) Hirsch, A. *Top. Curr. Chem.* **1999**, *199*.

(232) Banerjee, S.; Wong, S. S. *Journal of the American Chemical Society* **2004**, *126*, 2073.

(233) Banerjee, S.; Wong, S. S. *Nano Letters* **2004**, *4*, 1445.

(234) Lu, J.; Nagase, S.; Zhang, X. W.; Wang, D.; Ni, M.; Maeda, Y.; Wakahara, T.; Nakahodo, T.; Tsuchiya, T.; Akasaka, T.; Gao, Z. X.; Yu, D. P.; Ye, H. Q.; Mei, W. N.; Zhou, Y. S. *Journal of the American Chemical Society* **2006**, *128*, 5114.

(235) Campidelli, S.; Meneghetti, M.; Prato, M. *Small* **2007**, *3*, 1672.

(236) *http://www.sigmaaldrich.com/catalog*.

(237) Tomonari, Y.; Murakami, H.; Nakashima, N. *Chemistry-a European Journal* **2006**, *12*, 4027.

(238) Maeda, Y.; Kanda, M.; Hashimoto, M.; Hasegawa, T.; Kimura, S.; Lian, Y. F.; Wakahara, T.; Akasaka, T.; Kazaoui, S.; Minami, N.; Okazaki, T.; Hayamizu, Y.; Hata, K.; Lu, J.; Nagase, S. *Journal of the American Chemical Society* **2006**, *128*, 12239.

(239) Peng, X.; Komatsu, N.; Bhattacharya, S.; Shimawaki, T.; Aonuma, S.; Kimura, T.; Osuka, A. *Nature Nanotechnology* **2007**, *2*, 361.

(240) Peng, X. B.; Komatsu, N.; Kimura, T.; Osuka, A. *Journal of the American Chemical Society* **2007**, *129*, 15947.

(241) Valeur, B. *Molecular Fluorescence: Principles and Applications.*

(242) Chen, H.; Hu, X.; Ng, S.-C. *Journal of Polymer Science Part A: Polymer Chemistry (in press).*

(243) Frehill, F.; Vos, J. G.; Benrezzak, S.; Koos, A. A.; Konya, Z.; Ruther, M. G.; Blau, W. J.; Fonseca, A.; Nagy, J. B.; Biro, L. P.; Minett, A. I.; Panhuis, M. I. H. *Journal of the American Chemical Society* **2002**, *124*, 13694.

(244) Dresselhaus, M. S.; Dresselhaus, G.; Jorio, A.; Souza, A. G.; Pimenta, M. A.; Saito, R. *Accounts of Chemical Research* **2002**, *35*, 1070.

(245) Strano, M. S. *Journal of the American Chemical Society* **2003**, *125*, 16148.

(246) Samsonidze, G. G.; Chou, S. G.; Santos, A. P.; Brar, V. W.; Dresselhaus, G.; Dresselhaus, M. S.; Selbst, A.; Swan, A. K.; Unlu, M. S.; Goldberg, B. B.; Chattopadhyay, D.; Kim, S. N.; Papadimitrakopoulos, F. *Applied Physics Letters* **2004**, *85*, 1006.

(247) Fantini, C.; Jorio, A.; Souza, M.; Strano, M. S.; Dresselhaus, M. S.; Pimenta, M. A. *Physical Review Letters* **2004**, *93*.

(248) Maultzsch, J.; Telg, H.; Reich, S.; Thomsen, C. *Physical Review B* **2005**, *72*.

(249) Jorio, A.; Souza, A. G.; Dresselhaus, G.; Dresselhaus, M. S.; Swan, A. K.; Unlu, M. S.; Goldberg, B. B.; Pimenta, M. A.; Hafner, J. H.; Lieber, C. M.; Saito, R. *Physical Review B* **2002**, *65*.

(250) Piscanec, S.; Lazzeri, M.; Robertson, J.; Ferrari, A. C.; Mauri, F. *Physical Review B* **2007**, *75*.

(251) Miyata, Y.; Yanagi, K.; Maniwa, Y.; Kataura, H. *Journal of Physical Chemistry C* **2008**, *112*, 3591.

(252) Joselevich, E. *Angewandte Chemie-International Edition* **2004**, *43*, 2992.

(253) Kim, S. N.; Luo, Z. T.; Papadimitrakopoulos, F. *Nano Letters* **2005**, *5*, 2500.

(254) Hennrich, F.; Krupke, R.; Lebedkin, S.; Arnold, K.; Fischer, R.; Resasco, D. E.; Kappes, M. *Journal of Physical Chemistry B* **2005**, *109*, 10567.

(255) Weisman, R. B.; Bachilo, S. M. *Nano Letters* **2003**, *3*, 1235.

(256) Jones, M.; Engtrakul, C.; Metzger, W. K.; Ellingson, R. J.; Nozik, A. J.; Heben, M. J.; Rumbles, G. *Physical Review B* **2005**, *71*.

(257) Miyauchi, Y.; Oba, M.; Maruyama, S. *Physical Review B* **2006**, *74*.

(258) Li, L. J.; Glerup, M.; Khlobystov, A. N.; Wiltshire, J. G.; Sauvajol, J. L.; Tavlor, R. A.; Nicholas, R. J. *Carbon* **2006**, *44*, 2752.

(259) Traiphol, R.; Sanguansat, P.; Srikhirin, T.; Kerdcharoen, T.; Osotchan, T. *Macromolecules* **2006**, *39*, 1165.

(260) Quan, S. Y.; Teng, F.; Xu, Z.; Qian, L.; Hou, Y. B.; Wang, Y. S.; Xu, X. R. *European Polymer Journal* **2006**, *42*, 228.

(261) Stefanis, E.; Panayiotou, C. *International Journal of Thermophysics* **2008**, *29*, 568.

(262) Hansen, C. M. *Hansen Solubility Parameters: A User's Handbook*.

(263) Itoh, Y.; Yamashita, O.; Hachimori, A.; Kojima, M.; Suzuki, S. *Journal of Polymer Science Part a-Polymer Chemistry* **1995**, *33*, 137.

(264) Holden, D. A.; Ren, X. X.; Guillet, J. E. *Macromolecules* **1984**, *17*, 1500.

(265) Lu, J.; Lai, L.; Luo, G.; Zhou, J.; Qin, R.; Wang, D.; Wang, L.; Mei, W. N.; Li, G.; Gao, Z.; Nagase, S.; Maeda, Y.; Akasaka, T.; Yu, D. *Small* **2007**, *3*, 1566.

(266) Lee, C. W.; Weng, C. H.; Wei, L.; Chen, Y.; Chan-Park, M. B.; Tsai, C. H.; Leou, K. C.; Poa, C. H. P.; Wang, J. L.; Li, L. J. *Journal of Physical Chemistry C* **2008**, *112*, 12089.

(267) Kim, W.; Javey, A.; Tu, R.; Cao, J.; Wang, Q.; Dai, H. J. *Applied Physics Letters* **2005**, *87*.

(268) Zhang, L.; Zaric, S.; Tu, X. M.; Wang, X. R.; Zhao, W.; Dai, H. J. *Journal of the American Chemical Society* **2008**, *130*, 2686.

(269) Pan, X.; Li., L.-J.; Chan-Park, M. B. *Small* **2010**, *6*, 1311.

(270) Oyama, Y.; Saito, R.; Sato, K.; Jiang, J.; Samsonidze, G. G.; Gruneis, A.; Miyauchi, Y.; Maruyama, S.; Jorio, A.; Dresselhaus, G.; Dresselhaus, M. S. *Carbon* **2006**, *44*, 873.

(271) Yan, L. Y.; Li, W. F.; Fan, X. F.; Wei, L.; Chen, Y.; Kuo, J. L.; Li, L. J.; Kwak, S. K.; Mu, Y. G.; Chan-Park, M. B. *Small* **2010**, *6*, 110.

(272) L.Andrews, D.; Demidov, A. A. *Resonance Energy Transfer* **1999**, *JOHN WILEY & SONS*, 1-55.

(273) CRAIG, D. P.; THIRUNAMACHANDRAN, T. *Molecular Quantum Electrodynamics, An Introduction to Radiation-Molecule Interaction,* **1984**, *Academic Press*, 174-178.

(274) SALAM, A. *Molecular Quantum Electrodynamics, Long-Range Intermolecular Interactions,* **2010**, *John Wiley & Sons*, 311-369.

(275) Pan, X.; Chan-Park, M. B. *Journal of Polymer Science Part B: Polymer Physics (accepted)*.

(276) Cao, G. *Nanostructures & Nanomaterials synthesis, properties & applications,* **2004,** *Imperial college press*, 36-38.

Appendix: Publication

1. Kumar Raj, Xiaoyong Pan, Qing Zhang, Mary B. Chan-Park and Gao Pingqi, Chemically induced air- stable unipolar-to-ambipolar conversion of carbon nanotube field effect transistors, *Chem Phys Lett*, 470, 95-98, 2009

2. Xiaoyong Pan, Qin Jia Cai, Chang Ming Li, Qing Zhang, Mary B. Chan-Park, Species enrichment of SWNTs with pyrene alkylamide derivatives: is the alkyl chain length important? *Nanotechnology*, 20, 30, 2009

3. Wen Xiu Zhou, Ye Hai Yan, Xiaoyong Pan, Xu Rong, Mary B Chan-Park, Aggregation of silicone diacrylate varied molecular weight in the acrylate mixture on different substrates side surface, *J. Polym. Sci. Part B: Polymer Physics*, 48, 442–450, 2010

4. Xiaoyong Pan, Lain-Jong Li, Mary B. Chan-Park, Diameter and Metallicity Selective Enrichment of Single-Walled Carbon Nanotubes using Polymethacrylates with Pendant Aromatic Functional Groups, *Small*, 12, 1311-1320, 2010

5. Xiaoyong Pan, Mary B. Chan-Park, Separation of Single-Walled Carbon Nanotubes with Aromatic Group functionalized Polymethacrylates and Building Blocks Contribution to the Enrichmentment, *J. Polym. Sci. Part B: Polymer Physics, accepted.*

6. Xiaoyong Pan, Mary B. Chan-Park, Resonance Energy Transfer (RET) induced Intermolecular Pairing Force: a Tunable Weak Interaction and its Application in SWNT Separation. *submitted.*